Title
Neural Mechanisms of Inhibitory Control and Tic Generation in Persistent Tic Disorder

Author
Jurgiel, Joseph Alexander

Publication Date
2022

Peer reviewed|Thesis/dissertation

UNIVERSITY OF CALIFORNIA

Los Angeles

Neural Mechanisms of Inhibitory Control and Tic Generation in Persistent Tic Disorder

A dissertation proposal submitted in partial satisfaction of the

requirements for the degree of Doctor of Philosophy

in Bioengineering

by

Joseph Alexander Jurgiel

2022

ABSTRACT OF THE DISSERTATION

Neural Mechanisms of Inhibitory Control and Tic Generation in Persistent Tic Disorder

by

Joseph Alexander Jurgiel

Doctor of Philosophy in Bioengineering

University of California, Los Angeles, 2022

Professor Sandra K. Loo, Co-Chair

Professor Wentai Liu, Co-Chair

Persistent tic disorder (PTD) is a neuropsychiatric disorder characterized by involuntary and stereotypical movements called tics. Despite a multitude of research, questions still remain regarding the full neurological bases of tic generative activity, as well as the degree to which certain cognitive functions are impaired in children with PTD. This dissertation aims to further elucidate the atypical neural dynamics associated with PTD through an EEG perspective. To facilitate the investigation of these neural dynamics, we first evaluate an adapted approach for performing group-level analyses on localized EEG measures at the cortical source level and compares performance to classical methods. We examined three approaches (a voxel approach, a

region-of-interest (ROI) approach, and a k-means clustering approach) for detecting group differences in spectral activity in both a simulation analysis and visual attention task. Overall, we found that a voxel-approach produces reduced localization error, reduced spectral attenuation, and more accurate time-frequency detection of spectral effects, posing the method as an effective analysis approach. We then examined the degree to which behavioral performance and neural dynamics are atypical in children with PTD (compared to typically developing children) during an inhibitory control flanker paradigm, using measures of spectral power and effective connectivity. While task accuracy did not differ by diagnosis, children with PTD exhibited attenuated spectral activity in the anterior cingulate cortex (ACC), alongside greater information flow from the ACC to fronto-parietal network hubs relative to controls, while controls showed greater central and posterior connectivity. Correlations with clinical features (e.g., tic impairment) and task performance indicate these atypical activations may be neural adaptations from frequent engagement of inhibitory control pathways. Lastly, utilizing similar measures, we investigated the neural antecedents of tic expression, and the degree to which this activity is differentiable from normal resting state activity using a machine learning approach. Prior to tic occurrence, we observed increased spectral activity in the ACC, as well as changes in information flow in frontal, sensorimotor, and posterior regions, suggesting aberrant communication among multiple cognitive and sensory regions. These measurements were also found to be reliable discriminators between pre-tic activity and tic-free activity, using a Naïve Bayes classification model. We then discuss future directions for each of the three preceding studies, as well as a potential path for developing more effective treatment protocols in PTD.

The dissertation of Joseph Alexander Jurgiel is approved.

Agatha Lenartowicz

John Piacentini

Nanthia Suthana

Wentai Liu, Committee Co-Chair

Sandra K. Loo, Committee Co-Chair

University of California, Los Angeles

2022

To my parents,

who have always given me their unconditional love and support.

TABLE OF CONTENTS

LIST OF FIGURES

LIST OF TABLES

Acknowledgements

I would like to thank my PhD advisor, Sandra Loo, for her mentorship and guidance throughout my graduate studies, as well as my committee: Wentai Liu, Agatha Lenartowicz, John Piacetini, and Nanthia Suthana, for their insightful comments and kind words through these years.

I also want to extend my gratitude to my colleagues and collaborators, past and present, who have helped our work come to fruition. I would like to give special thanks to Iman Zadeh, for his support and mentorship in my early graduate research, and Makoto Miyakoshi, who has always been willing to share his clever thoughts and knowledge to any questions I may have.

This work has been supported by funding provided by National Institutes of Neurological Disease and Stroke grants 80160 and 97484 to Sandra Loo. The Swartz Center for Neural Computation, directed by Scott Makeig, was founded in 2001 by a generous gift from founding donor Dr. Jerome Swartz of The Swartz Foundation (Old Field, New York). All participants with persistent tic disorder were recruited through community advertisements, internet postings, and from an academic medical center anxiety and tic disorder clinic. We thank all the participants and their families who have volunteered their time.

Chapter 2 is a version of "Jurgiel, J., Miyakoshi, M., Dillon, A., Piacentini, J., Makeig, S., & Loo, S. K. (2021). Inhibitory control in children with tic disorder: Aberrant fronto-parietal network activity and connectivity. Brain Communications, 3(2), fcab067. https://doi.org/10.1093/braincomms/fcab067."

VITA

EDUCATION

2017 Master of Science, Bioengineering, University of California, Los Angeles, Los Angeles, California

2013 Bachelor of Science, Electrical Engineering, University of Connecticut, Storrs, Connecticut

PUBLICATIONS

Tan, P. Z., Rozenman, M., Chang, S. W., **Jurgiel, J.**, Truong, H. V., Piacentini, J., & Loo, S. K. (2021). The ERN as a Neural Index of Changes in Performance Monitoring Following Attention Training in Pediatric Obsessive-Compulsive Disorder. Biological Psychiatry

Jurgiel, J., Miyakoshi, M., Dillon, A., Piacentini, J., Makeig, S., & Loo, S. K. (2021). Inhibitory control in children with Tic Disorder: Aberrant fronto-parietal network activity and connectivity. Brain Communications, 3(2), fcab067.

Peris, T. S., Salgari, G., Perez, J., **Jurgiel, J.**, Vreeland, A., O'Neill, J., ... & Loo, S. K. (2020). Shared and Unique Neural Mechanisms Underlying Pediatric Trichotillomania and Obsessive Compulsive Disorder. Psychiatry Research, 113653.

Miyakoshi, M., **Jurgiel, J.**, Dillon, A., Chang, S., Piacentini, J., Makeig, S., & Loo, S. K. (2020). Modulation of frontal oscillatory power during blink suppression in children: Effects of premonitory urge and reward. Cerebral Cortex Communications.

Michelini, G., **Jurgiel, J.**, Bakolis, I., Cheung, C. H., Asherson, P., Loo, S. K., ... & Mohammad-Rezazadeh, I. (2019). Atypical functional connectivity in adolescents and adults with persistent and remitted ADHD during a cognitive control task. Translational psychiatry, 9(1), 137.

Salgari, G. C., Perez, J., **Jurgiel, J.**, O'Neill, J., Chang, S., Piacentini, J., ... & Loo, S. K. (2018). 4.30 Shared and Unique Neural Mechanisms Underlying Inhibitory Control in Trichotillomania and OCD. Journal of the American Academy of Child & Adolescent Psychiatry, 57(10), S214.

Coben, R., Mohammad-Rezazadeh, I., Frohich, J., **Jurgiel, J.**, & Michelini, G. (2017). Imaging brain connectivity in autism spectrum disorder. Autism Imaging and Devices, 261-302.

Chapter 1: Introduction

Persistent tic disorders (PTDs) including Tourette Syndrome (TS), are characterized by sudden, involuntary, and recurrent movements or vocalizations, referred to as tics. As one of the most common neurodevelopmental disorders, PTDs occur in approximately 1% of the childhood population worldwide (Robertson, 2008), and are often disruptive to typical childhood development through increased psychological distress and higher suicidal tendencies in individuals. Although tic severity often decreases by adulthood in a majority (75%) of cases (Bloch & Leckman, 2009), there is a need for more effective pediatric treatment protocols applicable during this critical developmental period given the modest efficacy of current treatment methods (Pedroarena-Leal & Ruge, 2017). However, it remains unclear the regions and mechanisms primarily responsible for tic/urge generation and the extent to which other related cognitive processes (such as inhibitory control) are impaired, information core to developing possible treatment targets and evaluating treatment efficacy among pediatric populations. The proposed studies contained in this dissertation aim to further elucidate the extent and locations of atypical cortical activity associated with affected cognitive and tic generative processes among children with tic disorders, utilizing an adapted method for more effectively detecting atypical cortical source-level EEG activity.

Over the years, a multitude of studies have investigated the pathophysiological characteristics of brain development and activity in individuals with tic disorders in order to better understand the driving factors for tic symptomology and disorder progression. Given one of the primary manifestations of the disorder's symptomology (i.e., motor tics), motor control pathways such as cortico-striato-thalamo-cortical (CSTC) circuitry have been a major focus of research

explorations. Structural deficits have been noted by a number of studies, including thinning of sensorimotor cortices (Sowell et al., 2008), atypical basal ganglia volumes (Greene et al., 2017; Peterson et al., 2003; Roessner et al., 2011), and abnormalities in white matter tract density among CSTC areas (Wen et al., 2016). Correlations between the degree of these structural abnormalities and tic severity (Wen et al., 2016), as well as longitudinal prediction of aberrant childhood basal ganglia volumes with adulthood tic severity (Bloch et al., 2005), provide support for relationships between neuroanatomical deficits and degree of clinical impairment.

Functional abnormalities using various brain imaging modalities have been reported amongst PTD populations across a number of cognitive paradigms, including resting state, suppression, inhibitory control, and voluntary movement tasks. Studies examining network dynamics have observed aberrant connectivity patterns among the well-researched CSTC circuitry (Worbe et al., 2012), as well as fronto-parietal, posterior, and default-mode networks (Church, Fair, et al., 2009) and urge-tic network nodes (Tinaz et al., 2015). Region-based studies have indicated localized aberrant activation amongst insula, motor cortex, precuneus, cingulate cortex, as well as frontal cortices (Cui et al., 2014; Jung et al., 2013). Findings have also implicated midcingulate and insular cortices in the urge-based component of tics (Jackson, Parkinson, Kim, et al., 2011; O'Neill et al., 2019). However, a number of uncertainties remain regarding the regions and networks associated with cognitive impairments among tic disorder populations. While many studies to date have been performed using functional magnetic resonance imaging (fMRI), there has been limited research on neural dynamics of tic disorders using time-resolved methods such as EEG, which can provide millisecond-resolution recording of atypical activation patterns. This may be in part due to frequent reports on subcortical abnormalities in PTD, which EEG has difficulty measuring due to physiological limitations. However, as described previously,

functional and structural MRI studies have indeed reported aberrant activity and anatomical development beyond these subcortical areas, extending to several cortical regions across the brain. Utilizing EEG to study cortical areas is thus an opportune method for further examining neural dynamics of the disorder with temporally resolved specificity.

Source-localized EEG activations, through methods such as independent component analysis (ICA), provide a way to enhance spatial localization of temporally resolved EEG activity in patient populations. Relative to scalp or electrode-level analysis, they may provide more effective localization of cortical sources (or dipoles) within neuroanatomical structures, an important feature for evaluating and interpreting any observed neural deficits. However, due to the uniqueness of source locations across subjects in ICA-based approaches, comparing source-level data between subjects and/or groups is nontrivial. To address this issue, group-level studies generally utilize clustering algorithms (e.g., k-means clustering) to group dipoles together based on spatial locations or signal characteristics, allowing analyses to be performed on these clusters. However, several subjective decision points exist within these methods that may result in non-optimal solutions, including a priori parameter selection (e.g., number of clusters, variables to include in clustering criteria, etc.), dependence of spatial specificity on cluster sizes, as well as impartiality to anatomical partitions of the brain (e.g., regions defined by Brodmann or other similar partitioning schemes that may be responsible particular cognitive processes). Variability in these parameter selections and clustering solutions may affect both interpretation of findings as well as replicability. Recent EEG analysis toolboxes including the Measure Projection Toolbox (MPT) (Bigdely-Shamlo et al., 2013) and groupSIFT (Loo et al., 2019) have worked towards resolving these issues by representing cortical sources as probabilistic volumes in order to facilitate group-level analyses while minimizing arbitrary parameter selection. In Chapter 2, this

probabilistic approach will be applied towards evaluating between-group differences in localized spectral activity in both simulated and real datasets. In this process, a region-of-interest (ROI) approach, based on the foundation of groupSIFT (Loo et al., 2019), and a voxel-based approach will be compared and contrasted to the classical k-means clustering approach utilized in EEGLAB (Delorme & Makeig, 2004) in their ability to effectively detect, localize, and replicate spectral activation findings.

The methods developed in Chapter 2 (if found to be beneficial over classical methods) will then be utilized in Chapters 3 and 4 to assess differing but potentially complementary aspects of tic symptomology and neural atypicality in children (ages 8-12 years old) with PTD. Chapter 3 will evaluate cognitive impairments beyond generally visible tic symptomology, specifically with regards to inhibitory control. Prior studies have presented contrasting findings regarding whether inhibitory control is impaired in children with PTD, with different studies indicating contrasting trends of both better and worse behavioral performance. Yet very few studies have evaluated whether inhibitory control networks associated with these deficits/advantages are similar to neurotypical controls. The Study aims to further explore whether cortical EEG activation patterns of children with PTD differ from typically developing controls during an inhibitory control paradigm (flanker task). Relationships between neural measurements and clinical/behavioral metrics were evaluated to determine the brain regions and networks utilized by children with tic disorders when performing a cognitive inhibitory control task. These results will provide further insight into neural mechanisms underlying inhibitory control among individuals with tic disorder along with better understanding of how cognitive functions tic are affected.

Chapter 4 will examine neural correlates of tic generation by examining brain activity prior to tic occurrence relative to tic-free resting state activity. Although several studies have reported neural activity associated with tic generation in various cortical regions (Bohlhalter et al., 2006; Lerner et al., 2007; Neuner et al., 2014; Stern et al., 2000), these studies have primarily focused on adult populations using fMRI or positron emission topography (PET). However, while adult populations may provide inferences about stable disorder states following disorder adaptation, evaluating pediatric populations are a necessity for examining the development and progression of the disorder. Furthermore, imaging methods such as fMRI and PET may not capture temporally precise activity associated with tic generation. Therefore, Chapter 4 aims to provide further knowledge regarding neural antecedents of tic occurrence by utilizing EEG to evaluate spectral activity and effective connectivity associated tic generation in children. Using a resting-state paradigm, the Study will evaluate whether pre-tic neural activity across the brain is differentiable from within subject average resting state activity in a cohort of children with PTD, and whether upcoming tics can be predicted from this activity. To support and validate the classifier identified in this study, an independent test sample of comparable children with PTD will be evaluated using the same criteria to determine whether the findings are generalizable to other children with PTD.

Altogether, these studies aim to first provide a foundation for more accurate and interpretable detection of cortical source-level activation patterns, and to secondly use this approach to further elucidate the neural locations and quantify brain network atypicality in PTD, with insight from currently unexplored temporally resolved spectral power and connectivity measurements.

Chapter 2: Development of a More Spatially Defined Method for Examining Group-Level, Cortical Source EEG Findings

2.1 Abstract

Independent component analysis (ICA) based source level electroencephalography (EEG) analyses, while providing better localizability and interpretability relative to scalp level analyses, involve solving a nontrivial dilemma at the group level due to unique source locations across participants. Current solutions (such as k-means clustering) often involve semi-arbitrary parameter selection by the researcher, which can negatively affect replicability of findings due to results being dependent on the parameters used. The present analysis evaluates the feasibility and benefits of alternative approaches for group-level spectral analysis, which require minimal parameter selection by the user. To do this, we utilize a region of interest (ROI) and voxel-based approach drawn from features of two prior toolboxes (Measure Projection Toolbox (Bigdely-Shamlo et al., 2013) and groupSIFT (Loo et al., 2019)) as applied towards group-level analysis of localized spectral activity. We compare these two proposed analysis methods towards the classical k-means clustering utilized in EEGLAB (Delorme & Makeig, 2004), with respect to robustness in detection, localization, and replicability of spectral effect findings in both a simulated and visual attention dataset.

2.2 Introduction

A fundamental caveat of using electroencephalography (EEG) to record brain activity is that the time series data obtained at each scalp sensor is a superposition of an unknown number of true underlying cortical sources, due to the propagative nature of electrical fields from the cortex.

Estimating the activity and location of these sources is commonly referred to as the EEG inverse problem. In an attempt to estimate a solution to this problem, independent component analysis (ICA) (Bell & Sejnowski, 1995) is frequently applied to learn a set of spatial filters which decompose scalp level EEG data into a linear combination of maximally independent processes (i.e., independent components). By using the electrode projection weights of these independent components (ICs), source activities may then be localized to cortical patches of dipolar activity within the brain (Delorme et al., 2012a).

Decomposing channel data into cortical sources using these prescribed methods provides multiple benefits for EEG analyses. One core benefit is the elimination of volume conductive characteristics present among spatially adjacent electrodes, which can otherwise negatively influence measurements such as neural connectivity due to spurious correlations. Second, it facilitates more effective physiological interpretations of findings, as measured activity is no longer at a projected scalp region but at the estimated cortical region of interest. However, there is a major pitfall, particularly with group-level analyses, which is that estimated dipole source locations are generally inconsistent across participants and, although to a lesser degree, recording sessions (Grandchamp et al., 2012). Thus, comparisons of cortical-source level measurements between participants become difficult, as not all subjects may possess a decomposed IC at a particular anatomical location. This is in contrast to scalp-level analyses where electrode montages are standardized and set to be consistent across subjects, thus making direct comparisons straightforward.

In an attempt to reconcile the spatial variability (and presence) of cortical sources across participants, different approaches have been introduced to allow for group-level comparisons to

be performed. A commonly used approach is k-means clustering, where dipoles from all participants are pooled and spatially separated into k clusters which minimize the squared error of within-cluster Euclidean distances between dipoles. Group-level analyses are then performed on these spatially distinct clusters by comparing the subset of dipoles between groups, circumventing the source inconsistency issue. However, several drawbacks are apparent when using this method. First, k-means (and several similar) clustering algorithms require a priori selection of semi-arbitrary clustering parameters, such as number of clusters or outlier threshold. However, the choice of parameter may affect study replicability as differing parameters may result in differing detection capabilities or specific locations of cortical findings. Secondly, clustering algorithms may unknowingly group ICs with effects of interest with other ICs displaying unrelated activity. This may result in diluted or attenuated effects when activations are averaged across ICs within a given cluster, particularly when the cluster number k is small, potentially resulting in failed detection of the effect of interest at the group level. While including spectral characteristics of interest in the clustering criteria may help evade this issue and provide better clustering solutions for a given effect, this can cause statistical "double-dipping" and inflation of type 1 error due to the variance reduction that occurs when grouping ICs by similarities in their activation patterns (Kriegeskorte et al., 2009). Lastly, given that cluster locations may not align well with the true anatomical locations of the effects of interest, relevant findings may be mislocalized, affecting both interpretation of findings and study replicability.

A more recent method, the Measure Projection Toolbox (MPT) (Bigdely-Shamlo et al., 2013), has utilized an alternative probabilistic approach, whereby dipole sources are smoothed across a brain model via a Gaussian kernel, transforming unipoint dipoles into a probabilistic dipole density. When applied to all dipoles, this smoothing results in a spatially continuous

distribution of dipole activations at the group level, allowing for analyses to be performed on these specific regions. This smoothing is substantiated by uncertainties which arise in dipole localization during head co-registration, differences in tissue conductivity across participants, or between-person differences in cortical organization/folding. Other tools have built upon this idea, particularly the groupSIFT toolbox (Loo et al., 2019), which utilizes the Gaussian smoothing application to examine source-level connectivity at the group level. Thus, an approach utilizing continuous dipole sources with appropriate statistical testing procedures may provide a better approach for examining source-level group differences.

The present study aims to expand on the approaches introduced in the MPT and groupSIFT plug-ins in order to address the aforementioned issues which may be present in typical cortical source-level clustering analyses, including a priori parameter selection, attenuation of effects of interest, and inaccurate localization of cortical findings. We explore two alternative approaches (relative to conventional k-means clustering) for performing group-level analyses of localized source-level spectral power activity: 1) a region of interest (ROI) approach using a set of 76 regions defined by the anatomical labeling atlas (AAL) (Tzourio-Mazoyer et al., 2002), and 2) a voxel-based approach, using a set of 8mm spaced voxels spanning across the brain. A simulation analysis is first performed, whereby we show that the voxel-based approach provides better spatial localization as well as reduced attenuation of cortical effects of interest, resulting in more consistent and valid anatomical interpretations. The methods are then applied to a spectral power study examining visual attention in a sample of healthy children during a visual attention paradigm, where the voxel-based approach is evaluated alongside the k-means and ROI approaches with respect to interpretability and localization of effects.

2.3 Methods

A simulation analysis was first performed to evaluate the effectiveness of three source-level analysis methods in detecting a spatially defined time-frequency activation pattern at the group-level. In brief, the simulation analysis consisted of four steps: 1) Resting state EEG data for a set of subjects was processed (including source localization) and artificially epoched into a Signal and Control condition. 2) A point in the cortex was randomly selected to be the center of the artificial activation pattern, with an 8-12Hz (random), 500ms wavelet added to Signal condition epochs of cortical sources nearby this point (simulating a spatially defined neural activation). 3) Three source-level analysis approaches (k-means clustering, ROI approach, and voxel approach) were implemented along with permutation-based statistical testing, with a goal of detecting the artificial effect in the Signal condition compared to the unaltered Control condition. 4) This procedure was iterated 100 times, with the location of the activation changing during each iteration, and with details of findings (relative to ground truth) recorded during each iteration (e.g., error in detected activation location, detected ROI vs true ROI, detected spectral power vs true spectral power, etc.).

2.3.1 Data Preprocessing

The simulation analysis utilized resting state EEG data (approximately 7.5 minutes in length) recorded from 33 typically developing children, aged 8-12 years old, using a 128-channel HydroCel net in an extended international 10-10 configuration (Electrical Geodesics Incorporated). Electrode impedances were lower than 50kΩ, based on manufacturer recommendation. EEG data was recorded at a sample rate of 1000Hz and referenced to channel

Cz. Spatial coordinates of electrodes were obtained using Polhemus, Inc. digitizer software, using the nasion and preauricular notches as anatomical reference points.

Using the EEGLAB toolbox, data were preprocessed and cleaned using a standard pipeline, including a 1Hz high-pass finite impulse response filter, followed by Artifact Subspace Reconstruction (ASR) (Kothe & Makeig, 2013) via the EEGLAB plug-in *clean_rawdata()* in order to remove and interpolate signal artifacts. Data was downsampled to 100Hz and cortical source activity (independent components (ICs)) was estimated using adaptive mixture independent component analysis (AMICA) (Palmer et al., 2011). Dipole locations of source activations were then estimated using the DIPFIT plug-in of the Fieldtrip toolbox (Oostenveld et al., 2010a). Non-neural ICs were rejected using the EEGLAB ICLabel plug-in, an algorithm trained to classify neural vs. non-neural ICs. ICs were also rejected if they were not spatially contained within the brain (based on coordinates), or if they displayed >15% residual variance relative to an equivalent dipole. A total of 439 dipoles were included in the analysis after data processing.

To prepare a condition for the artificial signal, source level activity within each subject was epoched into non-overlapping, contiguous 4-second segments (labeled as -2 to +2 seconds). Data trials were then separated into even-trial and odd-trial conditions using a split-half approach for each subject, resulting in a paired analysis of approximately 50 trials per condition per subject.

2.3.2 Establishing Ground Truth Spectral Activity

The simulation analysis was an iterative process, whereby a spectral activation pattern at a randomly selected region (i.e., voxel point) of the brain was first established during each iteration. The three analysis methods (k-means, ROI, and voxel) were then performed and evaluated for their

ability to detect this ground truth activation pattern. A general procedure for this simulation process is displayed in Figure 2-1, with the full detailed procedure as follows.

For each of the N = 100 simulations, a Signal condition and Control condition were first created for each subject by bootstrapping (with replacement) 50 data trials from the even-trial and odd-trial datasets, respectively. Next, a spatial location in the cortex was to be randomly selected as the centroid of the artificial activation pattern. A 3-dimensional (3-D) grid with 8mm spacing between grid points (voxels) was then placed on a standard brain model using the Measure Projection Toolbox, resulting in a set of 3908 voxels across the brain. To allow for a sufficient number of subjects to contain modified activations, and facilitate later ROI and voxel method implementations, only voxels which contained dipoles for at least 50% of subjects within a 50mm diameter sphere were included as potential centroids. This resulted in 1700 selectable voxels, one of which was then randomly chosen per iteration to be the spatial centroid of modified spectral activity. For the Signal condition, a simulated wavelet was then created and added to trials of dipoles within the 50mm sphere of the selected voxel for their Signal condition. This waveform consisted of a 500ms sine wave with frequency randomly selected from 8-12Hz, and an amplitude equal to the root-mean square (RMS) of data within the trial for a given dipole. The pure sine wave was then multiplied by a gaussian envelope ($\mu = 0.25$, $\sigma = 0.1$), in order to prevent edge artifacts from appearing in the time-frequency domain. The resulting signal was then added to the 500-1000ms portion of the trial. The process was repeated for all trials of all ICs within the spatial sphere, creating a ground truth spectral activation centered around 10Hz and 750ms in the Signal condition, and spatially localized around the selected voxel. The Control condition containing the original resting state EEG epochs was left unmodified.

Event-related spectral perturbation (ERSP), a time-frequency measurement of evoked changes in spectral power activity relative to a baseline, was utilized as the method for measuring the simulated time-frequency activation. To calculate ERSP for each of the two conditions, a sliding window of 1s in length was applied across each trial in 20ms steps to extract spectral magnitudes for each time-frequency bin of the trial. This resulted in a 100 frequency (3 to 50Hz) x 189 time (-1.5s to 1.5s) matrix of spectral magnitudes for each trial. Time-frequency matrices were then averaged within each subject, followed by baselining (divisive) of spectral magnitudes within each frequency using average power between -500ms to 0ms. These spectral magnitude ratios were then log-transformed to decibel (dB) units using the formula $10*log_{10}(X)$, creating a gain model describing changes in spectral power relative to the baseline (i.e., ERSP).

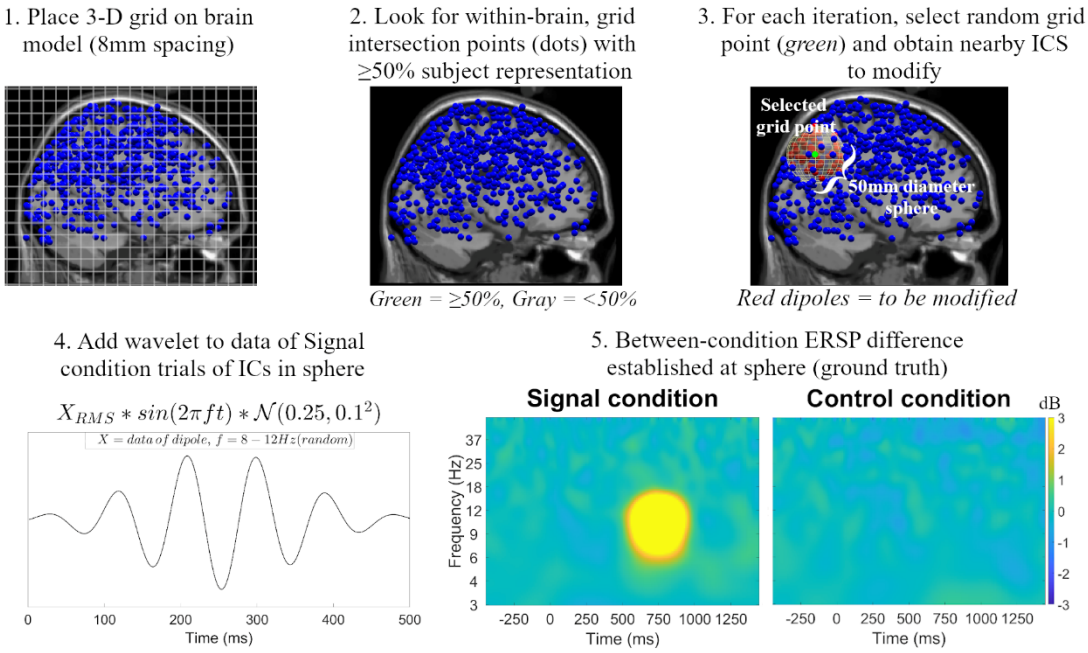

Figure 2-1. Creation of simulated ground truth spectral activation. (1) A 3-dimensional grid is placed on the brain model containing dipoles from all subjects. (2) Grid points (voxels) containing contributions from dipoles (defined by the dipole being within 25mm of the grid point)

from at least 50% of subjects are marked as potential locations for the artificial signal. (3) During each simulation iteration, dipoles contributing to the voxel are selected. (4) For each data trial, a wavelet of 8-12Hz (random) frequency, 500ms length, and amplitude equal to the root mean square of the data trial is added to the data trial. (5) Spectral plots indicate activation created in the 8-12Hz frequency band, and 500-1000ms time period of the epoch. ERSP = event-related spectral perturbation, IC = independent component.

2.3.3 Clustering Approaches for Detecting Ground Truth Signal

Three group-level cortical source analysis approaches were then evaluated on their ability to detect this between-condition (i.e., Signal vs Control) time-frequency difference in ground truth ERSP activation: a classical k-means clustering approach across a range of k-values, a ROI approach (using 76 regions defined by the anatomical labeling atlas), and a voxel approach (8mm spacing). A general overview of the three approaches is shown in Figure 2-2.

K-means clustering was implemented using the standard algorithm, which aims to separate data (here, dipoles) into K clusters which minimize the within-cluster squared Euclidean distances. Dipoles for all subjects were pooled together, and clustering solutions were obtained for values of $k = 5$ to $k = 15$, where dipole outliers spaced greater than 3σ from any cluster centroid were placed into an outlier group and not considered for the solution. For each cluster in a given solution, subject-level estimates of ERSP were obtained by taking within-subject averages of ICs in the cluster, resulting in a single ERSP for each subject.

The ROI approach employed 76 predefined anatomical ROIs from the anatomical labeling atlas (AAL). In order to estimate ERSP activity for each subject at each ROI, the previously described 8mm-spaced set of 3908 voxels was utilized. ROI labels were first assigned to these

voxels based on their Montreal Neurological Institute (MNI) coordinates relative to anatomical boundaries as defined by the AAL. Voxels with no corresponding ROI were left unlabeled. Dipoles were then smoothed into probabilistic spheres using a 3-D Gaussian kernel (full width half maximum of 20mm truncated at 3σ), as introduced in Bigdely-Shamlo et al. (2013). The Gaussian probability values of contributions from each dipole to nearby voxels was stored in a 439 (dipole) x 3908 (voxel) probabilistic weight matrix. For each subject in each ROI, a single ERSP matrix was calculated by using a weighted average of dipoles contributing to any voxels in the ROI, normalized such that the total probability contribution summed to one. ROIs with dipole contributions from fewer than 50% of subjects were excluded from the analysis.

The voxel approach followed a similar methodology as the ROI approach, but average ERSP for each subject was estimated at each voxel rather than atlas-based ROIs. Average ERSP for each subject at each voxel was calculated using a similar normalized within-subject, weighted average of dipole contributions to the respective voxel. A 50% subject inclusion requirement was similarly applied as well, resulting in a subject-level estimate of ERSP for 1700 of the original 3908 voxels.

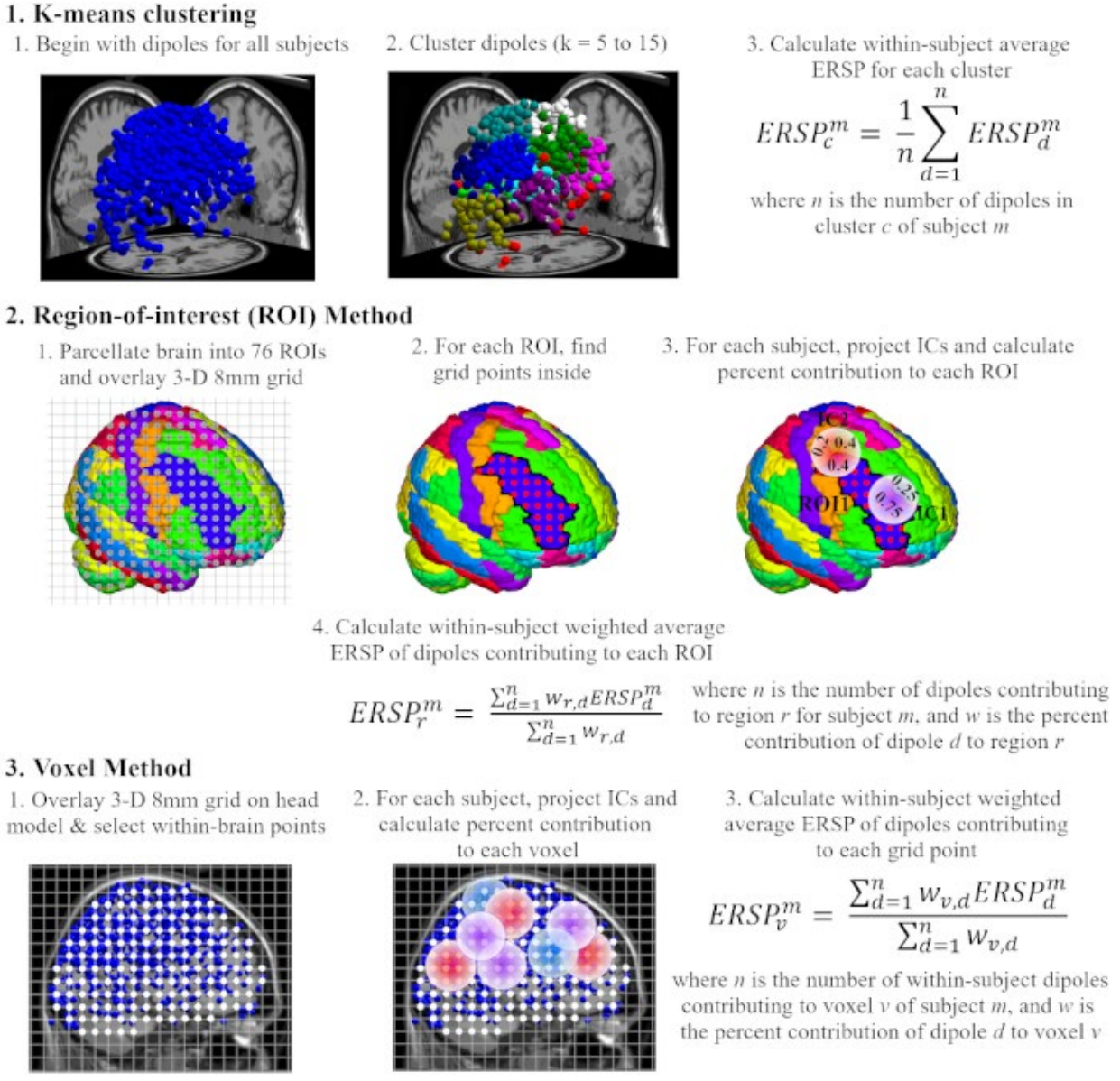

Figure 2-2. Overview of the three source-level analysis methods being compared.

2.3.4 Statistical Analysis

For both the ground truth modified sphere and results from each of the three detection methods, between-condition comparisons and statistics were calculated using a mass-univariate,

permutation testing approach on time-frequency ERSP matrices (Groppe et al., 2011; Pernet et al., 2015). The goal was to first examine the group-level ground truth differences in ERSP between the Signal vs Control condition at the modified sphere at a particular statistical threshold, and then test each method for their ability to replicate this finding at the same threshold.

For the ground truth, the group-level difference in ERSP between the two conditions was first evaluated based on ICs contained in the modified sphere. If a subject had more than one IC in the sphere, ERSP activity from these were averaged together, such that subjects had a single ERSP for the sphere. A mass-univariate statistical approach was utilized, whereby paired t-tests were run between conditions on each time-frequency pixel of the ERSP matrices for the sphere. Resulting t-statistic matrices were then masked using a $p = 0.001$ threshold, with nonsignificant bins set to zero. T-statistics of adjacent surviving pixels were summed to form t-statistic cluster masses, representing significant time-frequency ranges of between-condition ERSP effects. The time-frequency range of the ground truth effect was measured by the mask boundaries, and ground-truth ERSP averages for each condition were obtained by averaging ERSP values within this mask. No permutation tests were performed as the effect of interest was known.

For each of the detection methods, statistical comparisons between conditions were performed on their respective IC groupings using a similar mass-univariate testing approach. For k-means clustering, this meant on each cluster of each clustering solution; for the ROI approach, each ROI; and for the voxel approach, each voxel. For each method, paired t-tests and statistical masking at a $p < 0.001$ threshold were performed on each pixel of the ERSP matrices between conditions.

To account for multiple comparisons, cluster level correction was implemented using a permutation testing approach. For the k-means and ROI methods, t-statistic cluster masses were similarly formed by summing adjacent significant time-frequency pixels of the ERSP matrices, representing detected effects. For N = 1000 iterations, condition labels of each set of cluster/ROI ERSP matrices were shuffled. Statistical testing and cluster mass formation were repeated during each iteration, with the most extreme (absolute value) t-statistic cluster mass stored during each iteration to form a surrogate null distribution (one for each clustering solution and one for all ROIs). True-data cluster masses were then compared to this null distribution using a one-tail $p < 0.001$ significance threshold to obtain cluster level corrected results. Cluster masses from the true data that survived this thresholding/correction were considered significant.

2.3.5 Real Dataset Analysis (Visual Attention Task)

The three methods were then applied to a visual attention dataset in order to evaluate the ability of each method to detect evoked activations associated with related cognitive functions. In this dataset, each participant performed a modified Eriksen flanker task (Fig. 2-3), where for each trial a set of five horizontal white arrows appeared on a black screen either above or below a white fixation cross. The arrows could appear in congruent orientation, where all arrows pointed in the same direction, or in incongruent orientation, where the middle arrow points in the opposite direction of the four flanking arrows. The arrows remained on the screen for 250ms before disappearing. During the response period (1300ms), the participant used the left and right computer mouse buttons to select whether the central arrow was pointing to the left or right, respectively. The response period was followed by a jittered 800-1200ms intertrial interval. Each participant performed 72 congruent and 144 incongruent trials, lasting approximately 7 minutes in length.

Congruent trials with correct responses from each participant were epoched from -2000ms to +2000ms around the stimulus (arrows) presentation. Using a -550 to -50ms baseline, ERSP activity was analyzed during the 0-800ms post-stimulus period using the three approaches, along with the same statistical correction techniques described prior. Findings between the approaches were then compared and contrasted with respect to anatomical regions of detected effects.

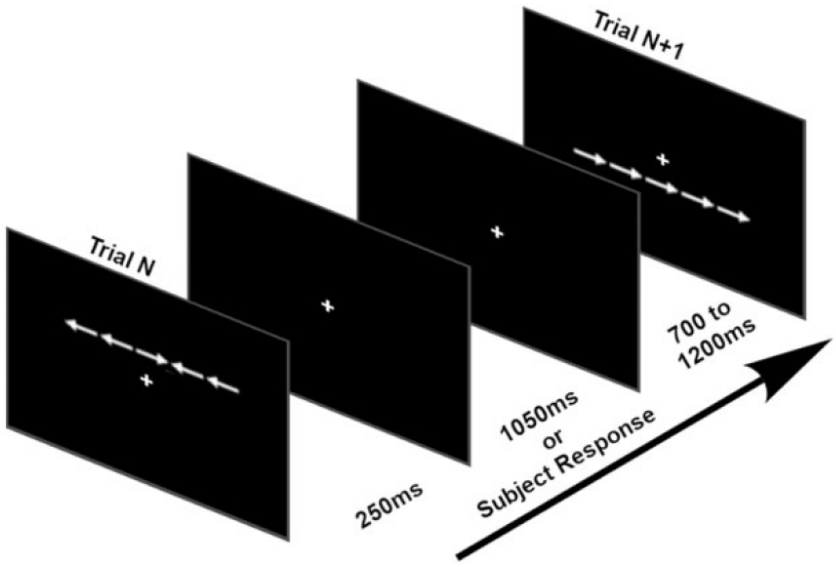

Figure 2-3. Modified Eriksen flanker task. The figure illustrates an incongruent flanker trial (in which the middle arrow points in a different direction than the flanking arrows) followed by a congruent flanker trial (in which all arrows point in the same direction).

2.4 Results

2.4.1 Comparison of Analysis Methods on Simulation Dataset

Several measures relating to the reliability and spatial accuracy of each detection method were extracted and compared, based principally on the types of measures that would be extracted from typical ERSP analyses.

The first metric evaluated was the localization error (Euclidean distance) between the centroid MNI coordinate of the detected effect compared to the centroid MNI coordinate of the established ground truth (i.e., the selected voxel). For k-means clustering, this MNI coordinate was the centroid of ICs in a particular cluster for a given clustering solution. For the ROI approach, this was the spatial centroid of voxels belonging to the ROI. For the voxel approach, this was the centroid of voxels contained in the detected spatial cluster mass of significant findings. As displayed in Figure 2-4, the voxel approach produced the smallest localization error of the three methods, with 6.1 ± 2.7 mm error for the voxel approach, 20.1 ± 5.4 to 22.8 ± 8.1 mm error for the k-means approach (increasing as cluster value k decreases), and 26.1 ± 9.0 mm for the ROI approach. One reasoning for this increased localization capability is the greater spatial resolution provided by the voxel method compared to the k-means and ROI methods. While the k-means method is limited to k = 5 to 15 centroids, and the ROI method is limited to 76 centroids, the voxel approach contains 1700 voxels (using 8mm resolution) which may be possible centroids of spatial activity.

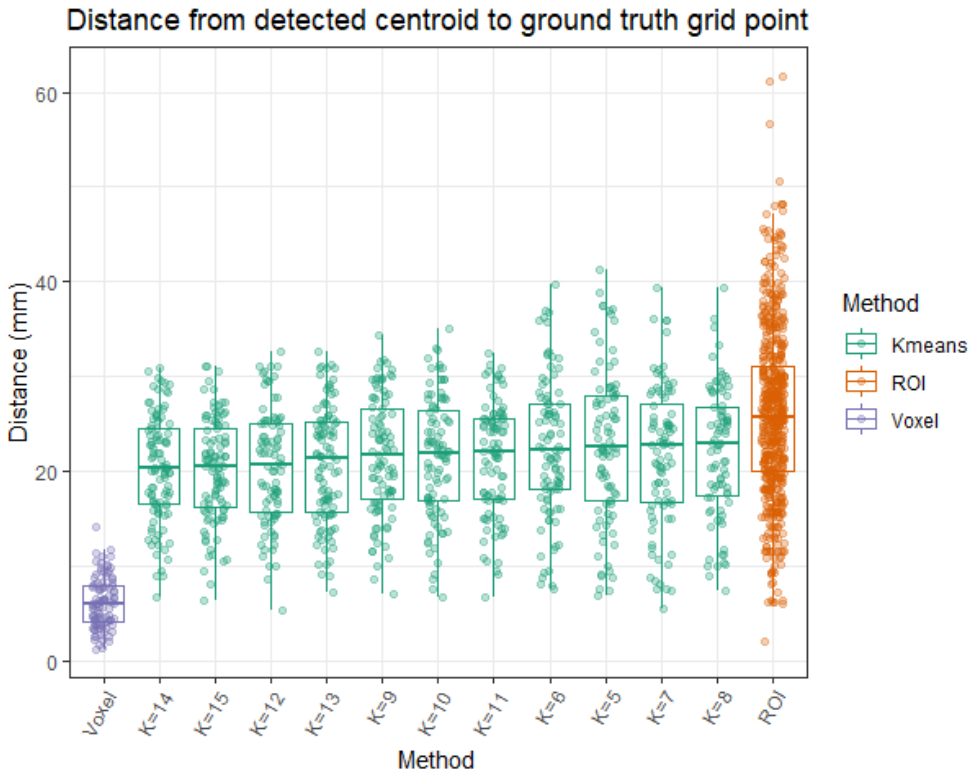

Figure 2-4. Localization error of each analysis method. Error is measured as Euclidean distance between the centroid MNI coordinate of the modified dipoles (ground truth) and the centroids of the activation detected in each of the three analysis methods. K values pertain to k-means clustering solutions for a given value of k.

Next, we assessed whether this decrease in localization error provided more accurate and reliable detection of the primary ROI of the ground truth activation, as interpretations of findings in applied EEG analyses may vary based on which ROI the effect is detected in. Two commonly used approaches were evaluated. The first was a centroid method, whereby the ROI label of the ground truth voxel (i.e., the centroid of modulated activity) was defined as the ground truth ROI. For the voxel approach, the detected ROI was defined by the ROI label of the central voxel of the detected spatial cluster mass. For the k-means approach, the detected ROI was defined by the ROI

label of the voxel nearest to the spatial centroid of a particular cluster. The ROI approach was not included as it included several ROIs detected per simulation, rather than a single ROI like the other two methods. The second was a percentage overlap method, where detected effects are considered a volume and are allowed to overlap multiple ROIs. For the ground truth, ROI labels were obtained for each voxel within the modified sphere, and ROI percentages were defined by the fraction of voxels (out of all voxels in the ground truth cluster mass) contained in a given ROI. For the voxel approach, ROI labels were obtained for each voxel in the detected spatial cluster mass, and overlap percentages were similarly calculated. For the k-means approach, distances between each IC and the centroid of a given cluster were calculated, and a sphere was created with radius equal to the 90% quantile of distances. This quantile percentage was used in order to reduce the impact of near-outlier dipoles on the diameter of the cluster. Overlap percentages were calculated similarly based on ROI labels of voxels in this cluster sphere. The ROI method was not included in this evaluation as there was no similarly unique ROI, nor percent overlap measure, for each iteration due to the approach used.

Match rates between the ROI detected from each method compared to the true ROI of the simulated signal across all 100 simulations are displayed in Figure 2-5. On average, the voxel method showed greater match rates for both the centroid (78%) and overlap (73%) approaches compared to the other two methods. K-means clustering displayed a 14-24% ROI detection rate (increasing as a function of cluster value k) using the centroid approach, and 24-34% ROI detection rate using the overlap approach, both exhibiting a decreasing trend as the k value decreased. Similar to the reasoning of the decreased localization error in the voxel approach, more effective ROI match rates (error) in the voxel and ROI approaches can be attributed to increased spatial resolution. However, while the ROI approach provides high sensitivity towards detection of

effects, it exhibits low specificity in rejection of ROIs where the signal is projected to but does not originate from.

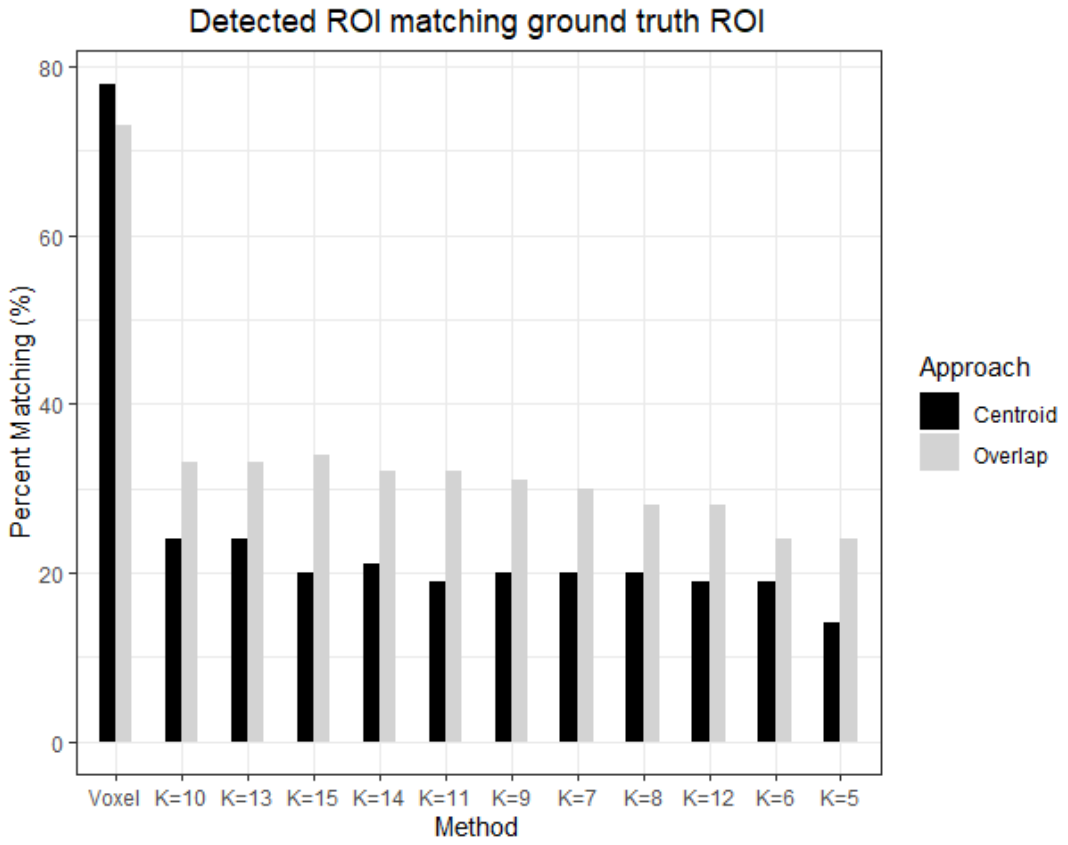

Figure 2-5. Percent of simulations where the primary ROI of the detected results matches the primary ROI of the ground truth. Two methods (centroid and overlap) are displayed. In the centroid approach, the ROI corresponding to the centroid of the ground truth is compared to the centroid of the detected voxels or k-means cluster. In the overlap approach, the ROI which has the greatest overlap with the ground truth sphere is compared to the ROI with the greatest overlap with the set of detected voxels or k-means cluster. Here, findings using the voxel approach show a high

degree of match (>70%) with the actual ground truth ROI. K values pertain to k-means clustering solutions for a given value of k.

We then aimed to evaluate the degree to which power attenuation/loss, that is the difference in masked ground truth activation power (dB) relative to masked detected activation power (dB), occurred in each approach. Since each approach is naïve to which dipoles are associated with the underlying effect, dipoles both associated and unassociated with the effect may be averaged together, attenuating the signal of interest. This power loss between the true signal and detected signal was calculated as the percent difference in averaged dB power (across the significance masked time-frequency indices) between the ground truth sphere and the detected group-level ERSP in each method. An ideal power loss of 0% would occur when the detected sphere and time-frequency cluster mass of activity perfectly matches/overlaps the ground truth.

Power loss between the ground truth and detection methods was evaluated using two possible significance masks: first by using the ground truth ERSP mask and applying it to the ERSP measured in each method, and second by using the detected ERSP mask from each method and applying it back to the ground truth ERSP. When using the ground truth mask, the lowest power attenuations were observed for the voxel and high k value clustering solutions, while the ROI approach showed greater attenuation across significant ROIs (Fig. 2-6A). When using the detected mask, the voxel approach showed lower power attenuation than all k value clustering solutions as well as the ROI method (Fig. 2-6B). The outcome of lower attenuation for the voxel approach using the latter detected mask but not the former ground truth mask is likely due to the unique masks among each spatially distinct voxel. Voxels closer to the edge of the detected spatial cluster mass are more likely to include only the most significant portions of the ground truth,

resulting in smaller time-frequency cluster masses in their ERSP matrices. Furthermore, greater variability was observed in the k-means and ROI approaches with respect to the degree of attenuation which occurred. For the k-means and ROI methods, this large variability is likely due to variations in how well the clustering (or ROI) solutions separated signal-associated and unassociated dipoles. If the modulated activity sphere was situated completely inside a particular cluster/ROI, power loss would be minimized, but if the sphere resided in more than one cluster/ROI, effects become diluted and attenuations in the signal occur.

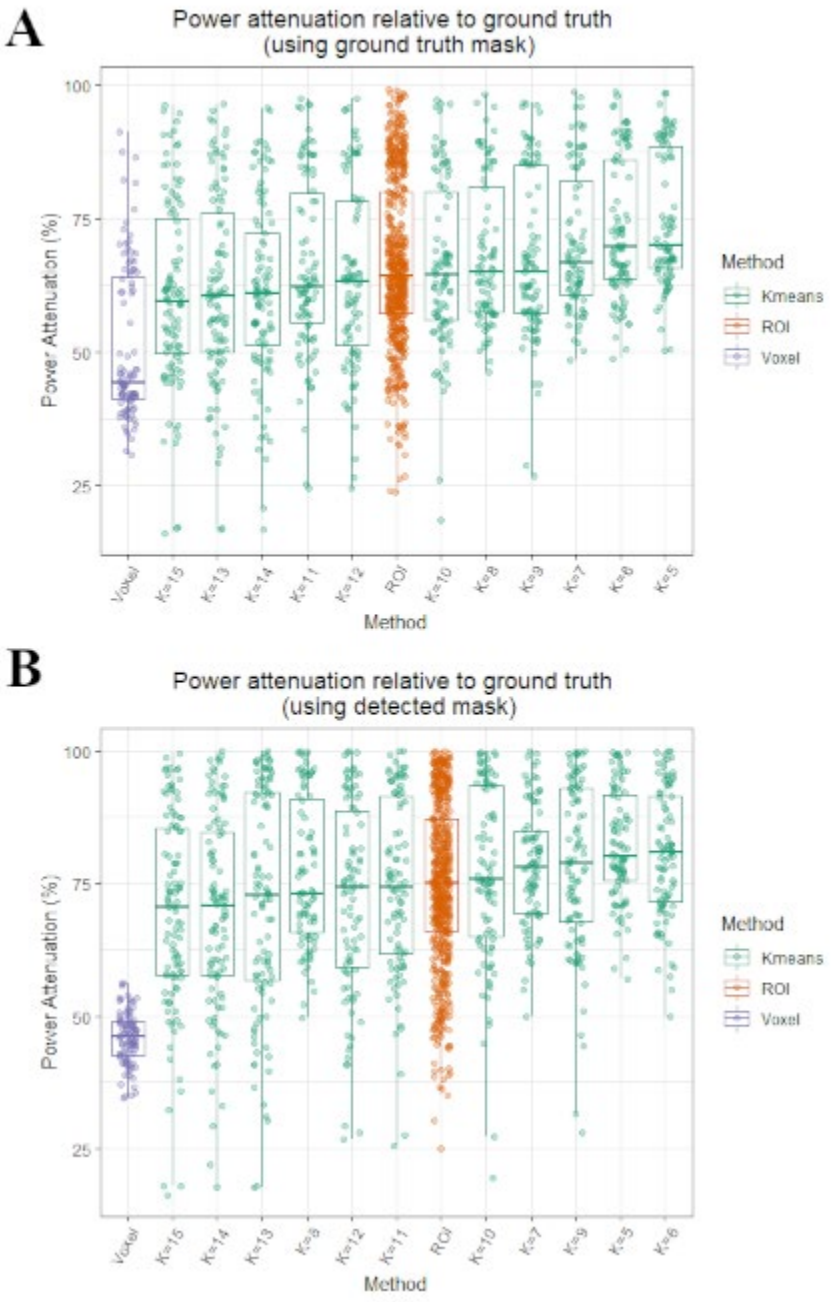

Figure 2-6. Attenuation of detected spectral power results relative to ground truth power. (A) Power attenuation between the ground truth spectral power and that detected in each analysis, using a time-frequency significance mask obtained by comparing the ground truth Signal condition to Control condition. (B) The same power attenuation measure but using a time-frequency

significance mask obtained from the resultant findings. Here, the voxel approach shows the lowest reduction in power, relative to the other two approaches, indicating an ability to better detect the true power of the underlying effect. K values pertain to k-means clustering solutions for a given value of k.

The ability of each approach to capture the true time-frequency ranges of the spectral effect was next evaluated. This effectiveness was measured by calculating the percent of time-frequency pixels in the ground-truth ERSP mask captured by (i.e., overlapping) the detected ERSP mask for each method. While the k-means and ROI methods each contained a single masked ERSP plot for each solution, there was more than one ERSP mask for the voxel approach as each voxel could have a unique mask. Therefore, the ERSP mask best representative of the voxel cluster mass was selected to be the mask contained at the most central voxel of the cluster mass. As displayed in Figure 2-7, the ERSP mask at the center of the voxel cluster mass showed a high degree of overlap (95 ± 4%) with the true time-frequency range of the effect, while the ROI and k-means methods displayed a lower degree of time-frequency overlap, with 65 ± 22% and 60 ± 22% to 66 ± 26% overlap (generally increasing as a function of increasing k value), respectively. This finding suggests a greater effectiveness of the voxel approach to capture the true time-frequency extent of the underlying spectral activity.

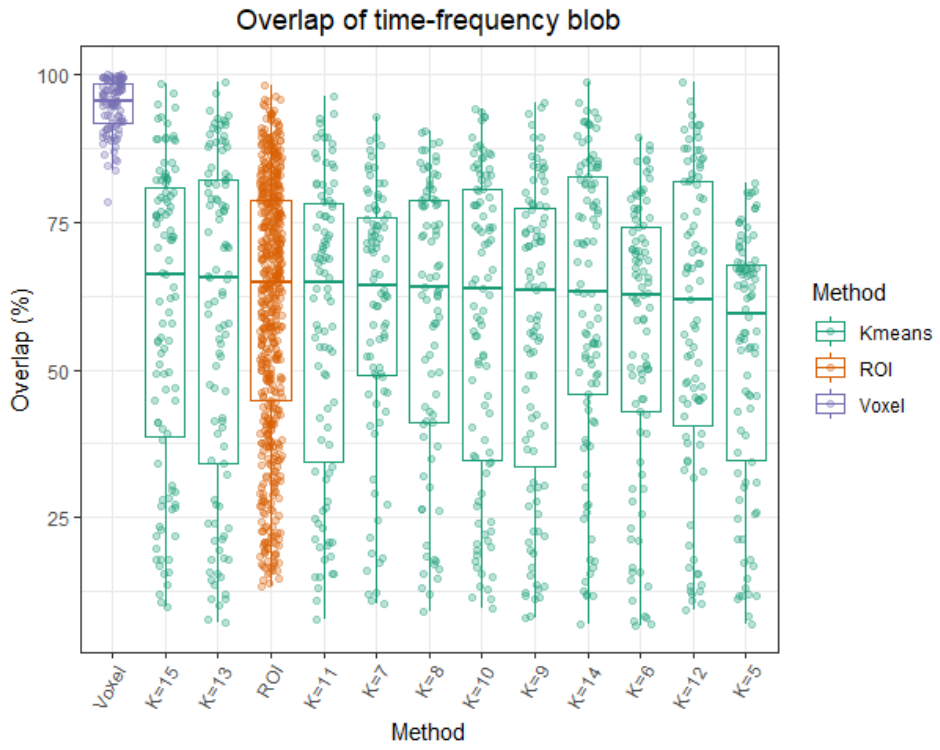

Figure 2-7. Percent overlap of detected time-frequency effects relative to ground truth effect. The time-frequency bins obtained in the significant findings for each method are compared to those which are significant in the ground truth. The greatest time-frequency overlap between the detected and ground truth effect was observed for the voxel approach, suggesting a better ability to accurately estimate both the temporal and frequency extent of the spectral effect. K values represent k-means clustering solutions for a given value of k.

Lastly, hit rates of signal detection were estimated for each method, quantified by the percent of simulations in which a significant difference in ERSP activity (associated with the ground truth activation) was detected in each method. Such detection "misses" could result from nonideal cluster locations relative to activation location, as well as attenuation of activation effects due to averaging with a high number of unrelated ICs. The simulation results indicated a 100% detection rate of the ground truth signal using the voxel approach, and a similar 100% detection

rate using the ROI approach. For the k-means method, however, lower detection rates were observed regardless of the cluster value k used, with a 10-19% false negative rate when using the same statistical threshold as the ground truth (Fig. 2-8). This decreased detection rate in the k-means approach is likely due to the occasional misalignment between the spatial location of the ground truth activity and the locations of the available clusters. Such misalignment may cause splitting of cortical sources associated with the effect of interest into different adjacent clusters, where the effect becomes diluted and unable to survive statistical comparisons and/or corrections.

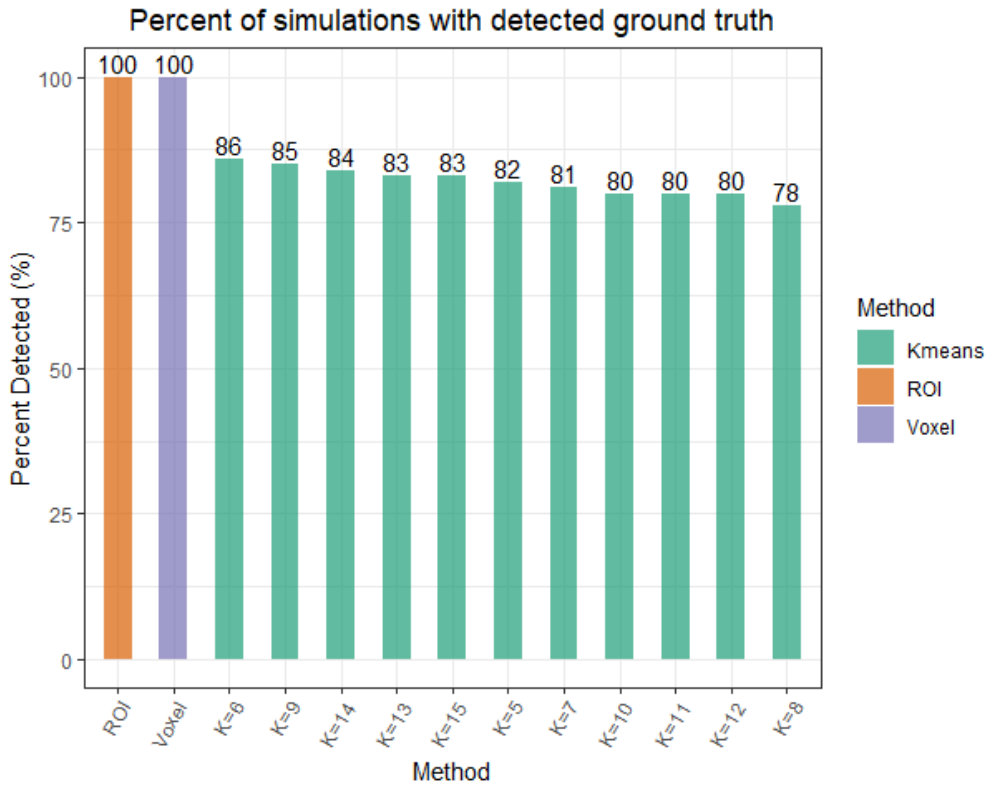

Figure 2-8. Percent of simulations with successful detection of ground truth activation by each method. Both the voxel and ROI approaches successfully detected the ground truth effect in 100% of the simulations, while the k-means approach only detected the effect in 78-86% of the

simulation iterations, dependent on the value of k (where k values represent k-means clustering solutions for a given value of k).

2.4.2 Comparison of Analysis Methods During Visual Attention Task

Given the superior effectiveness of the voxel method to provide more spatially accurate and interpretable detection of spectral activations based on the simulation analysis, we then applied this approach to correct congruent trials of an arrow flanker task for measuring effects of visual attention. The findings from this method were then compared and contrasted to those one would obtain using either a k-means or ROI approach.

The voxel method revealed three main ERSP effects, following pixelwise thresholding at $p < 0.001$ and cluster-level correction at $p < 0.05$ (Fig. 2-9). The first notable effect is an early increase in theta and alpha power, occurring from near stimulus presentation to around 800ms post stimulus. Beginning shortly after, an increase in theta power is observed more anterior and medially in the left supplementary motor and superior frontal cortices, occurring from approximately 250ms to 800ms post-stimulus. A decrease in alpha and beta power during the same time period was observed in a large portion of the posterior cortex, consisting of voxels primarily in the bilateral precuneus and occipital cortices. These findings are in line with prior oscillation-based MEG studies of visual attention, which have reported similar increases in frontal theta power and decreased posterior alpha power during a flanker paradigm (McDermott et al., 2017). Together these activations involve mechanisms associated with visual signaling to motor areas, which plan and execute the movement associated with the arrow stimuli.

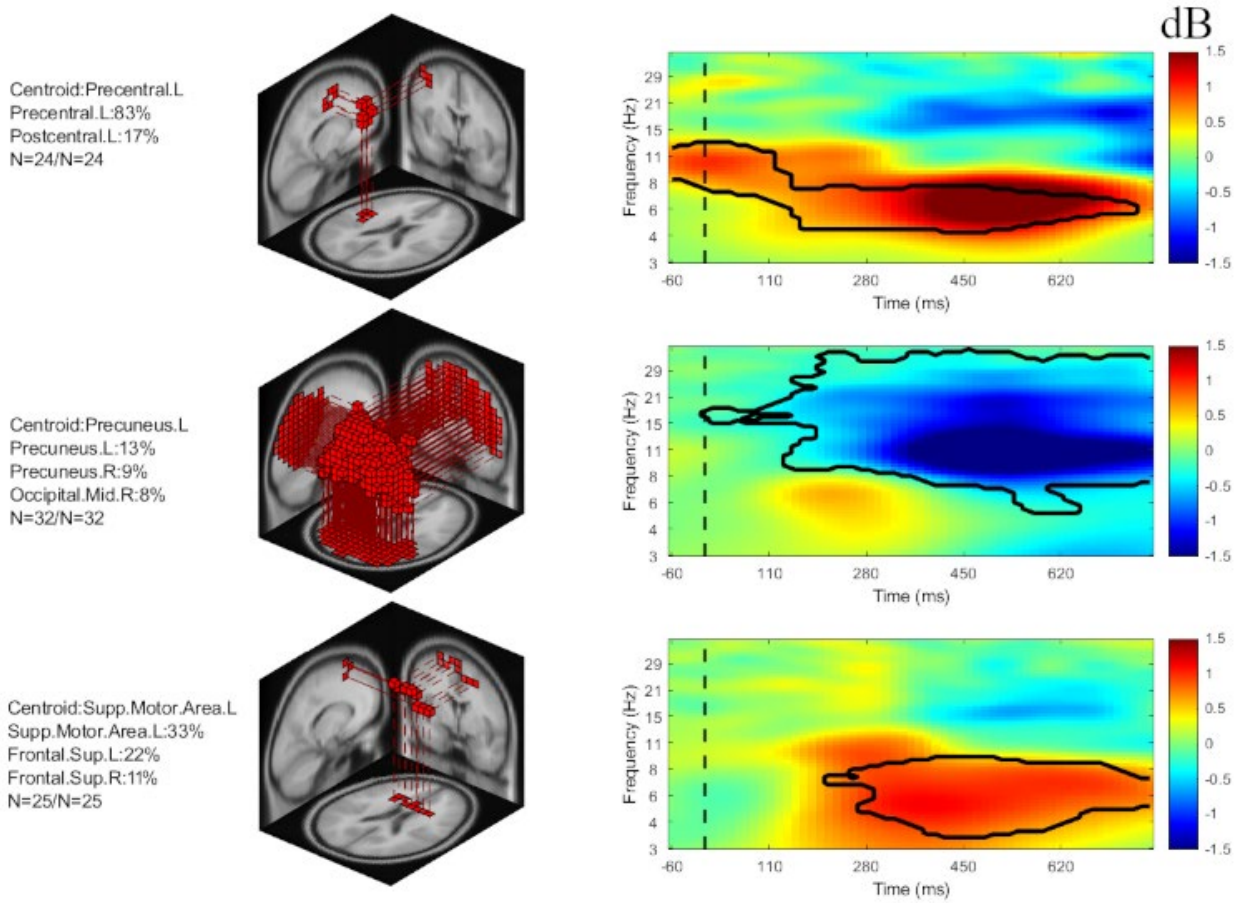

Figure 2-9. Significant spectral effects detected using the voxel approach during an arrow flanker paradigm.

Using a similar statistical thresholding and correction, the k-means and ROI approaches detected time-frequency activations comparable to the voxel approach (i.e., posterior alpha desynchronization and frontal theta synchronization). However, the regions of involvement and unique underlying effects were more vague (Fig. 2-10). For example, while a decrease in posterior alpha and beta power was clear in clusters of occipital and parietal regions, this decrease was also observed more anteriorly in the midcingulate and postcentral gyri, likely due to more posterior dipoles being included in the clusters. Using a clustering approach, it is more difficult to infer

where these activations are originating from in the cortex. Additionally, while the voxel approach detected a robust early alpha activation localized primarily to the left precentral cortex, this finding was not as pronounced in the clustering analysis as there was no precentral cortex cluster centroid. Instead, a smaller effect was obtained in a cluster with the postcentral cortex as the centroid, which only made up 17% of the detected voxel mass (the other 83% being the precentral cortex) in the voxel analysis. The activity detected in this cluster was likely attenuated due to a nonideal mapping of the cluster onto the location of the spectral effect.

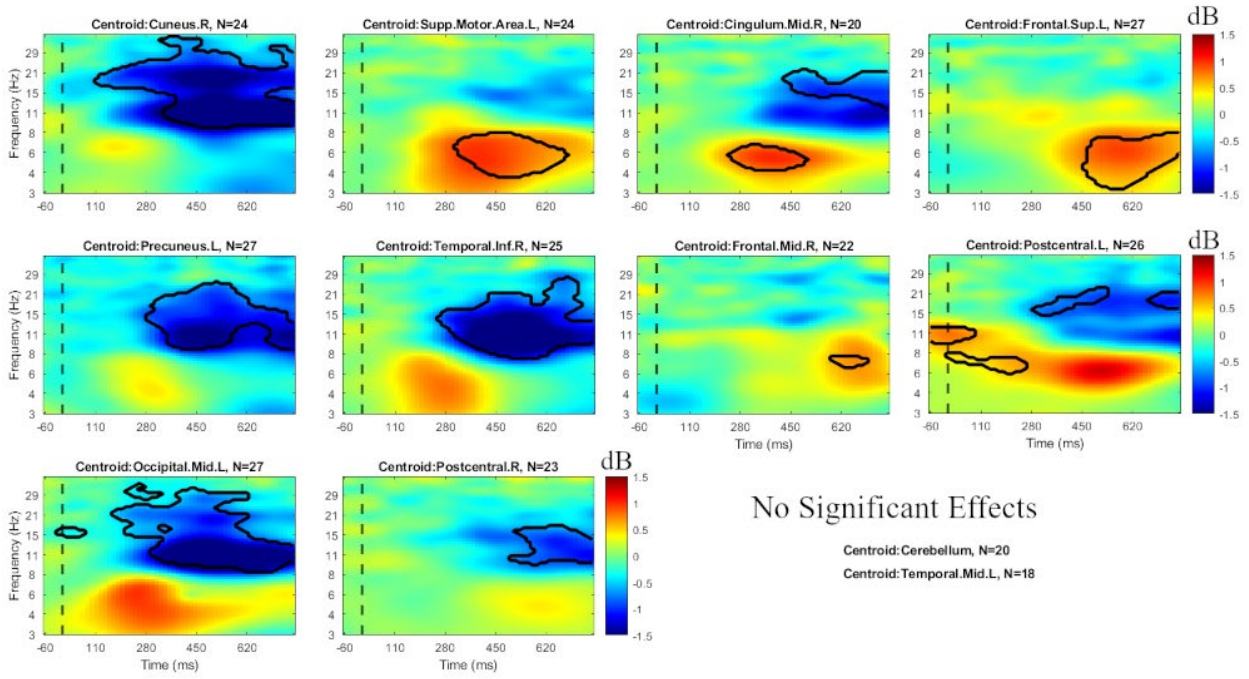

Figure 2-10. Surviving spectral effects from k-means clustering analysis. Spectral analysis using the classical k-means clustering approach (with a typical value of k = 12) indicated ten clusters with significantly increased or decreased spectral power. Two clusters (cerebellum, left midtemporal cortex) displayed no significant results. Two broad effects are observed: a significant increase in late theta power in three frontal clusters (left supplementary motor area, right midcingulate, and left superior frontal cortex). Several clusters in central and posterior regions

show a decrease in spectral power in the alpha and theta band. Inf = inferior, L = left, N = number of subjects in cluster, R = right, Sup = superior, Supp = supplementary.

While the ROI approach allowed for more effective mapping of analysis regions onto potential areas where spectral effects may exist, there was a reduction in the ability to localize effects to the principal ROIs due to the nature of the dipole smoothing onto nearby ROIs. As shown in Figure 2-11, a number of ROIs contained the effects observed in the voxel and k-means approaches. A first observation was that the increased alpha power observed directly after stimulus presentation in the left precentral cortex, which was also partially observed in the left postcentral cortex k-means cluster, was not observed in any of the left lateralized ROIs. The reasoning for this is likely due to the fact that the voxel approach was able to resolve this early alpha activity to the central portion of the precentral cortex ROI. These voxels made up a subset of those contained in the ROI and contained activity from a particular set of nearby dipoles, while the ROI approach was required to take additional dipoles (i.e., those contributing to other voxels of the ROI) contributing to the entire ROI into account for statistical comparisons. Thus, different dipoles containing different spectral activity may have attenuated this early effect, leading to it not surviving statistical correction.

A second observation regarding the ROI findings is the broader spatial volume detected to be associated with the increased frontal theta activity and decreased posterior alpha and beta activity. While increased frontal theta was localized primarily to the left precentral and left supplementary motor areas in the voxel approach, this effect was extended more medially towards the anterior cingulate as well as towards the right superior frontal and inferior frontal cortices. The decrease in posterior alpha and beta activity localized to the precuneus and occipital cortex in the

voxel approach additionally extended beyond these regions, with surviving findings obtained more anteriorly in the bilateral postcentral and midcingulate cortices. It can be seen that while the ROI approach provides similar detection of these broader effects, it loses both spatial accuracy with respect to the true cortical area of the effect, as well as sensitivity towards smaller effects which may be more localized in both the space and time-frequency domains (e.g., the early precentral alpha synchronization).

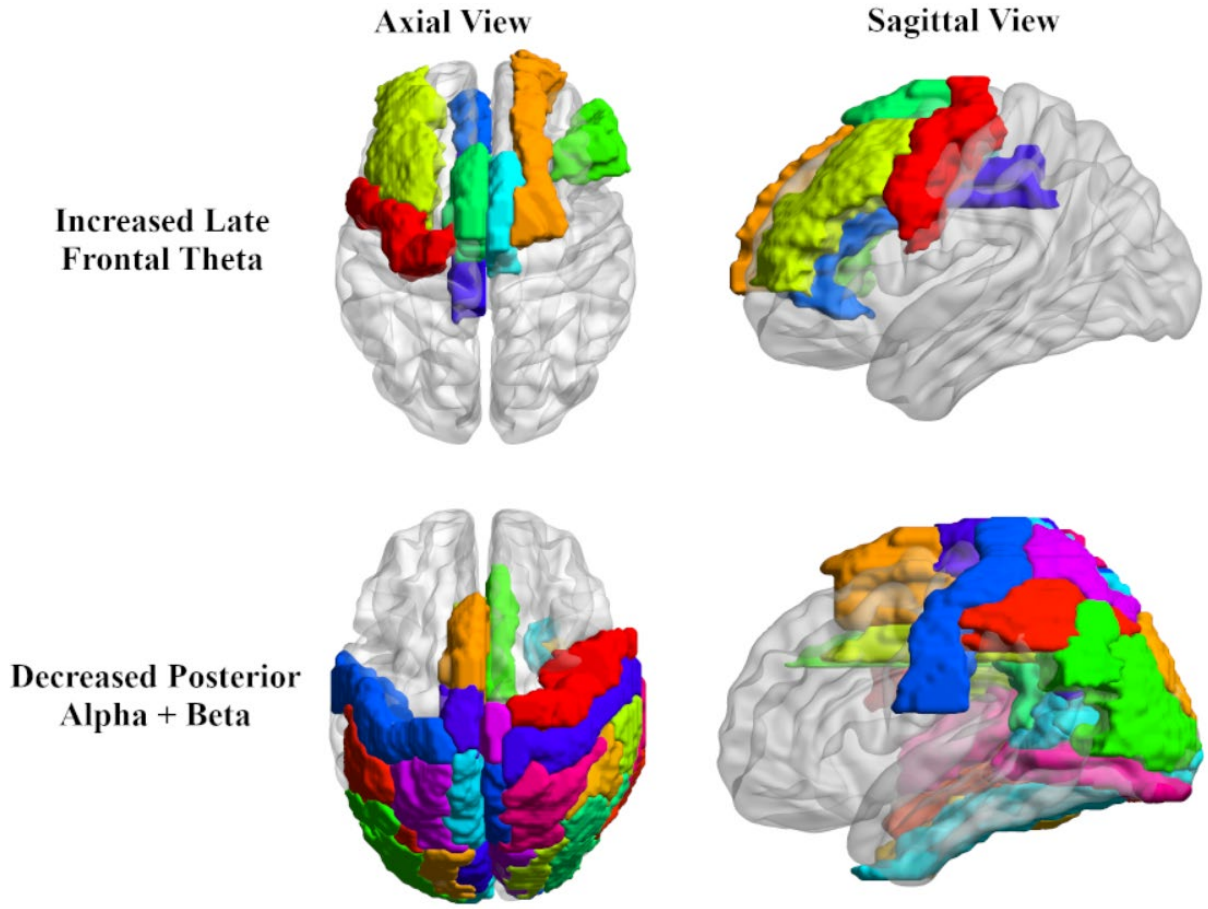

Figure 2-11. ROIs with significant time-frequency effects as obtained during the ROI analysis. Regions are marked as increased late frontal theta or decrease posterior alpha + beta, where these effects are comparable to those noted in the k-means clustering analysis.

2.5 Discussion

The present study evaluated two alternative approaches for group-level analysis of localized spectral activity (a voxel approach and a ROI approach), in comparison to the commonly used k-means clustering method. While k-means clustering is a straightforward approach to address the issues of dipole sparsity in source-level analyses, there are several downsides of the approach, including a priori parameter selection, lack of spatial resolution in effect detection due to the brain partitions (i.e., k clusters) created, and lack of control over where the clusters are located. We showed through a simulation analysis that a contiguous 3-D voxel approach is more effective at providing spatial localization and ROI estimation, minimizing power loss due to contributions from unrelated signals, detecting the true time-frequency range of a spectral effect of interest, as well as detecting the spectral effect itself. Applying these three methods to a study analyzing a visual attention task provided support for the voxel approach, which resulted in more effective spatial localization and ROI estimation of spectral effects of interest, as well as facilitating more accurate and compact anatomical interpretations of findings.

Spatial localization of the simulated effects in the voxel method showed a greater than 50% reduction in localization error relative to the k-means clustering and ROI methods. This can be attributed to multiple factors. The first is that spectral effects can be detected with higher (8mm) spatial resolution, rather than limited to the areas dictated by the k-means or ROI methods. Voxel-based cluster masses can be formed to the unique spatial volume of the effect of interest. In contrast, k-means clustering produces generally spherical clusters due to the minimization of squared error of Euclidean distances which occurs when forming the clusters. Interestingly, even while using a spherical ground truth activation, k-means clusters were still not as effective at

localizing the effects in this ideal scenario. In real datasets and analyses, activation effects are likely to be more spatially amorphous in both shape and size, which do not fit well with spherical clusters. Another factor may be that, for this and most other EEG studies performed, unique physiological parameters of subjects are not considered, including skull thickness, tissue conductivity, or variability in functionally equivalent cortical locations. It is plausible that the ROI method may show more effective localization if individual participant head model scans are available and utilized, such that ROIs may be more accurately created on a subject-by-subject basis.

Two other primary findings, which are both intertwined, are the reduced power loss and greater overall signal detection rate provided by the voxel approach compared to the k-means clustering approach in particular. Greater power loss occurs during clustering likely due to a misalignment between the location of the spectral effect and that of the cluster. For example, the present analysis simulated a spatially varying activation across iterations while the dipole locations of the dataset remained constant. Since repeated k-means clustering on this set of dipoles resulted in generally consistent clustering solutions across iterations, it is implausible that clustering solutions based solely on dipole locations will accurately localize the ground truth effect during each iteration. In real EEG analyses, a somewhat similar situation can occur when multiple cognitive tasks are concatenated and included in the ICA decomposition and dipole localization stages. While each task may have a cognitive effect which is of interest to the investigator (which exists in a particular area of the cortex), the clustering solution across the same set of dipoles will, for the most part, be similar regardless of task due to consistent dipole locations across tasks. It can be inferred that across all the tasks, cognitive effects which are not well-aligned with the clusters will not be picked up as easily (or at all) as those which are well-aligned. As discussed

prior, it is possible to include activity associated with the effect of interest in the clustering algorithm criteria to better cluster dipoles, but this may introduce increased type 1 error due to the variance minimization that occurs (Kriegeskorte et al., 2009).

The effectiveness of the voxel approach to measure and locate effects associated with visual attention during an arrow flanker paradigm was demonstrated, localizing increased theta activity to voxels of the left frontal cortex and decreases in posterior alpha activity to voxels of the precuneus and occipital cortex. With respect to the classical k-means method, in a similar fashion to the simulation analysis, comparable time-frequency activity was detected across a variety of clusters and clustering solutions. However, a mismatch between the clusters and the location of the effect based on the voxel approach was observed, where the voxel approach detected an early alpha increase primarily in the left precentral cortex, but the nearest k-means cluster centroid was in the left postcentral cluster. Based on the surviving time-frequency results, a less robust early alpha increase was detected as well as mislocalized. The ROI approach displayed a separate issue of decreased spatial resolution, and overestimation of where the effects were present due to the dipole smoothing performed. Early left precentral alpha activity was also not detected using this approach, possibly due to this activity only being present in a subset of voxels contained in the ROI as found in the voxel approach analysis. Detection capabilities of the ROI approach may therefore be related to the spatial size of the effect relative to the spatial size of the ROI.

While we have indicated that the voxel approach provides more effective and accurate localization of ERSP effects, there are some important considerations and caveats with this approach. Firstly, the true magnitude of the effect of interest, as well as subject sample size, may affect the ability of the effect to survive the multiple comparisons correction described in these

approaches. The effects analyzed in the simulation and visual attention task are fairly robust, and smaller effects (e.g., between two somewhat similar cognitive tasks) may be difficult to detect with the large number of voxels corrected over in the voxel approach. In these cases, a sacrifice between localization and detectability may need to be made, and the k-means or ROI approaches may be more useful for exploratory analyses. Secondly, if there are hypotheses regarding the specific ROIs in which the effects of interest are expected, the ROI approach may be particularly beneficial to use, where these regions are solely included in the analysis. This method is advantageous over the k-means approach, which has a potential risk of the clustering solution not being well aligned with the area of interest.

In conclusion, the present study examined the effectiveness of these methods through an ERSP-based view. However, the same conceptual pipeline and statistical procedures can be straightforwardly applied to other commonly used localized measures (event-related potentials, cross-frequency coupling, etc.). Together, such approaches can aim to further advance the interpretability and replicability of cortical source-level analyses.

Chapter 3: Neural Mechanisms of Inhibitory Control in Persistent Tic Disorder

3.1 Abstract

Persistent tic disorders, including Tourette Syndrome, are typically thought to have deficits in cognitive inhibition and top-down cognitive control due to the frequent and repetitive occurrence of tics, yet studies reporting task performance results have been equivocal. Despite similar behavioral performance, individuals with persistent tic disorders have exhibited aberrant patterns of neural activation in multiple frontal and parietal regions relative to healthy controls during inhibitory control paradigms. In addition to these top-down attentional control regions, widespread alterations in brain activity across multiple neural networks have been reported. There is a dearth, however, of studies examining event-related connectivity during cognitive inhibitory paradigms among affected individuals. The goal of this study was to characterize neural oscillatory activity and effective connectivity, using a case-control design, among children with and without persistent tic disorder during performance of a cognitive inhibition task. Electroencephalogram data was recorded in a cohort of children aged 8-12 years old (60 with persistent tic disorder, 35 typically developing controls) while they performed a flanker task. While task accuracy did not differ by diagnosis, children with persistent tic disorder displayed significant cortical source-level, event-related spectral power differences during incongruent flanker trials, which required inhibitory control. Specifically, attenuated broad band oscillatory power modulation within the anterior cingulate cortex was observed relative to controls. Whole brain effective connectivity analyses indicated that children with persistent tic disorder exhibit greater information flow between the anterior cingulate and other fronto-parietal network hubs (midcingulate cortex and

precuneus) relative to controls, who instead showed stronger connectivity between central and posterior nodes. Spectral power within the anterior cingulate was not significantly correlated with any connectivity edges, suggesting lower power and higher connectivity are independent (versus resultant) neural mechanisms. Significant correlations between clinical features, task performance and anterior cingulate spectral power and connectivity suggest this region is associated with tic impairment ($r = -0.31$, $p = 0.03$) and flanker task incongruent trial accuracy (r's = -0.27 to -0.42, p's = 0.0008 to 0.04). Attenuated activation of the anterior cingulate along with dysregulated information flow between and among nodes within the fronto-parietal attention network may be neural adaptations that result from frequent engagement of neural pathways needed for inhibitory control in persistent tic disorder.

3.2 Introduction

Persistent tic disorders (PTDs), including Tourette Syndrome (TS), are characterized by sudden, involuntary, and recurrent movements or vocalizations, referred to as tics. Given the frequent and repetitive occurrence of tics, it has been hypothesized that this atypical behavior is due, at least in large part, to deficits in motor inhibition and top-down cognitive control, as these processes are thought to mediate the selection of appropriate actions and behaviors. Numerous tasks have been used to evaluate the presence of inhibitory control deficits in PTD, however, results have been equivocal. For example, previous studies using different cognitive control paradigms have reported no differences in task performance between individuals with PTD and healthy controls (Ozonoff et al., 1998; Roessner et al., 2008). In contrast, others have observed worse performance (Crawford et al., 2005; Wylie et al., 2013) as well as better performance in PTD when compared to controls (Jackson, Parkinson, Jung, et al., 2011; Mueller et al., 2006),

leading to uncertainty as to the scope of potential deficits in cognitive control. A recent meta-analysis found a moderate effect (Cohen's d = 0.33) of general inhibitory deficits in PTD relative to typically developing controls, however, the effect size varied by task with commonly used inhibitory paradigms (Stop Signal, Flanker, and Go/No-go tasks) being not significantly different between diagnostic groups (Morand-Beaulieu et al., 2017). Findings of similar or better performance in individuals with PTD have been attributed to compensatory mechanisms developed from repeated voluntary tic suppression (Jackson, Parkinson, Jung, et al., 2011; Mueller et al., 2006).

The Eriksen flanker task is a common cognitive paradigm for measuring inhibitory control where the subject must quickly indicate the direction of a central arrow flanked by arrows pointing in a congruent or conflicting direction (Eriksen & Eriksen, 1974). Among healthy adults, activation of the anterior cingulate cortex (ACC) occurs during incongruent flanker trials (Fan et al., 2005), which is thought to play an important role in monitoring and/or resolving such conflict. The anterior insular cortex, precentral gyrus, intraparietal sulcus, and bilateral occipital cortices have also been reported to be involved in inhibitory control (Fan et al., 2007; Xuan et al., 2016). In contrast, typically developing children demonstrate developmental differences during inhibitory processing with activation of more central and posterior regions (premotor cortex, superior temporal gyrus, bilateral parietal and occipital cortices) relative to inferior and medial frontal gyri and ACC, potentially suggesting the inhibitory network is slower to develop in frontal areas (Bunge et al., 2002; Santhana Gopalan et al., 2019).

Despite similar inhibitory control task performance, individuals with PTD have exhibited aberrant patterns of neural activation in the supplemental motor area, anterior cingulate,

sensorimotor, inferior frontal and inferior parietal cortices relative to healthy controls (Baym et al., 2008; Ganos, Kahl, et al., 2014; Jung et al., 2013). Several of these same brain areas have been implicated in other experimental conditions such as resting state, voluntary movement, and voluntary tic suppression (Cui et al., 2014; Ganos et al., 2018; Loo et al., 2019; Tinaz et al., 2014; Zapparoli et al., 2019). While regional activation analyses are valuable for pathophysiological hypothesis testing, whole brain analysis using effective connectivity may be particularly useful yet underexplored in PTD. Prior studies and meta-analyses have suggested that alterations in brain activity are present across multiple neural systems (Hashemiyoon et al., 2017; Polyanska et al., 2017; Wen et al., 2016), and thus identification of mechanistic pathways of dysfunction may reveal greater insights than higher or lower neural activation.

Several studies examining resting state connectivity within PTDs have reported widespread atypical network connectivity that vary according to development. For example, pediatric studies have reported a trend of hypo- and immature connectivity among circuitry including fronto-parietal, posterior, and default-mode networks (Church, Fair, et al., 2009; Openneer et al., 2020; Wen et al., 2017). In contrast, adult studies suggest increased structural (Ramkiran et al., 2019; Worbe et al., 2015) and functional connectivity with decreased functional hub count (Worbe et al., 2012) within cortico-basal ganglia circuitry and urge-tic networks, with are positive correlated with tic severity (Tinaz et al., 2015; Worbe et al., 2012, 2015). Such differences may be due to the heterogenous and developmental nature of childhood PTD compared to the more stable state of adult PTD, as well as compensatory mechanisms that develop over time through learned self-regulation (Jackson, Parkinson, Jung, et al., 2011). Consistent with this are recent findings that functional connections that best discriminate individuals with PTD from controls are age-specific, with default mode and fronto-parietal connections providing the best discrimination among

children and salience, somatomotor, and default mode features best discriminating adults with PTD (Nielsen et al., 2020). Collectively, both biregional and whole-brain connectivity patterns among individuals with PTD are aberrant with the nature of deficit being across development.

Resting state paradigms, however, do not clarify the effect of differential neural connectivity on cognitive processes, nor whether particular connectivity patterns are adaptive or disruptive features of the disorder, an important factor for evaluating developmental trajectories. Across brain imaging modalities, aberrant connectivity during self-paced finger movements (Franzkowiak et al., 2012), waiting motor impulsivity (Atkinson-Clement et al., 2020), and face perception paradigms (Rae et al., 2018) have been noted among individuals with PTD. There is a notable dearth, however, of studies examining event-related connectivity during inhibitory control paradigms among individuals with PTD, particularly those using electroencephalography (EEG), which can reveal network activities with millisecond time resolution. There are two EEG-based studies that reported higher frontomesial and fronto-motor functional connectivity during voluntary tic suppression (Hong et al., 2013; Serrien et al., 2005) as well as during a Go/No-Go task (compared to controls) (Serrien et al., 2005). However, both studies were small (N = 9-10 children with PTD, 10 controls) and utilized a low number (10-19) of EEG channels. In addition, the studies examined scalp-level connectivity, where there is often concern of spurious connectivity measurements due to volume conduction between nearby scalp electrodes (Nunez et al., 1997). We have recently developed an algorithm for estimating cortical-source level, effective connectivity based on high density EEG (Koshiyama et al., 2020; Loo et al., 2019) and will apply that approach here to gain insight into putative atypical connectivity patterns within a sample of children with PTD while performing an inhibitory task. We hypothesized that children with PTD would not differ from typically developing controls in flanker task accuracy based on prior meta-

analytic findings (Morand-Beaulieu et al., 2017). We did, however, hypothesize that the diagnostic groups would diverge in terms of activation and connectivity patterns of top-down attentional control and inhibitory networks within frontal and parietal cortices.

3.3 Materials and Methods

3.3.1 Sample

The case-control study sample consisted of 95 children (60 with persistent tic disorder (PTD), 35 healthy controls (HC)), ages 8-12 years old. Participants were recruited through community advertisements, internet postings, and from an academic medical center anxiety and tic disorder clinic between 2013 and 2019. Verbal and written explanations of study criteria were provided to participants and their parents, and written parent permission/assent were obtained prior to study participation. All study procedures and consents were approved by the local Institutional Review Board.

3.3.2 Procedure

All participants participated in a single experimental session that lasted approximately 2-3 hours, during which time diagnostic interviews, cognitive testing, and EEG recording were administered. Psychiatric diagnoses were determined using a semi-structured diagnostic interview, the Anxiety Disorder Interview Schedule, Child Version (ADIS) (Silverman, 1996) modified to assess persistent tic disorders. Diagnostic interviews were administered either by supervised graduate level psychologists or directly administered by a licensed psychologist, who confirmed the presence of DSM-5 psychiatric diagnoses. The ADIS was supplemented by the clinician-administered Yale Global Tic Severity Scale (YGTSS) (Leckman et al., 1989), Child Yale-Brown

Obsessive-Compulsive Scale (CYBOCS) (Scahill et al., 1997), and Strengths and Weaknesses of ADHD symptoms and Normal behavior (SWAN) scale (Swanson et al., 2012). Estimated intelligence (IQ) was assessed using the Wechsler Abbreviated Scale of Intelligence (WASI) (Wechsler, 1999).

Participants were included in the study if they met the following criteria: 1) male or female aged 8-12 years; 2) resided with their primary caretaker for at least 6 months prior to consent; 3) both participant and guardian(s) were able to complete all study measures in English; and 4) capable of completing all required study procedures (as determined by psychologist). Individuals with PTD were required to have a primary DSM-5 diagnosis of Persistent Motor Tic Disorder, Persistent Vocal Tic Disorder, or Tourette Disorder as diagnosed by ADIS and confirmed by diagnostic interview, as well as YGTSS ≥ 15 at baseline. Individuals with PTD were excluded from participation if they had a history of any of the following: 1) head injury resulting in concussion; 2) diagnoses of autism, major depression, bipolar disorder, panic disorder, or psychosis; 3) estimated Full Scale IQ < 80; or 4) YGTSS < 15 (PTD only). Individuals taking stimulant medication for comorbid ADHD discontinued use for 24 hours prior to their visit. Other psychotropic medications were included as covariates of no interest in analyses. Healthy controls were excluded if they had any major Axis I diagnosis or were on a psychoactive medication.

3.3.3 Experimental Task

Participants performed a modified Eriksen flanker task (Eriksen & Eriksen, 1974) while EEG was recorded (Fig. 3-1). Each trial consisted of five white arrows appearing horizontally across a black screen either above or below a centralized, static white fixation cross. Each arrow spanned 1.2° x 1.2° visual angle with 0.6° spacing between arrows. The arrows remained on the

screen for 250ms before disappearing. Following subject response or trial expiration due to lack of response after 1300ms from stimulus onset, a jittered 700-1200ms intertrial interval succeeded the trial until the next set of arrows appeared. The arrows could appear in congruent orientation, where all arrows pointed in the same direction, or incongruent orientation, where the central arrow pointed in the opposite direction of the side flanking arrows. The subject used a computer mouse with their right hand to press the left or right mouse button to select the respective direction of the central arrow. The task consisted of a high number of incongruent trials (n = 144) versus congruent trials (n = 72) to increase the inhibitory control required, which was a primary focus of the study. Trials were presented in random order and the task lasted approximately 7 minutes; dependent variables were percent accuracy, reaction time (on correct trials only), and reaction time variability.

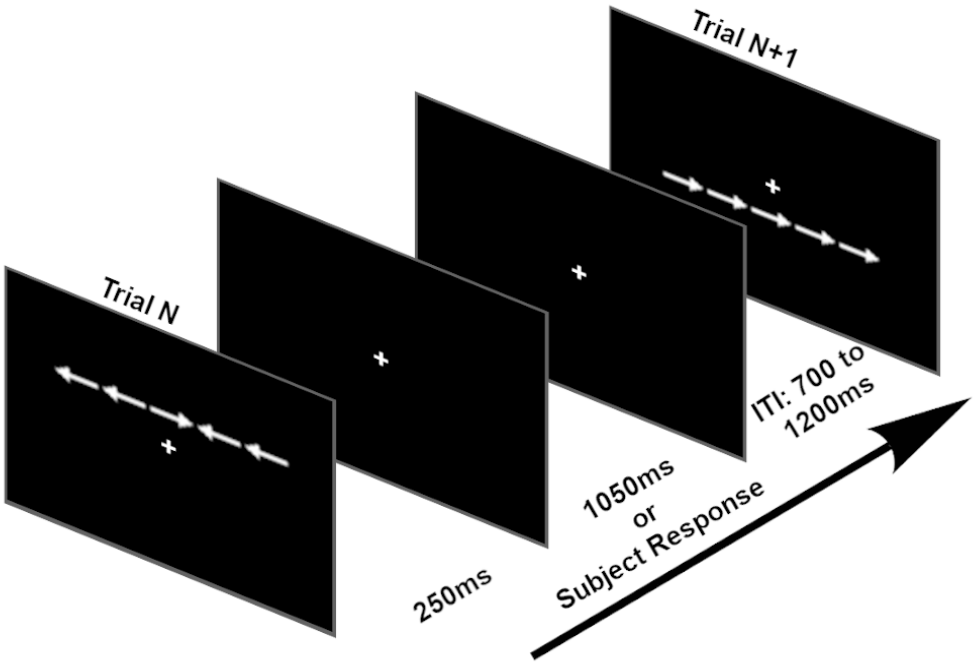

Figure 3-1. Modified Eriksen flanker task. The figure illustrates an incongruent flanker trial (in which the middle arrow points in a different direction than the flanking arrows) followed by a congruent flanker trial (in which all arrows point in the same direction).

3.3.4 EEG Recording and Processing

EEG was recorded using a 128 Hydrocel electrode net in an extended international 10-10 configuration (Electrical Geodesics Incorporated). Electrode scalp coordinates were transcribed through Polhemus, Inc. digitizer software, using the nasion and preauricular notches as anatomical reference points. Data were sampled at 1000Hz, referenced to Cz, and electrode impedances were lower than 50kΩ (per manufacturer recommendation). Task event markers from E-Prime software were merged with raw EEG signals using Lab Streaming Layer (LSL, https://github.com/sccn/labstreaminglayer).

Data cleaning and processing was performed using EEGLAB (Delorme & Makeig, 2004). Spectral power analyses utilized data that were down sampled to 250Hz and filtered using a 0.5-55Hz bandpass filter. To remove channel artifacts, Artifact Subspace Reconstruction (ASR) (Blum et al., 2019; Chang et al., 2018; Kothe & Makeig, 2013; Mullen et al., 2015) was employed via EEGLAB plug-in *clean_rawdata()*, which removed channels with over 5 seconds of flat signal as well as those poorly correlated ($r < 0.85$) with adjacent channels. ASR additionally helped to remove and interpolate non-stationary high amplitude bursts. Scalp signals were then decomposed into independent source level activations, also known as independent components (ICs), using adaptive mixture independent component analysis (AMICA) (Delorme et al., 2012b; Hsu et al., 2018; Palmer et al., 2011). This was performed within EEGLAB on the full EEG dataset, using approximately 525,000 data points (35 minutes of data sampled at 250Hz) for 128-channel decomposition. IC rejection was performed using the EEGLAB plug-in ICLabel (Pion-Tonachini et al., 2017), an algorithm trained to detect neural vs non-neural IC activations. ICs were rejected if the brain was not the highest probability source. Dipole locations of source activations were subsequently estimated using Fieldtrip (Oostenveld et al., 2010b). For the effective connectivity analysis, EEG data was down sampled to 100Hz to reduce model complexity and the potential influence of line noise. Each subject was also restricted to their top 10 ICs based on variance accounted for. This facilitated proper fitting of a multivariate autoregressive (MVAR) model using a sufficient data point ratio as proposed in Korzeniewska *et al.* (2008) based on the equality:

$$\frac{K^2(p+1)}{NsNt} \leq 0.1$$

where K denotes the number of ICs, p is the model order, N_s is the number of samples in the sliding window, and N_t is the number of trials. This equation was modified slightly (using K^2 instead of

K) based on recommendations from the Source Information Flow Toolbox (SIFT) (Delorme et al., 2011).

To perform event-related analyses, the preprocessed source-level data was epoched (from -2000ms to 2000ms around stimulus) into three trial types: congruent trials with correct responses, incongruent trials with correct responses, and incongruent trials with incorrect responses. Congruent trials with incorrect responses were excluded due to sparsity.

3.3.5 Event-Related Spectral Power

Event-related spectral perturbation (ERSP) is a time-frequency analysis method that measures event-related changes, relative to baseline, in spectral power evoked by a stimulus (see Fig. 3-2). To calculate ERSP, a sliding window of 1-second in length was applied across each epoch in 25ms steps from which the average amplitude spectra of each frequency interval was calculated for each window using a Morlet kernel and the EEGLAB function *newtimef()*. These values were first averaged across trials, baseline normalized using average power between -550 to -50ms prior to stimulus, and then converted into decibel (dB) values using $10*log_{10}(X)$, producing time-frequency plots of log-scale spectral power. This time selection for baseline ensured that prior trial response phenomena were not included. Average ERSP values in frequency bands (Theta [4-7Hz], Alpha [8-12Hz], Low Beta [13-20Hz], High Beta [20-30Hz]) and time ranges related to stimulus presentation (0-200ms) and conflict resolution/response preparation (250-600ms) were extracted.

Dipoles were spatially grouped at the study level using k-means clustering weighted by dipole location (dimension, 3; weight, 10), event-related potential (dimension, 4; weight, 1), ERSP (dimension, 4; weight, 1), and scalp map (dimension, 6; weight, 1) to create a 12-cluster solution.

Clusters that contained at least 70% of unique subjects were included in the spectral power analysis.

3.3.6 Connectivity Analysis

To examine network information flow, source-level effective connectivity was measured in the form of renormalized partial directed coherence (rPDC), a frequency-domain measurement of causal (directed) information flow between multivariate time series (see Fig. 3-2) (Schelter et al., 2009). This was done using the EEGLAB plugin *groupSIFT* (Loo et al., 2019), which utilizes the EEGLAB-compatible SIFT plug-in to calculate subject-level multivariate effective connectivity and perform group-level analyses. For each subject, rPDC was calculated between ICs using a MVAR model fitted from the Vieira-Morf algorithm. A 1-second sliding window was applied to the epoched data in 20ms steps, along with 30 log-scaled frequencies from 2 to 49 Hz. This resulted in a 150 timepoint x 30 frequency matrix of rPDC values for each connection.

A challenge of source-space analyses is the variability in the locations of estimated dipole locations for each subject, which makes group-level comparisons of connectivity between regions difficult. To resolve this issue, *groupSIFT* utilizes a 3-D gaussian kernel to "smooth" dipoles from single points into probabilistic dipole densities. The full width at half maximum was set to 20mm and the gaussian was truncated to 3σ, resulting in a density radius of 25.5mm. The automated anatomical labeling (AAL) atlas (Tzourio-Mazoyer et al., 2002), customized to integrate non-cortical regions into upper and lower basal regions to avoid misleading use of subcortical regions as EEG sources, was then referenced to segment a brain model into 76 regions of interest (ROI). From this, each subject maintained a four-dimensional matrix of size 76 (region, leaders) x 76 (region, followers) x 30 (frequency) x 150 (time). Distributed dipole density for all subjects were

placed in this voxelized brain model, and ROIs which contained overlapping smoothed dipoles for at least 70% of unique subjects were included in the analysis.

3.3.7 Correction for Multiple Comparisons

For each connection in the whole-brain connectivity analysis, pairwise t-tests between diagnostic groups were performed on each rPDC time-frequency plot at the pixel level and masked at $p < 0.01$ significance. Groups of neighboring pixels with surviving t-statistics were combined and summed to "t-statistic cluster masses", representing time-frequency ranges of significant group differences. To correct for multiple comparisons, cluster-level correction (Groppe et al., 2011; Korn et al., 2004a) was implemented for control of familywise error rate (FWER) using a non-parametric permutation test (N = 10,000) by shuffling diagnostic group labels of rPDC matrices. For each iteration, pairwise t-tests, significance thresholding, and t-statistic cluster generation were repeated using the prior method. Observing across all graph edges, the second largest t-statistic cluster mass was stored to form a surrogate null distribution. True-data cluster masses were then compared to the surrogate null distribution using a one-tail $p < 0.05$ significance threshold to obtain across-edge corrected results. This implementation of cluster-level correction ensured that the number of false discoveries did not exceed a chosen value of $u = 1$, with at least 95% confidence (Korn et al., 2004a).

In order to examine potential relationships between connectivity and spectral power findings, separate ROI analyses were run on regions with significant spectral power findings. This ROI analysis was achieved using a similar statistical procedure as the whole-brain analysis, except that the surrogate distribution was instead created from the largest cluster mass from each

permutation/iteration of the single graph edge of interest (rather than across all edges). This resulted in within-edge control of FWER.

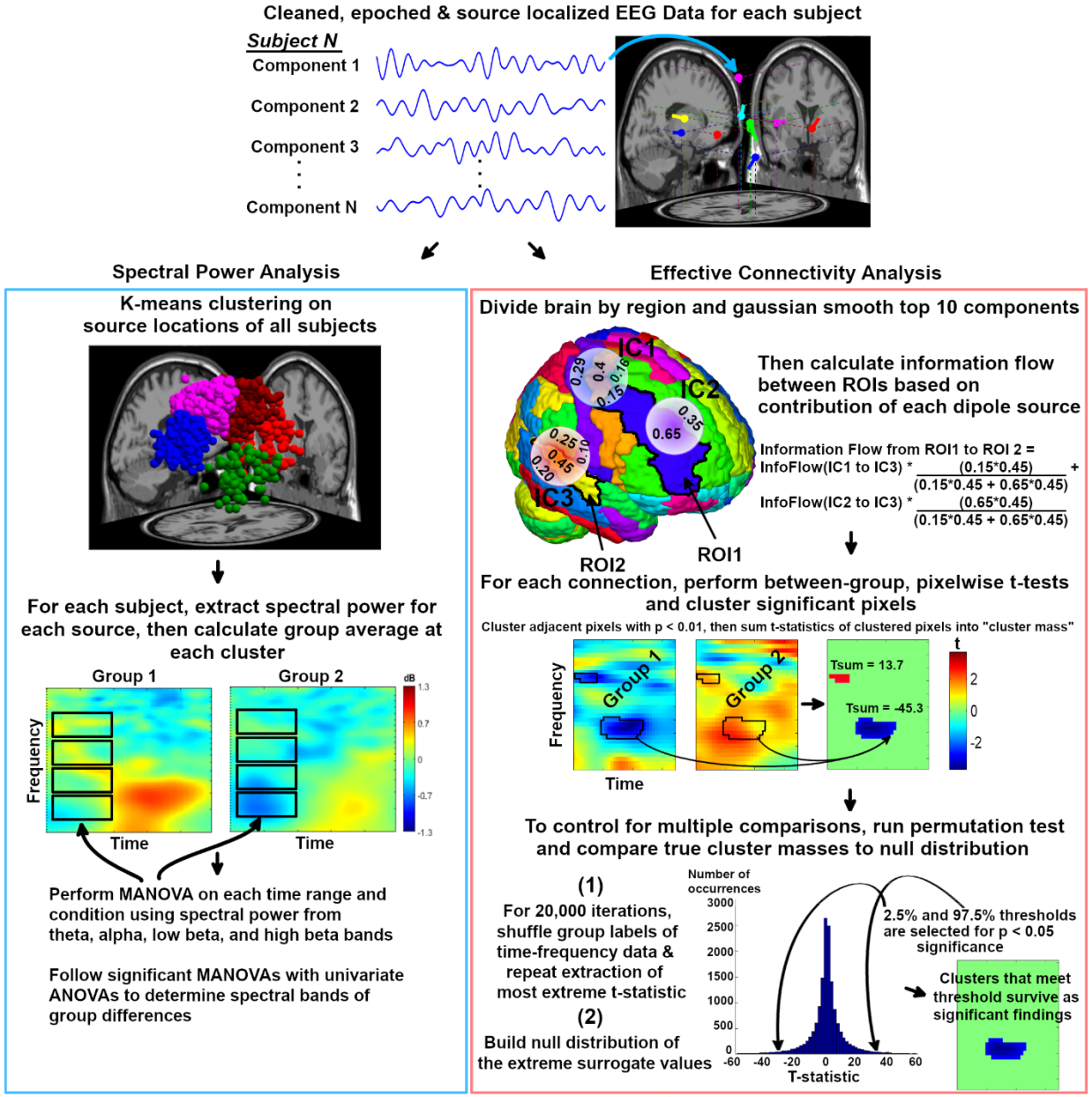

Figure 3-2. Summary of EEG analysis methods for spectral power and effective connectivity. ANOVA = analysis of variance, IC = independent component, MANOVA = multivariate analysis of variance, ROI = region of interest

3.3.8 Statistical Analysis

All analyses were run in the R programming environment (R Core Team, 2020) using customized scripts. In summary, we used the following analysis path for obtaining and interpreting results. First, spectral power calculations were performed on k-means clustered sources to examine localized group differences in spectral power in pre-selected time and frequency ranges. To aide in functional interpretation, Pearson partial correlations (controlling for age) were then run between significant spectral power findings and clinical metrics (YGTSS scores) along with task performance. Next, whole-brain effective connectivity was examined along with supplemental ROI connectivity analyses on any regions with significant spectral power findings. Pearson partial correlations were run between significant connectivity findings and task performance, and with any corresponding spectral power differences to investigate potential compensatory relationships between local power and regional connectivity. Previous EEG analyses among children with and without PTD indicated large effect sizes in brain measurements during voluntary movement (Loo et al., 2019). Although the tasks differ across studies, our current sample size (N = 95) had sufficient power (>80%) to detect an alpha of 0.05 with a medium effect size (f = 0.20) (Cohen, 1988).

Flanker task behavioral data were tested for diagnostic group differences using analysis of variance (ANOVA) for the dependent variables (accuracy, reaction time, reaction time variability) from congruent and incongruent trials separately. Effects of covariates (gender, age, and ADHD/OCD comorbidity) on significant group differences were tested by re-running ANCOVAs with each covariate. To reduce dimensionality and type 1 error rate within the EEG spectral power analyses, multivariate analysis of variance (MANOVA) tests were used to examine significant

group differences in spectral power. MANOVAs were run for each trial type, source cluster, and time period, with theta, alpha, low beta, and high beta band spectral power as dependent variables. MANOVAs with significant diagnostic group differences ($p < 0.05$) were followed by univariate ANOVAs to test the effect of diagnostic group on the spectral power of each frequency band. Effects of covariates (gender, age, and ADHD/OCD comorbidity) on significant group differences were tested by re-running ANCOVAs with each covariate. Statistical procedures to control type 1 error for the connectivity analysis were performed in the *groupSIFT* toolbox described prior.

3.4 Results

Participants in the HC (N = 35) and PTD (N = 60) groups were well matched in age (HC = 9.6 ± 1.4, PTD = 10.0 ± 1.4, t = -1.2, p = 0.25). Estimated intelligence (IQ) was above the average range in both groups but modestly lower in the PTD group (HC = 115 ± 15, PTD = 110 ± 13, t = 2.1, p = 0.04), which has been reported for other clinical samples (Debes et al., 2011). Gender ratio differed, as the HC group was 46% male and the PTD group was 80% male ($\chi^2 = 10.3$, p = 0.001). To account for this imbalance, significant spectral power results were re-run using gender and IQ as covariates. The PTD group had an average YGTSS Total score of 27 ± 8.6, suggesting moderate clinical impairment. Within the PTD group, 10 had comorbid OCD, 15 had comorbid ADHD, and nine had both OCD and ADHD comorbidities, which is similar to rates of comorbidity for ADHD and/or OCD in other samples (Kumar et al., 2016). A total of 10 participants were on non-stimulant psychotropic medication and one patient with PTD was taking a stimulant, which was discontinued for 24 hours prior to their visit.

3.4.1 Flanker Performance

Significant diagnostic group differences on behavioral performance measures in reaction time for congruent and incongruent trials emerged, reflecting faster reaction times in the PTD group relative to controls (see Table 3-1). Accuracy and reaction time variability for both trial types were not significantly different across groups. When controlling for covariates, the congruent trial reaction time differences remained significant, while the incongruent trial reaction time differences continued to be significant when controlling for age and IQ, but not gender, OCD or ADHD symptoms.

Table 3-1. Spectral Power Group Differences

Cluster	Time (ms)	Freq	ERSP, HC (dB)	ERSP, PTD (dB)
Anterior Cingulate	0-200	Theta*	0.00 (1.06)	-0.42 (0.71)
		Alpha**	0.30 (0.82)	-0.26 (0.67)
	250-600	Theta*	0.48 (0.80)	0.03 (0.83)
		Alpha**	0.36 (0.76)	-0.11 (0.76)
		Low Beta**	0.06 (0.67)	-0.34 (0.52)
		High Beta*	0.12 (0.80)	-0.23 (0.55)

** $p < 0.01$, * $p < 0.05$. Analyses revealed significant between-group differences in spectral power solely in the anterior cingulate cortex cluster during incongruent trials with correct responses. Values in the ERSP column represent mean spectral power and standard deviation (in parenthesis), measured in decibels (dB), relative to baseline.

3.4.2 Oscillatory Dynamics - Clustering Solution

From the 12-cluster solution, three clusters (left temporal, right temporal, and inferior occipital) were excluded after using 70% unique subject criteria. The resulting nine clusters and

their corresponding scalp topographies are described in Figure 3-3. Montreal Neurological Institute (MNI) coordinates of cluster centroids were used to estimate Brodmann areas for each cluster via the Yale BioImage Suite (Lacadie et al., 2008).

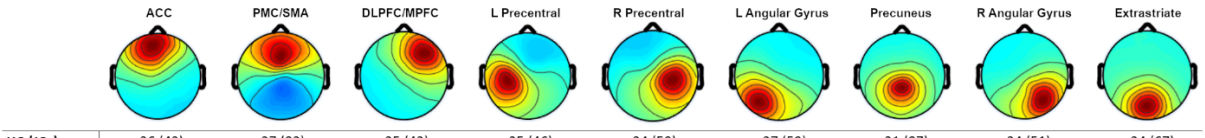

	ACC	PMC/SMA	DLPFC/MPFC	L Precentral	R Precentral	L Angular Gyrus	Precuneus	R Angular Gyrus	Extrastriate
HC (ICs)	26 (43)	27 (82)	25 (42)	25 (46)	24 (59)	27 (59)	31 (87)	24 (51)	24 (67)
CTD (ICs)	48 (85)	44 (112)	46 (68)	47 (87)	51 (105)	51 (129)	46 (115)	50 (111)	55 (136)
BA	32	6	9	4	4	39	7	39	19
X mm (SD)	-11 (16)	1 (11)	32 (12)	-40 (12)	40 (13)	-38 (14)	-2 (16)	39 (11)	1 (13)
Y mm (SD)	42 (15)	8 (14)	27 (15)	-15 (15)	-15 (14)	-61 (14)	-48 (14)	-63 (14)	-82 (12)
Z mm (SD)	14 (19)	52 (16)	18 (15)	51 (13)	49 (15)	20 (17)	64 (14)	31 (14)	32 (13)

Figure 3-3. Source-level independent component cluster topographies. Scalp map views of propagated activity from the nine underlying source-level clusters included in the spectral power analysis. Number of subjects and independent components (ICs) within each cluster are listed for healthy control (HC) and persistent tic disorder (PTD) groups, as well as corresponding Brodmann Area (BA). Coordinates reflect cluster centroid with standard deviation of locations for all ICs in that cluster. ACC = anterior cingulate cortex, DLPFC = dorsolateral prefrontal cortex, L = left, MPFC = medial prefrontal cortex, PMC = premotor cortex, R = right, SD = standard deviation, SMA = supplementary motor area.

3.4.3 Spectral Power During Inhibitory Control

Oscillatory power during flanker performance was examined in the nine clusters selected for analysis for three conditions: congruent trials with correct responses, incongruent trials with correct responses, and incongruent trials with incorrect responses. MANOVA results were significant only for correct incongruent flanker trials, suggesting that task difficulty and successful management of conflict were important factors for evoking neural activation patterns unique to affected individuals. These group differences were present specifically in the ACC cluster during

both the 0-200ms (Wilk's $\Lambda = 0.86$, $F(4,69) = 2.8$, $p = 0.03$) and 250-600ms (Wilk's $\Lambda = 0.85$, $F(4,69) = 3.0$, $p = 0.03$) time periods (Table 3-1; Fig. 3-4). Univariate ANOVAs revealed that directly after incongruent flanker presentation (0-200ms), individuals with PTD exhibited attenuated theta ($F(1,72) = 4.2$, $p = 0.04$) and alpha ($F(1,72) = 10.1$, $p = 0.002$) band power in the ACC relative to controls. In the subsequent 250-600ms period, the HC group exhibited greater ACC spectral power compared to the PTD group in theta ($F(1,72) = 5.2$, $p = 0.03$), alpha ($F(1,72) = 6.5$, $p = 0.01$), low beta ($F(1,72) = 8.1$, $p = 0.006$), and high beta ($F(1,72) = 4.9$, $p = 0.03$). Group differences remained significant after controlling for gender, age, and IQ, with the exception of ACC theta power during the 0-200ms period, which was reduced to a trend level finding.

Controlling for age, partial correlations among spectral power, task performance, and clinical measures indicated significant negative association between early (0-200ms) alpha power with YGTSS Impairment ($r = -0.31$, $p = 0.03$) and later (250-600ms) high beta power with incongruent trial accuracy ($r = -0.25$, $p = 0.04$). These results indicate that higher tic-related impairment and lower incongruent flanker accuracy were associated with EEG power modulations seen in PTD.

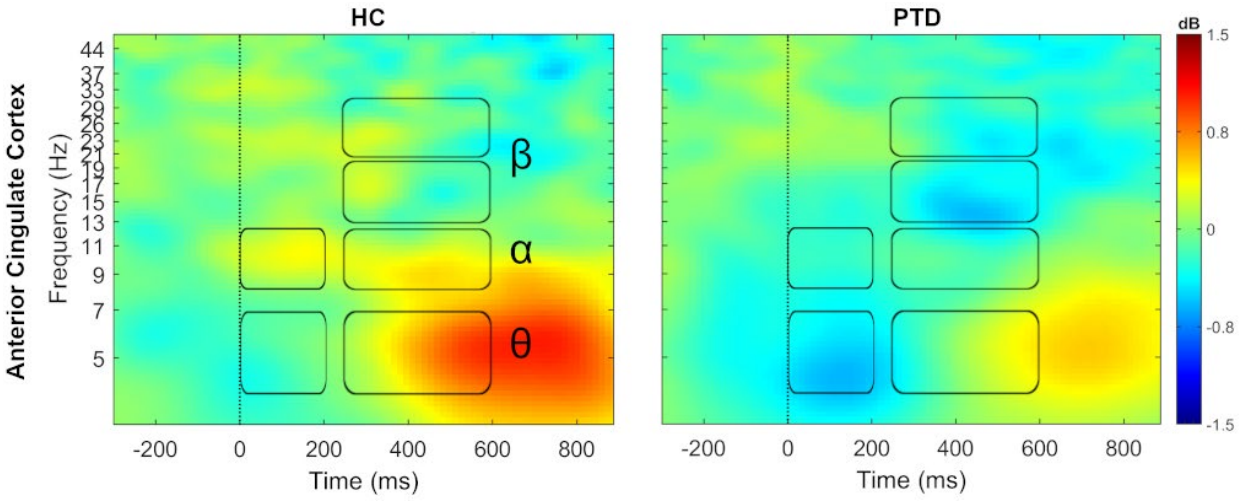

Figure 3-4. Attenuated ACC power in persistent tic disorder. During incongruent trials, subjects with persistent tic disorder (PTD) showed broadband attenuation in spectral power in the anterior cingulate cortex. Time-frequency ranges of significant between-group differences are marked by boxes for theta (θ, 4-7Hz), alpha (α, 8-12Hz), and low (13-20Hz) and high beta (β, 20-30Hz) frequency bands.

3.4.4 Connectivity Dynamics

Following findings of diagnostic group differences in spectral power exclusively on correct incongruent trials, effective connectivity was examined solely in this condition. In addition to whole-brain connectivity, we examined connectivity edges involving the ACC due to significant group differences in spectral power. Together, these two analyses revealed 10 connections (seven from the whole-brain analysis and three from the ACC analysis) with significant group differences in information flow. Each connection involved a minimum of 66 subjects using the 70% unique subject thresholding criteria. Notably, all connections were associated with bilateral precuneus or midcingulate cortex nodes, regions within the fronto-parietal network that have been shown to be highly involved in processes of cognitive control, integration of information, and mental imagery

(Margulies et al., 2009; Shackman et al., 2011). These hubs showed differences in both information inflow and outflow with eight other anatomical regions located in mid-frontal, left motor, left temporal, and bilateral occipital cortices.

Topographically, controls exhibited greater information flow within the central and posterior brain regions through integration of the precuneus with left precentral, left mid-temporal, and right occipital cortical sources (Fig. 3-5A). In contrast, individuals with PTD exhibited stronger effective connectivity along the midline and with anterior frontal areas, including the ACC and superior medial frontal cortex. Examination of the time dynamics of group differences revealed that differences in information flow occurred throughout the period from stimulus presentation until subject response (Fig. 3-5B). The HC group, however, displayed a notable period of relatively stronger information flow directly after stimulus presentation.

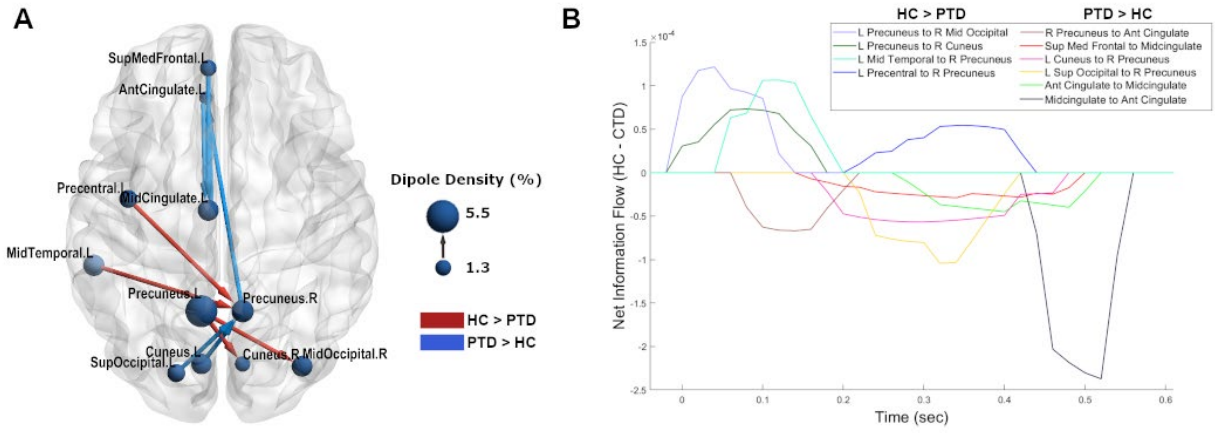

Figure 3-5. Network view of effective connectivity during inhibitory control. **A)** The persistent tic disorder (PTD) group exhibited greater information flow along the midline and with frontal regions (blue), while greater causal flow among central and posterior regions was observed in the healthy control (HC) group (red). The arrows represent the direction of information flow for a

given connection, and node sizes represent dipole density for a given node. The brain model was visualized using BrainNet Viewer software (Xia et al., 2013). **B)** Time series representation of outflow for significant between-group connections from (A). Information flow which is stronger in the HC group is represented by positive values while stronger in the PTD group is represented by negative values. Stimulus onset was at t = 0; mean response time was ~600ms, averaged across both groups. Ant = anterior, L = left, Med = medial, R = right, Sup = superior.

Controls exhibited greater information flow from the left precentral gyrus to right precuneus from 200-400ms, revealing the first appearance of motor cortex differences in the study and suggesting atypical motor signaling from this area in individuals with PTD (Fig. 6). While controls displayed greater early left precuneus to right occipital communication, the PTD group showed stronger early connectivity from the right precuneus to ACC (Fig. 7), possibly representing different stimulus appraisal strategies. Recruitment of additional frontal regions for task processing in PTD was further indicated by greater information flow from the superior medial frontal cortex to midcingulate (Fig. 3-6), as well as greater bidirectional connectivity between the ACC and left midcingulate (Fig. 3-7). Given their timing (200-500ms), these connections suggest atypically greater signaling of frontal conflict processing/response preparation mechanisms in individuals with PTD.

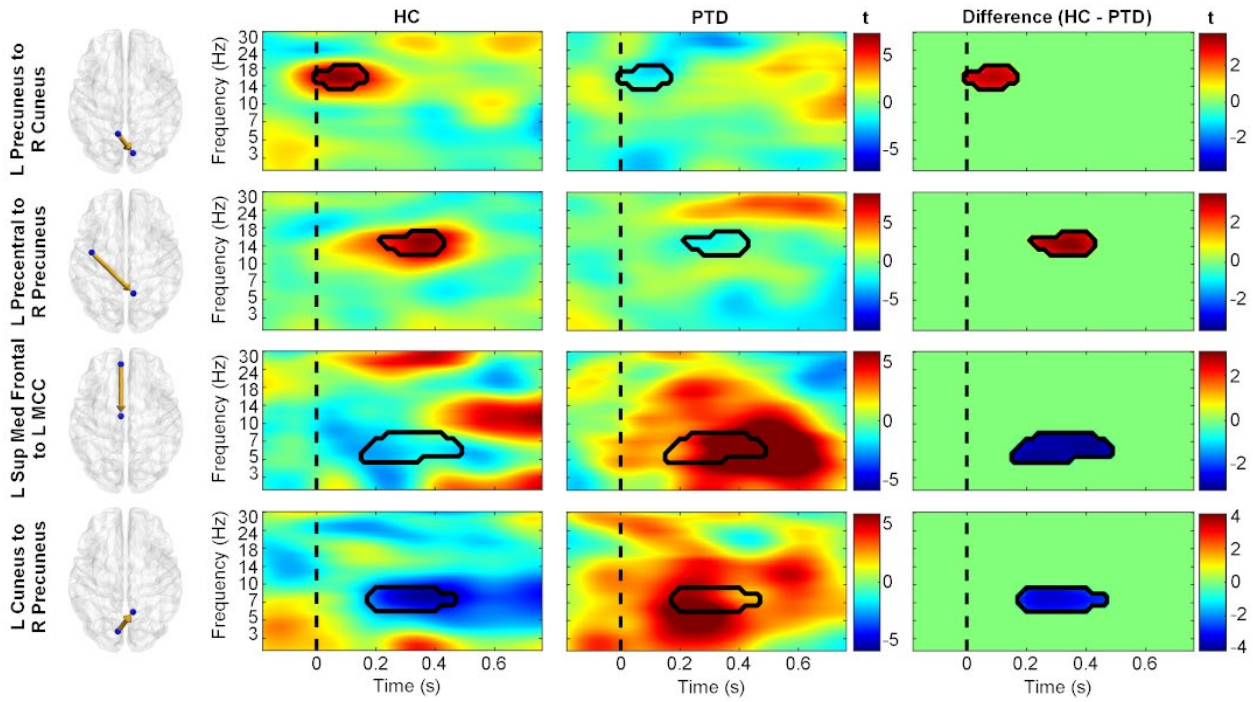

Figure 3-6. Diagnostic group differences in causal information flow. Time-frequency plots of effective connectivity patterns (represented as t-statistics) for healthy controls (HC, left), individuals with persistent tic disorder (PTD, middle), and the between-group differences (right). The precuneus in the HC group displayed greater connectivity with the right occipital and left precentral gyrus (red in difference plots), while the PTD group showed greater information flow with frontal and left occipital cortices (blue in difference plots). The dashed line represents stimulus presentation at t = 0. L = left, Med = medial, MCC = midcingulate cortex, R = right, Sup = superior.

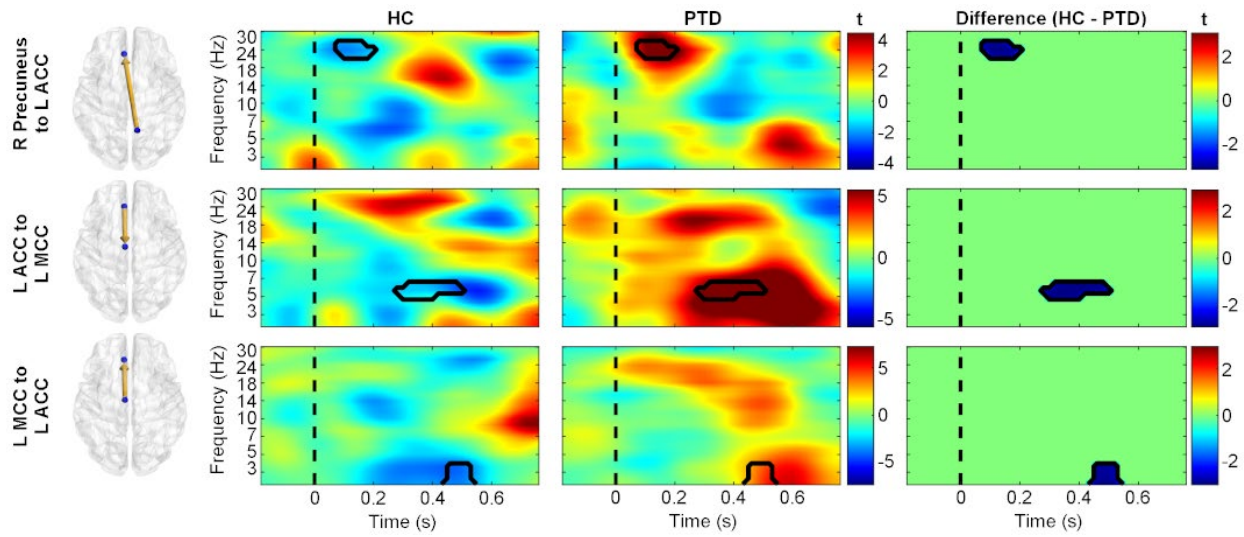

Figure 3-7. Significant causal interactions involving the anterior cingulate. Time-frequency plots of effective connectivity patterns (represented as t-statistics) for healthy controls (HC, left), individuals with persistent tic disorder (PTD, middle), and the between-group differences (right). Individuals with PTD exhibited greater effective connectivity (blue in difference plots) from the right precuneus to anterior cingulate cortex (ACC), as well as bidirectionally between the ACC and midcingulate cortex (MCC). The dashed line represents stimulus presentation at t = 0. L = left, R = right.

3.4.5 Correlations with Behavior and Performance

Partial correlations (controlling for age) between rPDC information flow and incongruent trial performance metrics indicated significant associations with several connections ($p < 0.05$). Accuracy was negatively correlated with left precentral to right precuneus ($r = -0.27$, $p = 0.03$) connectivity (which was stronger in controls) as well as with frontal connections (all of which were stronger in PTD) between the left superior medial frontal and midcingulate ($r = -0.25$, $p = 0.04$), ACC to midcingulate ($r = -0.35$, $p = 0.003$), midcingulate to ACC ($r = -0.42$, $p = 0.0004$),

and right precuneus to ACC ($r = -0.42$, $p = 0.0008$). Midcingulate to ACC connectivity was also negatively correlated with incongruent trial reaction time ($r = -0.31$, $p = 0.009$). Correlations between ACC connectivity and spectral power were not significant (all p's > 0.05), suggesting: 1) these are separate neural mechanisms that are not resultant from one another, and 2) higher connectivity between frontal and midcingulate regions was an alternative neural pathway utilized by individuals with PTD that resulted in faster response times but similar accuracy.

3.5 Discussion

The present study provides the first report of cortical source-resolved, event-related brain oscillatory dynamics and effective connectivity during inhibitory processing in PTD. Overall, children with PTD exhibited lower spectral power in the ACC but higher causal information flow between the ACC and other midline central and posterior regions, despite similar levels of task accuracy, relative to typically developing controls. In addition, whole-brain connectivity analyses indicated that the midcingulate and precuneus serve as fronto-parietal network hubs whose connections with several motor and sensory areas such as left precentral, left temporal, and bilateral occipital nodes were atypical in PTD. Finally, attenuated ACC activation and higher information flow between and among nodes within the fronto-parietal attention network were significantly associated with tic impairment, faster reaction time, and worse inhibitory performance, suggesting these alternate cortical patterns may be a putative neural adaptation among individuals with PTD.

Significant differences in neural dynamics were observed between controls and individuals with PTD despite equivocal differences in inhibitory task performance, a finding that is consistent with other event-related potential (ERP) and functional MRI cognitive control studies (Baym et

al., 2008; Ganos, Kühn, et al., 2014; Jung et al., 2013). Interestingly, these differences in dynamics were observed solely in incongruent trials despite the group differences present in congruent trial reaction time. A potential explanation for this may be found from the correlation analyses, which revealed significant EEG correlations primarily with incongruent trial accuracy. This could be due to a greater sensitivity of the EEG measurements used to neural mechanisms associated with accuracy rather than network activity related to reaction time, which may be widely distributed.

Within the current study, the ACC showed between-group differences in both activation and connectivity patterns, suggesting it plays a key role in the cognitive inhibition process. The involvement of this region is well supported, as the ACC has repeatedly been shown to be engaged during monitoring of conflict (Botvinick et al., 2004; Fan et al., 2003; Van Veen & Carter, 2002). In PTD, studies have reported structural and neurochemical ACC deficits among affected individuals, including lower grey matter in adults (Müller-Vahl et al., 2009) and lower γ-aminobutyric acid (GABA) levels in youth (Freed et al., 2016). Aberrant ACC activity has also been observed in pediatric and adult samples during inhibitory control tasks (Jung et al., 2013; Marsh et al., 2007) as well as prior to tic occurrence (Wang et al., 2011), suggesting the ACC subserves multiple roles common to both tic occurrence and inhibitory control in PTD. This hypothesis is further supported by negative correlations observed here between alpha band power in the ACC and higher YGTSS Impairment scores, indicating greater tic impairment was associated with attenuated ACC activity during inhibitory processing.

Several additional brain regions exhibited aberrant effective connectivity, suggesting widespread atypical network communication in individuals with PTD during inhibitory control. The precuneus and midcingulate were involved with nearly all significant connections. Both

regions are known to be associated with the integration of various processing areas and cortical functions, including cognitive control (Cavanna & Trimble, 2006; Fan et al., 2003; Shackman et al., 2011), and have been implicated in PTD during an adaptive control paradigm (Church, Wenger, et al., 2009). The precuneus communicates with peripheral visual, frontal, and motor regions (Margulies et al., 2009), and the presence of altered hub connectivity in PTD may indicate difficulties with the integration of multimodal information that is required when performing sensory-driven movements. The precuneus is also associated with internally guided attention (Cavanna & Trimble, 2006) as well as with attention shifting between object features (Nagahama et al., 1999). Given that the paradigm was designed for assessing features of attentional control (Fan et al., 2002), altered connectivity patterns between the precuneus and visual cortex could suggest mechanistic and/or procedural differences in attention shifting between important stimulus features (e.g., arrow directionality) in PTD, as reflected by contrasting directions of information flow between the precuneus and bilateral occipital cortices by diagnostic group. Together these would suggest individuals with PTD utilize atypical communication patterns between attention, visual and sensorimotor networks

While the involvement of the MCC in cognitive control and response selection is well established, greater engagement of the midcingulate with other frontal areas could provide support for an urge-based motoric role that has been previously hypothesized (Jackson, Parkinson, Kim, et al., 2011). In particular, this hypothesis proposes a separation between a "urge-driven action" network involving the insula and MCC and a "willed, intentional action" network primarily involving the premotor and parietal cortices. The present findings fit well with this anatomical separation, as while a premotor and parietal-based connectivity pattern was observed in controls, an additional MCC-based network was present in the PTD group. This idea is also supported by

the fact that negative, rather than positive, correlations were observed between MCC connectivity and accuracy as well as reaction time, indicating that the influence of the MCC did not necessarily help participants perform better on the task. Additionally, the involvement of the MCC in goal-directed (including impulsive and body-directed) actions (Caruana et al., 2018) could signify greater impulsive signaling within these motor pathways in PTD and help explain the EEG-behavior relationships.

Whole brain effective connectivity analyses revealed greater information flow among the central and posterior network hubs in the HC group, while the PTD group exhibited greater connectivity along the midline fronto-parietal axis during inhibitory processing. Greater fronto-parietal connectivity is typically considered to be a developmentally mature neural pattern (Church, Fair, et al., 2009), which may arise among children with PTD as a result of frequent inhibition of tics and the need to control tic expression (Ganos et al., 2018; Nielsen et al., 2020). On the other hand, integration of the ACC into the fronto-parietal network as opposed to the cingulo-opercular control network is an immature developmental pattern observed in youth with PTD that is most commonly seen among typically developing children but not adolescents or adults (Church, Fair, et al., 2009). Thus, these results suggest altered network connectivity patterns that cannot be characterized as unidirectional along the developmental spectrum.

While qualitatively different developmental trajectories of neural connectivity has been reported previously (Nielsen et al., 2020), we note that another reason these results don't map directly onto previous findings may be the lack of comparable studies given the dearth of task dependent, event-related connectivity studies in PTD. Many MRI-based studies reporting functional or structural connectivity have been performed on resting state, which may differ

significantly from task dependent effective connectivity due to increased top-down control of cortico-striatal-thalamic activity under task conditions (Zapparoli et al., 2017). While several studies have examined connectivity dynamics during tic suppression and other inhibitory control paradigms (Zapparoli et al., 2015), of the two EEG-based studies examining scalp-based connectivity, children with PTD exhibited higher coherence values relative to controls in fronto-central connections during tic suppression (Hong et al., 2013) and motor inhibition (Serrien et al., 2005). Our results are thus consistent with these previous studies and extend the findings with a higher density electrode montage and cortical-source level effective connectivity, allowing identification of directional information flow to specific nodes along the fronto-parietal network with precise timing. In light of these associations, altered task-dependent network connectivity patterns within PTD appear to have greater involvement of frontal regions than is generally reported for typically developing children. We hypothesize that greater frontal connectivity is likely a neural adaptation to coping with the illness, but one that does not necessarily result in better behavioral performance.

A strength of this study is the large sample size of children with and without PTDs (N = 95) who are within a relatively tight age range of 8-12 years. In addition, state of the art EEG recording and processing techniques allowed for sub-second quantification of oscillatory activity and effective connectivity with greater spatial resolution of cortical-source resolved generators. One limitation is that pediatric populations are developmentally heterogenous and at the early stages of diagnosis, which may make it difficult to generalize findings towards older individuals with tic disorder. Nevertheless, evaluations of early diagnostic stages are prudent for examining disorder progression and optimizing early intervention techniques. A second limitation is that EEG is blind to activity from deeper subcortical sources within the cortico-striato-thalamo-cortical

network, which are thought to play a key role in tic generation within PTDs (Ganos et al., 2013). Key distinctions have been made, however, between the neural mechanisms that generate tics versus those that play a role in suppression of involuntary and voluntary movements, as well as inhibition of internally driven versus externally triggered events (Ganos et al., 2018). Recent studies and a meta-analysis of task-based neuroimaging studies did not find significant diagnostic group differences in activation and network disruptions involving basal ganglia or thalamic regions (Polyanska et al., 2017; Wen et al., 2016, 2017), suggesting there are clear cortical dysfunctions that contribute meaningfully to PTD phenomenology that can be assessed with EEG. Furthermore, the atypical cortical activity reported here may provide potential non-invasive neuromodulation targets for future treatment of PTD. A final consideration is that the PTD sample contained more boys and some subjects with comorbid OCD and ADHD. The occurrence of comorbid disorders in patients with PTD is typical but creates potential issues when attempting to interpret results and their association with PTD. However, most group differences remained significant after controlling for sex as well as ADHD and OCD symptoms, suggesting that the group differences observed are not systematically associated with gender or diagnostic comorbidity.

In summary, we have provided evidence of aberrant activation and communication patterns within the fronto-parietal network, specifically in the anterior cingulate cortex, which had attenuated spectral power but greater causal information flow with several fronto-parietal hub regions, particularly the midcingulate and precuneus, in PTD. Further research into these temporally resolved mechanisms will better elucidate neural mechanisms and potential patterns of atypical network communication that lead to tic expression and suppression in PTD.

Chapter 4: Neural Dynamics Preceding Tic Expression in Persistent Tic Disorder

4.1 Abstract

Persistent tic disorders (PTDs) are characterized by stereotypical and involuntary movements referred to as tics. Prior EEG and imaging-based studies have indicated a number of cortical and subcortical regions with aberrant activity in the seconds preceding tic expression. Of the EEG studies examining the neural activity preceding tic events, however, none have taken a whole-brain approach, particularly with respect to measurements of causal information flow, which may provide insight into the temporally resolved cortical mechanisms and regions driving tic expression. The goal of this study was to further examine these neural antecedents of tic expression using EEG measures of spectral power and effective connectivity in a whole-brain approach in a sample of children with PTD (N = 50) during a free ticcing resting state paradigm. Using a Tic condition made up of tic-locked activity, and a NoTic condition made up of resting state activity without tics, changes in spectral power and effective connectivity were evaluated. Following detection and localization of significant changes activity, these significant measures were used as features in a Naïve Bayes classifier to determine the differentiability between the Tic and NoTic epochs. The classifier was first trained using a cross-validation approach and was afterwards tested using comparable measures extracted from an independent set of children (N = 15) with PTD performing the same task. Spectral power analyses indicated significant increases in activity in the anterior cingulate cortex prior to tic expression relative to typical resting state activity. Changes in information flow were detected across the brain, implicating frontal, sensorimotor, and posterior regions, suggesting aberrant communication among multiple

cognitive, sensory, and motor-based regions. High classification accuracies (both sensitivity and specificity) were observed in the both the training and test datasets, indicating these changes in spectral power and information flow to be reliable discriminators of tic generative processes.

4.2 Introduction

Tics are the core symptom of persistent tic disorders (PTD), consisting of stereotypical and involuntary movements performed by individuals with the disorder. Prior to tic expression, there are a number of neurological mechanisms which are hypothesized to be involved, including excessive activity in motor pathways, insufficient inhibitory control, and strong premonitory urges (Conceição et al., 2017; Wang et al., 2011). These premonitory urges, which show apparent increasing rates as development progresses (Banaschewski et al., 2003), are generally described as a feeling of discomfort that is relieved by performing the tic, and are particularly unique in that they notify individuals of instances of symptomatic activity. Despite the often involuntary and habitual nature of tics, many individuals with PTD are able to direct internalized attention towards these sensory urges to voluntarily detect and suppress oncoming tics to some degree (Himle & Woods, 2005). Thus, there appear to be neurological processes associated with tic generation and expression that are able to be consciously and internally intercepted before the tic is expressed. These tic-generative processes may also provide an avenue for external interception through non-invasive intervention approaches such as neurostimulation, assuming that they can be adequately localized and detected (with high temporal resolution) relative to typical resting state periods without tics.

Neurophysiological studies have investigated the neural dynamics involved in tic generation and expression, with reports of several cortical and subcortical regions activated prior

to tic onset. In adults with Tourette syndrome, atypical activations upwards of 2 seconds prior to tic onset have been observed in the anterior cingulate cortex (ACC), insular cortex, supplementary motor area (SMA), primary motor cortex (M1), somatosensory cortex (SMC), and parietal operculum during tic freely conditions in functional magnetic resonance imaging (fMRI) studies (Bohlhalter et al., 2006; Neuner et al., 2014). One second prior to tic onset, both cortical and subcortical regions have also been implicated, including the extrastriate visual cortex, putamen, amygdala, and cerebellum (Neuner et al., 2014). Activation during tic occurrence of limbic areas including the insula and ACC, as well as SMA have been similarly supported by positron emission topography (PET) studies (Lerner et al., 2007; Stern et al., 2000). The insula has also been indicated to display atypical connectivity with fronto-striatal nodes of the urge-tic network in adult patients (Tinaz et al., 2015), and its involvement in urge-related behavior is supported by other tic disorder and behavioral studies (Jackson et al., 2020; Jackson, Parkinson, Kim, et al., 2011).

Electroencephalographic (EEG) approaches have been sparsely utilized to examine cortical activity prior to tic occurrence, primarily in the sensorimotor cortices. Early event-related potential (ERP) studies have suggested an absence of readiness potentials prior to tic onset in some (Obeso et al., 1981), but not all patients with tic disorders (Karp et al., 1996). Reasoning for this discrepancy has been theorized to be related to the presence (or absence) of internal tic-related urge phenomena, which varies from patient to patient. A lack of beta band power decrease or desynchronization has also been reported in motor cortices prior to tics, in contrast to the desynchronization observed prior to voluntary movements, suggesting tics may engage a unique set of brain regions not involved in volitional movements, including insular, cingulate, and subcortical basal-ganglia regions reported in prior studies (Maiquez et al., 2020). Although connectivity changes prior to tics have remained mostly unexplored, one study has reported

changes in thalamo-cortical (motor cortex) coherence beginning approximately one second prior to tic occurrence (Bour et al., 2015), suggesting that atypical communication patterns prior to tics may be present.

While the majority of previous studies have solely focused on fMRI, or applying EEG/ERP approaches to sensorimotor cortices, there is a gap in the literature regarding whether there are detectable oscillation-based EEG activations driving tic expression in other cortical regions. Furthermore, there is a lack of research regarding the causal, rather than functional, mechanisms of cortical-cortical communication involved in tic generation, which may facilitate understanding of cortical regions driving tics. The present study aimed to address this topic by utilizing high-density EEG to examine cortical source-level, whole-brain spectral power and effective connectivity during the time periods directly preceding spontaneous tic events. Utilizing a tic freely resting state paradigm, the goals of the study were two-fold. Firstly, the study aimed to identify cortical regions exhibiting atypical spectral dynamics prior to tic events, relative to periods of no tic activity. Secondly, the study aimed to measure the degree to which this tic-associated activity was discriminable from periods of no tic activity using a classification approach. We first trained a classifier and examined performance using the primary dataset, and then evaluated the classifier model on EEG data from an independent dataset of similar-aged children with PTD. Based on prior studies, we hypothesized that tic-associated activity, and discriminable features, would consist of activations and connections among sensorimotor and cingulate cortices, and that these activation patterns would be associated with both tic and urge severity.

4.3 Methods

4.3.1 Sample

The primary study sample consisted of 50 children, aged 8-12 years old, with persistent tic disorder recruited from the community from radio and newspaper advertisements, local schools, an academic medical center anxiety and tic disorder clinic between 2013 and 2020. Prior to screening and any study procedures, participants and their parents received verbal and written explanations of study criteria and provided written permission/assent. All studies procedures and consents were approved by the local Institutional Review Board.

During a single experimental session that lasted approximately 2-3 hours, participants underwent semi-structured diagnostic interviews, cognitive testing, and a comprehensive EEG recording. Participants were required to be male or female aged 8-12 years, possess a primary DSM-V diagnosis of Persistent Motor Tic Disorder, Persistent Vocal Tic Disorder, or Tourette Disorder from both the Anxiety Disorder Interview Schedule, Child Version (ADIS) (Silverman, 1996) and diagnostic interview, as well as have a tic severity score ≥15 on the Yale Global Tic Severity Scale (YGTSS) (Leckman et al., 1989). Presence and strength of premonitory urges were evaluated using the Premonitory Urge for Tics Scale (PUTS) (Woods et al., 2005). Comorbidity of ADHD was diagnosed using the Strengths and Weaknesses of ADHD-symptoms and Normal-behavior (SWAN) scale (Swanson et al., 2012), and obsessive-compulsive disorder (OCD) using the Child Yale-Brown Obsessive-Compulsive Scale (CYBOCS) (Scahill et al., 1997). Estimated intelligence (IQ) was assessed using the Wechsler Abbreviated Scale of Intelligence (WASI) (Wechsler, 1999).

Exclusion criteria included an estimated Full Scale IQ < 80, or a history of head injury resulting in concussion, autism spectrum disorder, major depression, bipolar disorder, panic disorder, or psychosis. Individuals taking stimulant medication for comorbid ADHD discontinued

use for 24 hours prior to their visit. Other psychotropic medications were included as covariates of no interest in analyses.

An independent test sample of children with persistent tic disorder, for usage only in testing the classifier model, was obtained from the baseline visit of a prior published behavioral intervention study (McGuire et al., 2022). This sample consisted of 15 subjects, aged 8-14 years old, recruited under comparable inclusion and exclusion study criteria.

4.3.2 Experimental Task

Participants performed a resting-state, eyes open paradigm while EEG was recorded. The task lasted for 7.5 minutes, with a static dot shown on the center of the computer screen for the entirety of the task. Participants were instructed to keep their attention towards the screen and were free to tic as needed. High-definition video (at 30fps) of each participant was simultaneously recorded during the EEG session. Following the EEG recording session, a trained staff member performed a frame-by-frame review of the session video for tic events and marked the time point of each tic onset throughout the resting-state paradigm in the EEG data stream. From this task, a "tics per minute" dependent variable was calculated for each participant.

4.3.3 EEG Recording and Processing

EEG was recorded using a 128 Hydrocel electrode net in an extended international 10-10 configuration (Electrical Geodesics Incorporated). Electrode scalp coordinates were transcribed through Polhemus, Inc. digitizer software, using the nasion and preauricular notches as anatomical reference points. Data were sampled at 1000Hz, referenced to Cz, and electrode impedances were lower than 50kΩ (per manufacturer recommendation).

Processing of data was performed using the EEGLAB toolbox (Delorme & Makeig, 2004). Data was first downsampled to 250Hz and filtered using a 0.5-55Hz bandpass filter. Artifact subspace reconstruction (ASR) (Blum et al., 2019; Chang et al., 2018; Kothe & Makeig, 2013; Mullen et al., 2015) was the employed by the EEGLAB plug-in *clean_rawdata()* for removing large artifacts, bad channels, and line noise. Scalp signals were then be decomposed into independent source level activations, also known as independent components (ICs), using adaptive mixture independent component analysis (AMICA) (Delorme et al., 2012a; Hsu et al., 2018; Palmer et al., 2011). Dipole locations of source activations were then subsequently estimated using Fieldtrip (Oostenveld et al., 2010b). To remove muscle, ocular, and line noise source components, the EEGLAB plug-in ICLabel, a classifier trained to detect neural vs non-neural IC activations, was utilized to select only brain-based sources, with non-neural sources being rejected from the data. In order to ensure model stability in the effective connectivity analysis, each subject's dataset was limited to the top 15 ICs, ranked based on the percent of EEG variance accounted for.

Preprocessed source-level resting state data was epoched into two sets of trials: a Tic condition and NoTic condition. The Tic condition consisted of tic-locked epochs -4000ms to 0ms relative to the start of each tic. In order to prevent contamination from motor artifacts of preceding tic events, epochs were excluded if a preceding tic was within 5000ms of the tic. The NoTic condition consisted of non-overlapping epochs selected from portions of the data where there were no tics, and neither pre-tic activity nor post-tic artifacts occurred. To achieve this, epochs were matching in length (4000ms), with the left edge of the epoch required to be at least 2000ms after any tic event and right edge required to be 3000ms prior to any tic event.

4.3.4 Measures

Two measurements were implemented at the cortical source level to examine changes in both local neural activity and region-to-region communication.

Local activation at each cortical source was measured using event-related spectral perturbation (ERSP), a time-frequency analysis method that measures event-related changes in spectral power relative to a baseline. ERSP was estimated using the EEGLAB function *newtimef()*, using a similar sliding window of 1-second in length with 25ms step size was applied. Spectral magnitudes were averaged across trials, baselined using a divisive gain model of average magnitudes from the -3500ms to -2500ms baseline period, and log transformed to decibel (dB) units.

Information flow between pairs of cortical sources within subjects was measured using renormalized partial directed coherence (rPDC), a frequency-domain form of effective connectivity (Schelter et al., 2009), as implemented in the groupSIFT (Loo et al., 2019) and SIFT (Delorme et al., 2011) plug-ins for EEGLAB. For each subject, connectivity was estimated between sources using a multivariate autoregressive model fit from the Vieira-Morf algorithm, with 30 log-scaled frequencies from 2 to 40Hz, along with a 1-second sliding window of 25ms step size. Connectivity values were baselined by subtracting average connectivity from the preceding -3500ms to -2500ms baseline period.

In order to facilitate group-level analyses on these cortical sources and measures, a source projection methodology was applied to dipoles (Loo et al., 2019). The method employed a 3-D Gaussian kernel (full-width half maximum of 20mm truncated at 3σ) to spatially smooth dipoles from single points into probabilistic dipole densities. A 3-dimensional, 8mm-spaced voxel system was then placed on the brain model. For the ERSP analysis, estimates of ERSP activity for each

subject were calculated at each voxel using a within-subject weighted average of dipole densities contributing to the voxel. This produced a Voxel x Time x Frequency ERSP matrices for each subject. Voxels that had dipole contributions from at least 50% of subjects were included in the analysis. For the connectivity analysis, the brain model was parcellated into 76 regions of interest (ROI) using the automated anatomical labelling atlas (Tzourio-Mazoyer et al., 2002). For each subject, connectivity was then calculated between ROI pairs based on contributions of dipoles to each ROI using a within-subject weighted average, producing a *ROI* x *ROI* x *Time* x *Frequency* connectivity matrix. ROIs which had dipole contributions from at least 80% of subjects were included in the analyses. To note, greater subject inclusion criteria was achievable in the ROI approach (compared to the voxel approach) due to their larger anatomical size and thus greater dipole contribution. These inclusion criteria values were selected on the basis of maintaining sufficient statistical power (from subject inclusion) while also ensuring a sufficient portion of the cortex was included in the analysis.

4.3.5 Statistical Analysis

A mass univariate approach was utilized in the time-frequency domain for comparing the Tic and NoTic condition epochs for both the spectral power (ERSP) and effective connectivity (rPDC) analyses. For each time-frequency pixel of each measure, a paired t-test was performed between the two conditions. Significance values were then masked at a threshold of $p < 0.05$, and t-statistics among surviving adjacent pixels were summed together to form statistical cluster masses. To control for familywise error rate (i.e., correct for multiple comparisons), cluster level correction was performed using an iterative permutation approach ($N = 1000$) by shuffling condition labels of spectral power and connectivity time-frequency matrices. During each iteration,

pairwise statistical testing and cluster mass formation were repeated, with the second largest cluster mass across all voxels/ROIs (for spectral power and connectivity, respectively) recorded and stored to form a surrogate null distribution. Using the second largest cluster mass ensured that the number of false discoveries did not exceed u = 1, with 95% confidence (Korn et al., 2004b). True data time-frequency cluster masses were compared to the null distribution using a $p < 0.05$ threshold. Following the whole-brain effective connectivity analysis, an additional ROI-specific connectivity analysis was performed on regions showing significant changes in activity in the spectral power analysis. Multiple comparisons were accounted for through false discovery rate (FDR) control at $p = 0.05$.

In an effort to examine clinical interpretations of EEG findings, Pearson correlations were run in the R environment (R Core Team, 2020) between behavioral scores (including clinical scales and tic-related metrics) and significant findings from the spectral power and connectivity analyses.

4.3.6 Classification of Tic and NoTic Conditions

A kernel naïve Bayes classifier, run in the MATLAB environment, was utilized to determine the discriminability between trial-averaged activity of Tic trials from that of NoTic trials. Broadly, this supervised classifier assigns outcome labels to observations based on a probabilistic model learned from applying Bayes Theorem to features from a set of training data. Predictors/features consisted of significant spectral power and connectivity measures obtained from the group-level analysis, while observations (N = 100) were made up of the 50 subjects, each with two conditions (pre-tic and rest). The classifier was first trained through a training and validation set using a 10-fold cross-validation approach, obtaining measures of overall classifier accuracy (sensitivity and specificity) as well as area under the curve (AUC). The classifier model

was then applied to predict labels of unseen data from the independent test set of 15 subjects with the same two conditions (Tic and NoTic).

4.4 Results

4.4.1 Demographics

Demographic data for the primary study sample as well as classifier test sample are described in Table 4-1. The primary sample displayed moderate tic severity with a mean total YGTSS score of 27.4 ± 8.6. Comorbidities of ADHD, OCD, or an anxiety disorder were present in 70% of participants, as is typical for such populations (Hirschtritt et al., 2015).

Table 4-1. Demographics and clinical characteristics of participants.

Demographics	**Primary Sample**	**Test Sample (only for classifier)**
N	50	15
Age, M (SD)	9.8 (1.6)	11.8 (2.0)
Sex, males, N (%)	38 (76%)	11 (73%)
Full Scale IQ, M (SD)	113 (15)	109 (13)
Clinical Characteristics		
ADHD, N (%)	25 (50%)	3 (20%)
OCD, N (%)	21 (42%)	6 (40%)
Generalized anxiety disorder, N (%)	14 (28%)	3 (20%)
No comorbidities, N (%)	15 (30%)	6 (40%)
YGTSS, M (SD)		

Total score	27.4 (8.6)	26.1 (5.1)
Impairment	26.8 (8.7)	29.0 (6.3)
Motor	16.5 (3.4)	15.5 (2.8)
Vocal	11.2 (6.5)	10.6 (4.1)
PUTS, M (SD)		
Urge presence	4.4 (2.2)	N/A
Urge strength	4.2 (2.1)	N/A
Tic frequency	5.2 (2.1)	N/A
CBCL total, M (SD)	56.8 (11.3)	60.7 (8.5)
SWAN, M (SD)		
Inattention	24.8 (8.9)	25.5 (10.4)
Hyperactivity	24.3 (7.9)	25.2 (7.7)
CYBOCS, M (SD)	9.5 (10.6)	N/A
Medication		
No medication, N (%)	37 (74%)	11 (73%)
Stimulant, N (%)	1 (4%)	0
Psychotropic, N (%)		
α -2 agonist	7 (14%)	0
Antidepressant	6 (12%)	2 (13%)
Anticonvulsant	1 (2%)	0
Antipsychotic	2 (4%)	1 (7%)
Antihypertensive	2 (4%)	3 (20%)

Note: M = mean, SD = standard deviation, IQ = intelligence quotient, ADHD = attention-deficit/hyperactivity disorder, OCD = obsessive-compulsive disorder, YGTSS = Yale Global Tic Severity Scale, PUTS = Premonitory Urge for Tics Scale, CBCL = Child Behavior Checklist, SWAN = Strengths and Weaknesses of ADHD-symptoms and Normal-behavior scale, CYBOCS = Child Yale-Brown Obsessive-Compulsive Scale

4.4.2 Tics During EEG Recording Session

Tics included in the analysis consisted of visible motor-related movements located above the waist. While nearly all patients possessed vocal tics in addition to motor tics, verbal tics were not analyzed as no audio was available for the post-session video review. Parent and clinician-reported ticcing behavior indicated ocular tics to be the most frequent (90% of subjects), followed by shoulder/head (74%), facial (58%), and truncal (32%) tics. The number of tics exhibited by patients during the 7.5 minute recording session ranged from 1 to 9.5 (mean of 4.2 ± 2.1) tics per minute. When tics occurred in a quick sequence (less than 1s apart), they were considered as a single tic with the beginning of the sequence noted as the onset time.

4.4.3 Localized Spectral Power

Comparisons of spectral power during Tic periods vs. NoTic periods revealed distinct changes in local neural activity prior to tic onset among voxels located bilaterally in the ACC (centroid Montreal Neurological Institute (MNI) coordinates x = 2, y = 32, z = 19). Significant increases in spectral power (relative to the -3500 to -2500ms baseline period) occurred in the ACC during the -1700 to -500ms period prior to tic onset, primarily in the theta and alpha frequency ranges (Fig. 4-1). There were no significant relationships between ACC spectral power and behavioral measures of tic severity or urge (all p's > 0.05).

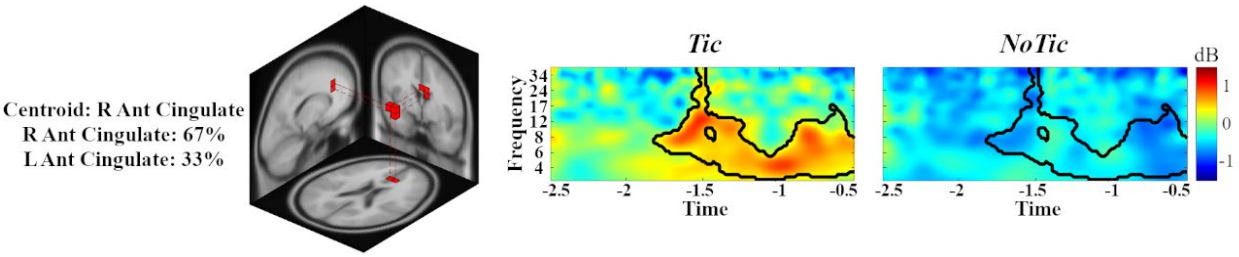

Figure 4-1. Voxels with significant spectral activity between Tic and NoTic conditions. A localized increases in spectral activity (primarily in theta and alpha bands) was observed in the anterior cingulate cortex prior to tic events. Time-frequency plots are masked at pixelwise p = 0.05. Ant = Anterior, dB = decibel, L = left, R = right.

4.4.4 Regional Connectivity

In the effective connectivity analysis, changes in information flow prior to tic occurrence were observed in several cortical regions across the brain, involving a number of bilateral frontal sensorimotor regions as well as left posterior areas of the parietal and occipital cortex (Fig. 4-2, 4-3). Amongst frontal areas, decreases in information flow were observed notably from the midcingulate cortex (MCC) to several other frontal nodes, including the left midfrontal gyrus, right precentral gyrus (primary motor cortex), and bilateral postcentral gyrus (somatosensory cortex). A decrease in connectivity was also noted from the right superior frontal gyrus (SFG) to left SMA, as well as long-distance connectivity from the left angular gyrus to right SFG. These changes occurred throughout the -2500 to -500ms period preceding tic onset, and together indicate acute decreases in communication among cognitive, motor, and sensory-based regions prior to tics.

Increased connectivity was observed from the left midtemporal to left precuneus and left cuneus to left superior parietal cortex during the -1500 to -500ms preceding the tic. Following the detection of local changes in ACC power, the ROI analysis on this region indicated increased

information flow from the ACC to MCC during the -1000 to -500ms immediately preceding the tic event.

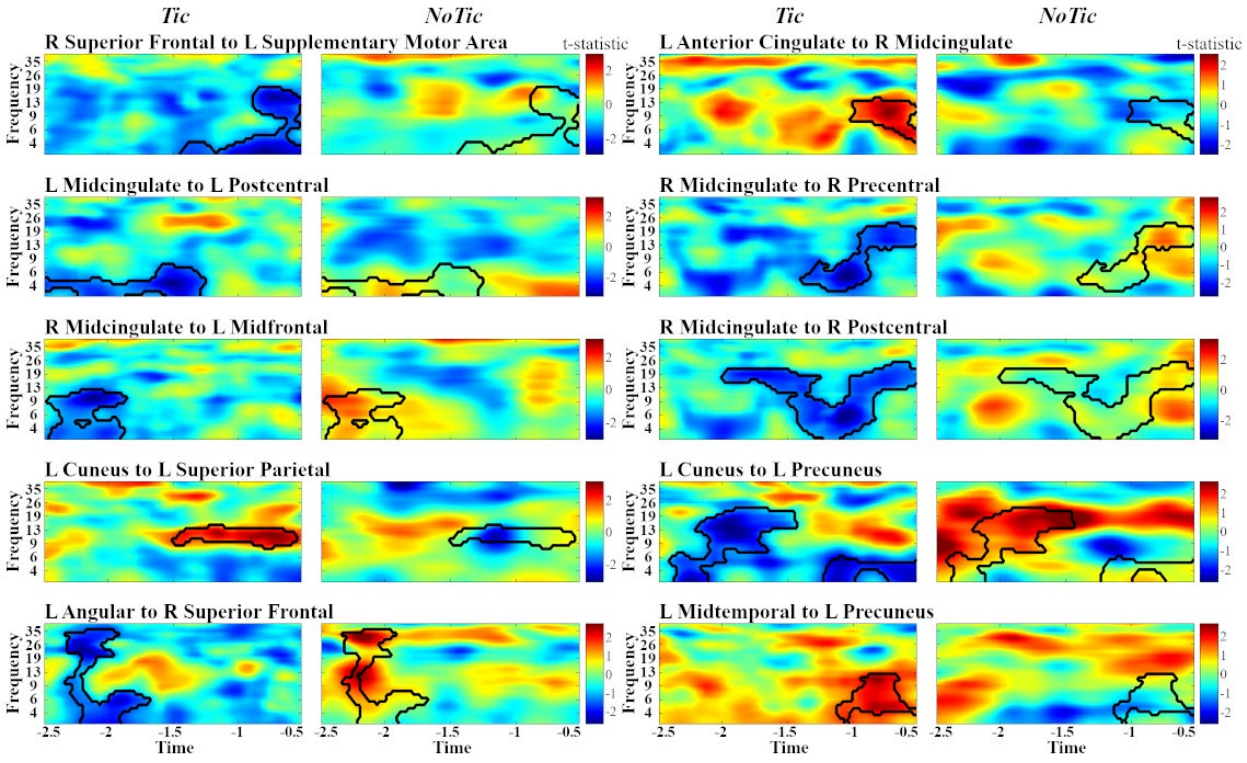

Figure 4-2. Regional connections with significant changes in information flow prior to tic onset. Time-frequency plots are shown with t-statistics, where the statistic at a given pixel is based on a t-tests between connectivity at that pixel and the average baseline (-3500 to -2500ms) connectivity value. Plots are masked at pixelwise p = 0.05. L = left, R = right.

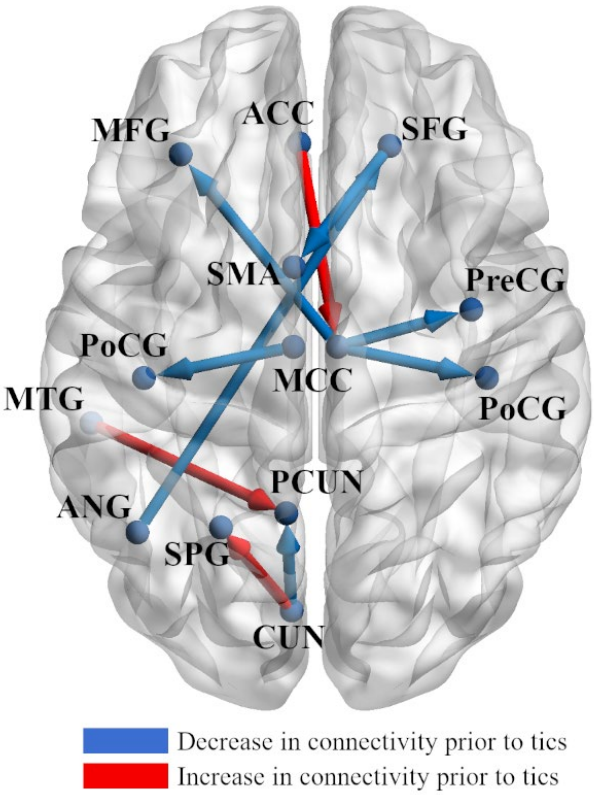

Figure 4-3. Brain plot of significant changes in information flow prior to tic occurrence. Blue connections indicate decreases in information flow (relative to -3500 to -2500ms baseline) prior to tic onset, while red connections indicate increases in information flow. ACC = anterior cingulate cortex, ANG = angular gyrus, CUN = cuneus, MCC = midcingulate cortex, MFG = midfrontal gyrus, MTG = midtemporal gyrus, PCUN = precuneus, PoCG = postcentral gyrus, PreCG = precentral gyrus, SFG = superior frontal gyrus, SPG = superior parietal gyrus, SMA = supplementary motor area.

4.4.5 Behavioral Correlations

Correlation analysis between pre-tic changes in connectivity and PTD-related behavioral measures indicated several significant relationships (Table 4-2). Lower severity scores for YGTSS total and YGTSS impairment scores were associated with greater decreases in information flow

values among several MCC connections as well as the left angular gyrus to right SFG, as well as with greater increases in left cuneus to left superior parietal information flow. Measures of tic frequency (i.e., PUTS tic frequency and tics per minute) were also correlated with connectivity changes in the same direction as the severity scores, with lower tic frequency being associated with greater atypical changes in information flow for all but two connections (left MCC to left postcentral gyrus and left ACC to right MCC) for either PUTS tic frequency or tics per minute. Only one connection was found to be correlated with PUTS urge presence, which indicated greater decreases in right MCC to left midfrontal information flow to be correlated with lower urge presence. PUTS urge strength was not found to be associated with any changes in information flow.

Table 4-2. Pearson correlations between EEG measures and behavioral scores

	YGTSS Total	YGTSS Impairment	PUTS Urge Presence	PUTS Urge Strength	PUTS Tic Frequency	Tics per minute
R Sup Frontal to L Supp Motor Area	0.26	0.19	0.21	0.10	0.24	**0.38***
L Ant Cingulate to R Midcingulate	-0.18	-0.19	-0.02	0.20	-0.05	-0.26
L Midcingulate to L Postcentral	0.01	**0.32***	0.03	0.02	0.17	-0.04
R Midcingulate to R Precentral	**0.33***	**0.34***	0.19	-0.09	**0.42****	0.25
R Midcingulate to L Midfrontal	**0.34***	0.26	**0.40***	0.19	**0.47****	**0.32***
R Midcingulate to R Postcentral	**0.32***	0.27	0.25	-0.04	**0.47****	**0.38***
L Cuneus to	**-0.40****	-0.30	-0.11	0.01	-0.31	**-0.38***

L Sup Parietal						
L Cuneus to L Precuneus	0.11	0.08	0.03	-0.21	**0.38***	0.08
L Angular to R Sup Frontal	**0.40****	**0.35***	0.23	-0.04	**0.35***	**0.35***
L Midtemporal to L Precuneus	-0.08	-0.21	-0.21	-0.16	**-0.43****	-0.12
Anterior Cingulate Cortex	0.20	0.13	0.11	0.24	0.31	-0.26

Note: YGTSS = Yale Global Tic Severity Scale, PUTS = Premonitory Urge for Tics Scale, R = right, Sup = superior, L = left, Supp = supplementary, Ant = anterior. *P < 0.05, **P < 0.01

4.4.6 Classification of Trial-Averaged Activity

The significant findings (one spectral power, 10 connectivity) obtained in the aforementioned analyses were utilized as features in a classification analysis to test the degree of discrimination between Tic and NoTic activity. For each subject, values within the significant time-frequency mask were averaged together to obtain a single value for each feature for each subject. Subjects who did not have data available for a particular feature (as described in Methods) were considered as "missing" for that feature. Given the two conditions (Tic and NoTic), this resulted in an input feature matrix for the classifier consisting of 100 observations (50 subjects, two conditions) and 11 features. Using a kernel naïve Bayes classifier along with 10-fold cross-validation approach, an overall 86% classification rate of condition labels was observed with 90% sensitivity (Tic intervals accurately predicted), and 82% specificity (NoTic intervals accurately predicted). An ROC curve analysis showed an AUC of 0.90, suggesting high discrimination between Tic and No-tic activity.

4.4.7 Independent Test Sample Validation

The obtained model was then evaluated on the independent test sample of 15 subjects by extracting spectral power and connectivity values from the respective region and connections. This resulted in a feature matrix of 30 observations (15 subjects, Tic and NoTic conditions) and 11 features. Classification of these observations resulted in an overall 90% accuracy on this novel dataset, with 100% sensitivity and 80% specificity, indicating these changes in information flow and spectral power to be robust discriminators and indicators of Tic periods relative to NoTic periods.

4.5 Discussion

The present study is the first EEG-based analysis to investigate whole-brain dynamics, using localized spectral power and cross-regional effective connectivity, during the period leading up to tic expression in children with persistent tic disorder. In the 2.5 seconds preceding tic onset, increases in spectral activity were detected amongst voxels of the ACC compared to resting state periods without tics. Changes in information flow were also detected, principally among several frontal and sensorimotor cortex nodes, as well as left temporal, parietal, and occipital cortices, suggesting aberrant communication among multiple cognitive, sensory, and motor-based regions. Using a naïve Bayes classifier to evaluate the discriminability of Tic intervals compared to NoTic intervals, results suggest high specificity and sensitivity in classification rates in both the training and independent test sets, indicating the identified spectral power and connectivity measures are reliable discriminators of tic generation processes.

With respect to evoked local spectral power, tic movements were preceded by increased spectral power in voxels of the ACC. Similar findings of increased ACC activity prior to and

during spontaneous tic exhibition have been frequently reported in prior imaging studies of PTD (Bohlhalter et al., 2006; Neuner et al., 2014; Stern et al., 2000). The ACC has also been implicated in experimental paradigms in PTD, with atypical activity noted during attention-based cognitive control paradigms (Jung et al., 2013; Jurgiel et al., 2021), as well as tic-related cognitive efforts such as voluntary tic suppression (Peterson et al., 1998). The involvement of the ACC in pre-tic processes prior is highly plausible, given the hub-like role in integrating affective, sensory, and cognitive information from thalamic and other cortical regions, as well as involvement in attentional processes and decision-based premotor processing (Devinsky et al., 1995; Paus, 2001; Stevens et al., 2011). Furthermore, the influence of attentional (Herrmann et al., 2019; Misirlisoy et al., 2015) and affective (Ruhrman et al., 2021) processes on tic frequency and severity provide support for the involvement of an integrative region like the ACC. There are several neurological processes for which the increased activity observed here may be representing. One explanation is the attentional detection of a mismatch or conflict between the intended movement (tic) and sensory information from the external environment. Alternatively, the ACC could also be processing internal decision-making on whether to allow or counteract (suppress) this oncoming mismatched tic movement, as well as attempting to initiate inhibition of the upcoming movement. However, it is difficult to discern the degree to which this decision-making is unconscious/autonomic versus conscious. While participants were informed that they could tic as needed, some individuals may have engaged in symptom-reducing behavior, either consciously or unconsciously. Given that there were no observed relationships between ACC spectral power or connectivity and clinical measures of urge or tics, this activity may be more indicative of broader cognitive control processes.

The effective connectivity findings suggest the involvement of several bilateral frontal and left lateralized posterior regions in tic-related processes. The largest number of connectivity differences were found to be associated with the MCC, which is thought to be an information hub for communicating goal-directed behavior towards motor regions (Caruana et al., 2018; Shackman et al., 2011). Decreased information flow towards the precentral and postcentral cortices, two regions have been implicated in prior fMRI studies of tic generation (Hampson et al., 2009; Neuner et al., 2014; Wang et al., 2011), may represent dysregulated communication of motor and sensory-based information, resulting in aberrant motor activation patterns. Additionally, the MCC has been hypothesized to be involved in the "urge-to-action" of both general (e.g., urge to cough) and symptomatic (e.g., urge to tic) behaviors (Jackson, Parkinson, Kim, et al., 2011). Despite being posed as a plausible region for tic-related urge processes, most significant correlations observed with the MCC were associated with measures of tic severity and frequency rather than urge. However, this may be due to using a broader clinical score of urge as opposed to an empirical measure from the recording session. Dysconnectivity was also noted towards the MCC anteriorly from the ACC. This finding is in agreement with two prior EEG connectivity studies of tic suppression and motor inhibition (Hong et al., 2013; Serrien et al., 2005), as well as a prior study on this dataset during inhibitory control (Jurgiel et al., 2021), which observed similar trends of higher frontomesial connectivity in PTD. Given the prior cognitive involvement of this connection, increased connectivity may suggest the engagement of conflict processing or suppression mechanisms prior to tic exhibition, despite no explicit requirement of tic suppression.

Additional reductions in information flow were observed from the right SFG to left SMA, as well as towards the right SFG from the left angular gyrus. Studies have indicated the right SFG to have a broad role in executive functions both as a mediator in motor-based decision making as

well as motor urgency/impulsivity (Hu et al., 2016; Schilling et al., 2012). The SMA similarly takes on a number of roles with respect to decisional movements, including sequencing and performing both simple and complex movements based on intention as well as inhibiting potentially unwanted movements (Nachev et al., 2008). Dysregulated information flow from the left angular gyrus, which has been thought to take more of a sensory and attentional reorientation role (Seghier, 2013), may result in impaired internal decision making and impulsivity downstream among the SFG and SMA regions.

More posteriorly, both increased and decreased communication amongst left occipital and parietal nodes were observed. Connectivity changes involving the left superior parietal, cuneus, and precuneus nodes may be reflective of blink related processes, given prior reports on connectivity and activation changes in these regions during control of eye movements, blink suppression, and cued eye blinks (Asscheman et al., 2015; Berman et al., 2012; Lerner et al., 2009; Loo et al., 2019). The presence of blink-related processes may also be supported by the fact that the ocular tics were the most frequently reported tics observed in this study, as is typical among PTD samples (Ganos et al., 2015).

An interesting relationship emerged between behavioral measures and tic-related connectivity changes, whereby the magnitudes of these atypical changes (i.e., deviations away from NoTic connectivity patterns) were also associated with both lower tic severity and frequency. One possible explanation for this is the involvement of regulatory neural mechanisms, whereby children with greater tic severity are less able to modulate network communication patterns. This would suggest that the communication patterns observed may be related to processes attempting to handle, or counteract, aberrant sensory or motor signals. Another explanation is related to the

fact that tics of various types, with respect to both body part involved and complexity, were included in the analysis. The direction of correlations observed could suggest unique degrees of evoked information flow patterns dependent on the type of tic performed. While classes of parent and child-reported tic behaviors (e.g., ocular, facial, etc.) were obtained during screening, we did not classify the specific tics which occurred during the recording session during the marking procedure. However, prior studies have suggested varying effectiveness of tic inhibition depending on the body part involved, where the most effective inhibition was for body parts exhibiting the fewest tics (Ganos et al., 2015). This dependency may translate to unique neural signatures for different types of tics, which may be detectable with respect to differential magnitudes of activity prior to tic events.

When used as features in a naïve Bayes classification model, the observed changes in spectral power and information flow were found to be robust in their discrimination capabilities, showing high classification rates in both the primary dataset as well as in a novel set of individuals previously unseen by the classifier. Although several studies have evaluated significant differences in neural activations prior to tics, there have been minimal attempts to use observed pre-tic activations in a classification model to evaluate the separability of these tic states from background resting-state activity. One area where this degree of discriminability can be particularly important is for closed-loop neurostimulation treatment protocols, where anomalous tic activation patterns need to be detected amongst typical resting resting-state activity. While we did not perform single-trial training/testing as is needed in such an approach, as preprocessing methods were not optimized towards maximizing single-trial signal detection, the regions causally driving pre-tic activity observed in the present study may pose as suitable targets for further analysis in such an approach.

While the availability of two unique and independent subject samples strengthens the present findings, several limitations should be considered regarding the present analysis and interpretations. Firstly, as the study's primary investigation focus was on motor tics and their neural correlates, vocal tics were not included in the analysis. Given the less frequent occurrence of vocal tics amongst tic disorder populations relative to motor tics, it is possible that other unique regions may be involved with vocal tics, such as those associated with speech. A second limitation expands on this point, such that different neurological mechanisms may be associated with different types of tics, as well as suppression of these tics. Since the EEG recording period was relatively short (~7 minutes), there were not enough tic events to feasibly categorize each (i.e., ocular, facial, etc.) without greatly sacrificing statistical power. A longer resting state analysis where tics are categorizable may be beneficial towards understanding whether different regions and mechanisms are involved in different types of tics. A final limitation is that tic-related activity observed in the present pediatric study may not be fully representative of what occurs in adults with persistent tic disorders, given that studies have indicated unique neural activation patterns across the age spectrum (Nielsen et al., 2020). Considering that children in the present sample are closer to the typical age of onset, they may be less aware of premonitory urges associated with oncoming tics. Reports suggest urges may not apparent until a few years after the onset of tics (Leckman et al., 2006), though this may be simply due to increased somatic awareness as cognitive development occurs through childhood (Banaschewski et al., 2003). Various developmental and adaptive changes in neural functionality occurring up to adulthood may also result in the engagement of additional mechanisms, either consciously or unconsciously, prior to tic onset. Further studies examining both pediatric and adult populations, or the longitudinal progression of

the disorder, may be beneficial towards understanding how tic disorder phenomena change across development.

In summary, the present study used cortical source-level EEG to demonstrate that prior to tic occurrence, acute changes in spectral activity and effective connectivity occur amongst several sensorimotor and left posterior regions, and that this activity is highly discriminable from tic-absent resting state activity. Further analysis of changes in effective connectivity as a function of tic type among the regions described here, both from a trial-averaged and single trial approach, may provide a better understanding of the unique range of neural signatures associated with tics, as well as provide insight towards more effective and targeted treatments.

Chapter 5. Conclusions and Future Directions

The preceding studies discussed in this thesis have attempted to evaluate the degree to which neural activity and cortical-cortical causal communication are impaired or atypical in children with tic disorders during inhibitory control and tic generation. We first presented and validated an alternative approach for performing cortical source-level EEG analyses at the group level for localized spectral power activity. Through a simulation analysis and data from a visual attention task, we demonstrated that the voxel-based approach has better performance for accurately detecting both the location and magnitude of spatially resolved spectral effects. This increase in detectability better ensures both replicability and interpretability of source-level findings. Event-related spectral perturbation was used as a measure of local activity and this method can easily be applied to any type of localized EEG measurement as a future application. As a secondary future direction, evaluations between this ICA dipole-based voxel method and distributed source models such as the Minimum Norm Solution (Hämäläinen & Ilmoniemi, 1994) can be performed in order to compare and contrast these two source estimation approaches with respect to detection, location, and magnitude of particular effects of interest.

Whole-brain spectral power and effective connectivity were then explored in children with PTD (relative to typically developing controls) during an inhibitory control paradigm. Despite minimal differences in accuracy between groups, children with PTD displayed faster reaction times as well as atypical fronto-parietal connectivity and ACC spectral activity during conflict trials. As discussed prior, there have been conflicting reports of inhibitory control deficits among patients with PTD, and while meta analyses point to a moderate effect of general inhibitory control deficits (Morand-Beaulieu et al., 2017), the cognitive paradigm used may play a factor in these

conflicting findings. Further research comparing both behavioral performance and neural dynamics across different types of inhibition tasks may provide more details regarding the specific inhibitory control mechanisms that may be atypical in PTD, and in turn provide a potential resolution to these conflicting findings.

Although treatment methods involving various pharmacotherapies and cognitive behavioral training (such as habit reversal therapy) are frequently employed in an effort to reduce tic symptomology (see Essoe *et al.* (2019) for review), mixed effectiveness as well as medication side-effects often present issues for patient populations. Several studies have explored alternative non-invasive neurostimulation treatment approaches for children with PTD, such as transcranial magnetic stimulation (TMS), and have thus far observed moderate success in reducing symptom severity (Kwon et al., 2011; Le et al., 2013). Further success in this domain, however, may be attainable with personalized and/or closed-loop treatment protocols, where stimulation timing, parameters, and location are selected based on each individual's unique symptomatology and disorder severity as it occurs across time (Pedroarena-Leal & Ruge, 2017). Support for these types of closed-loop systems has been provided in treatment studies of other movement disorders such as Parkinson's disease, where greater efficacy has been observed relative to open-loop systems (Little et al., 2013, 2016). Age has also been indicated to be a factor in treatment efficacy, where young patients appear to be more receptive to brain stimulation treatment with regards to symptom reduction (Grados et al., 2018). To develop a closed-loop system in tic disorders, a critical first step is identifying biomarkers of tic generation among children and adolescents, which are usable as effective features for determining stimulation timing or other parameters.

The final study on EEG antecedents of tic generation provided preliminary findings towards to this goal, with changes in both cortical spectral power and regional information flow observed prior to tic events in children. While some other studies using fMRI have similarly investigated pre-tic antecedents, fMRI measurements potentially lack the temporal resolution to effectively detect pre-tic activity during the short period before the tic is performed. This can pose an issue if the therapeutic stimulation is intended as a counteractive mechanism for tic generative processes, as these processes may only be active for a short period of time before the tic occurs. While the presented analysis did not evaluate tic epoch classification from a single trial approach, successful classification of trial-averaged epochs indicates the observed features and regions to be suitable areas for future exploration using a single trial approach, either as treatment targets or potential indicators for stimulation timing.

The studies presented here provide further insight into the atypical cortical dynamics present in children with PTD during different experimental paradigms. Continued exploration of unique source-level activity present in this patient groups, both from a single-trial standpoint and according to specific classes of tics, may assist in the continued advancement of treatment protocols as applied to the early stages of PTD diagnosis.

References

Asscheman, S. J., Thakkar, K. N., & Neggers, S. F. W. (2015). Changes in Effective Connectivity of the Superior Parietal Lobe during Inhibition and Redirection of Eye Movements: Supplementary Issue: Behavioral Neuroscience. *Journal of Experimental Neuroscience*, *9s1*, JEN.S32736. https://doi.org/10.4137/JEN.S32736

Atkinson-Clement, C., Porte, C.-A., de Liege, A., Klein, Y., Delorme, C., Beranger, B., Valabregue, R., Gallea, C., Robbins, T. W., Hartmann, A., & Worbe, Y. (2020). Impulsive prepotent actions and tics in Tourette disorder underpinned by a common neural network. *Molecular Psychiatry*, 1–10. https://doi.org/10.1038/s41380-020-00890-5

Banaschewski, T., Woerner, W., & Rothenberger, A. (2003). Premonitory sensory phenomena and suppressibility of tics in Tourette syndrome: Developmental aspects in children and adolescents. *Developmental Medicine & Child Neurology*, *45*(10), 700–703. https://doi.org/10.1111/j.1469-8749.2003.tb00873.x

Baym, C. L., Corbett, B. A., Wright, S. B., & Bunge, S. A. (2008). Neural correlates of tic severity and cognitive control in children with Tourette syndrome. *Brain*, *131*(1), 165–179. https://doi.org/10.1093/brain/awm278

Bell, A. J., & Sejnowski, T. J. (1995). An information-maximization approach to blind separation and blind deconvolution. *Neural Computation*, 1159.

Berman, B. D., Horovitz, S. G., Morel, B., & Hallett, M. (2012). Neural correlates of blink suppression and the buildup of a natural bodily urge. *NeuroImage*, *59*(2), 1441–1450. https://doi.org/10.1016/j.neuroimage.2011.08.050

Bigdely-Shamlo, N., Mullen, T., Kreutz-Delgado, K., & Makeig, S. (2013). Measure Projection Analysis: A Probabilistic Approach to EEG Source Comparison and Multi-Subject Inference. *NeuroImage*, *72*, 287–303. https://doi.org/10.1016/j.neuroimage.2013.01.040

Bloch, M. H., & Leckman, J. F. (2009). Clinical course of Tourette syndrome. *Journal of Psychosomatic Research*, *67*(6), 497–501. https://doi.org/10.1016/j.jpsychores.2009.09.002

Bloch, M. H., Leckman, J. F., Zhu, H., & Peterson, B. S. (2005). Caudate volumes in childhood predict symptom severity in adults with Tourette syndrome. *Neurology*, *65*(8), 1253–1258. https://doi.org/10.1212/01.wnl.0000180957.98702.69

Blum, S., Jacobsen, N. S. J., Bleichner, M. G., & Debener, S. (2019). A Riemannian Modification of Artifact Subspace Reconstruction for EEG Artifact Handling. *Frontiers in Human Neuroscience*, *13*, 141. https://doi.org/10.3389/fnhum.2019.00141

Bohlhalter, S., Goldfine, A., Matteson, S., Garraux, G., Hanakawa, T., Kansaku, K., Wurzman, R., & Hallett, M. (2006). Neural correlates of tic generation in Tourette syndrome: An event-related functional MRI study. *Brain*, *129*(8), 2029–2037. https://doi.org/10.1093/brain/awl050

Botvinick, M. M., Cohen, J. D., & Carter, C. S. (2004). Conflict monitoring and anterior cingulate cortex: An update. *Trends in Cognitive Sciences*, *8*(12), 539–546. https://doi.org/10.1016/j.tics.2004.10.003

Bour, L. J., Ackermans, L., Foncke, E. M. J., Cath, D., van der Linden, C., Visser Vandewalle, V., & Tijssen, M. A. (2015). Tic related local field potentials in the thalamus and the effect of deep brain stimulation in Tourette syndrome: Report of three cases. *Clinical Neurophysiology*, *126*(8), 1578–1588. https://doi.org/10.1016/j.clinph.2014.10.217

Bunge, S. A., Dudukovic, N. M., Thomason, M. E., Vaidya, C. J., & Gabrieli, J. D. E. (2002). Immature Frontal Lobe Contributions to Cognitive Control in Children: Evidence from fMRI. *Neuron*, *33*(2), 301–311. https://doi.org/10.1016/S0896-6273(01)00583-9

Caruana, F., Gerbella, M., Avanzini, P., Gozzo, F., Pelliccia, V., Mai, R., Abdollahi, R. O., Cardinale, F., Sartori, I., Lo Russo, G., & Rizzolatti, G. (2018). Motor and emotional behaviours elicited by electrical stimulation of the human cingulate cortex. *Brain*, *141*(10), 3035–3051. https://doi.org/10.1093/brain/awy219

Cavanna, A. E., & Trimble, M. R. (2006). The precuneus: A review of its functional anatomy and behavioural correlates. *Brain*, *129*(3), 564–583. https://doi.org/10.1093/brain/awl004

Chang, C.-Y., Hsu, S.-H., Pion-Tonachini, L., & Jung, T.-P. (2018). Evaluation of Artifact Subspace Reconstruction for Automatic EEG Artifact Removal. *Conference Proceedings: ... Annual International Conference of the IEEE Engineering in Medicine and Biology Society. IEEE Engineering in Medicine and Biology Society. Annual Conference*, *2018*, 1242–1245. https://doi.org/10.1109/EMBC.2018.8512547

Church, J. A., Fair, D. A., Dosenbach, N. U. F., Cohen, A. L., Miezin, F. M., Petersen, S. E., & Schlaggar, B. L. (2009). Control networks in paediatric Tourette syndrome show immature and anomalous patterns of functional connectivity. *Brain*, *132*(1), 225–238. https://doi.org/10.1093/brain/awn223

Church, J. A., Wenger, K. K., Dosenbach, N. U. F., Miezin, F. M., Petersen, S. E., Schlaggar, B. L., & Marsh, R. (2009). Task control signals in pediatric Tourette syndrome show evidence of immature and anomalous functional activity. *Frontiers in Human Neuroscience*, *3*. https://doi.org/10.3389/neuro.09.038.2009

Cohen, J. (1988). *Statistical Power Analysis for the Behavioral Sciences*. Academic Press.

Conceição, V. A., Dias, Â., Farinha, A. C., & Maia, T. V. (2017). Premonitory urges and tics in Tourette syndrome: Computational mechanisms and neural correlates. *Current Opinion in Neurobiology*, *46*, 187–199. https://doi.org/10.1016/j.conb.2017.08.009

Crawford, S., Channon, S., & Robertson, M. M. (2005). Tourette's syndrome: Performance on tests of behavioural inhibition, working memory and gambling. *Journal of Child Psychology and Psychiatry*, *46*(12), 1327–1336. https://doi.org/10.1111/j.1469-7610.2005.01419.x

Cui, Y., Jin, Z., Chen, X., He, Y., Liang, X., & Zheng, Y. (2014). Abnormal baseline brain activity in drug-naïve patients with Tourette syndrome: A resting-state fMRI study. *Frontiers in Human Neuroscience*, *7*. https://doi.org/10.3389/fnhum.2013.00913

Debes, N. M. M. M., Lange, T., Jessen, T. L., Hjalgrim, H., & Skov, L. (2011). Performance on Wechsler intelligence scales in children with Tourette syndrome. *European Journal of Paediatric Neurology: EJPN: Official Journal of the European Paediatric Neurology Society*, *15*(2), 146–154. https://doi.org/10.1016/j.ejpn.2010.07.007

Delorme, A., & Makeig, S. (2004). EEGLAB: An open source toolbox for analysis of single-trial EEG dynamics including independent component analysis. *Journal of Neuroscience Methods*, *134*(1), 9–21. https://doi.org/10.1016/j.jneumeth.2003.10.009

Delorme, A., Mullen, T., Kothe, C., Akalin Acar, Z., Bigdely-Shamlo, N., Vankov, A., & Makeig, S. (2011). EEGLAB, SIFT, NFT, BCILAB, and ERICA: New Tools for Advanced EEG Processing. *Computational Intelligence and Neuroscience*, *2011*, 1–12. https://doi.org/10.1155/2011/130714

Delorme, A., Palmer, J., Onton, J., Oostenveld, R., & Makeig, S. (2012a). Independent EEG Sources Are Dipolar. *PLoS ONE*, *7*(2), 14.

Delorme, A., Palmer, J., Onton, J., Oostenveld, R., & Makeig, S. (2012b). Independent EEG Sources Are Dipolar. *PLOS ONE*, *7*(2), e30135. https://doi.org/10.1371/journal.pone.0030135

Devinsky, O., Morrell, M. J., & Vogt, B. A. (1995). Contributions of anterior cingulate cortex to behaviour. *Brain*, *118*(1), 279–306. https://doi.org/10.1093/brain/118.1.279

Eriksen, B. A., & Eriksen, C. W. (1974). Effects of noise letters upon the identification of a target letter in a nonsearch task. *Perception & Psychophysics*, *16*(1), 143–149. https://doi.org/10.3758/BF03203267

Essoe, J. K.-Y., Grados, M. A., Singer, H. S., Myers, N. S., & McGuire, J. F. (2019). Evidence-based treatment of Tourette's disorder and chronic tic disorders. *Expert Review of Neurotherapeutics*, *19*(11), 1103–1115. https://doi.org/10.1080/14737175.2019.1643236

Fan, J., Byrne, J., Worden, M. S., Guise, K. G., McCandliss, B. D., Fossella, J., & Posner, M. I. (2007). The relation of brain oscillations to attentional networks. *The Journal of Neuroscience: The Official Journal of the Society for Neuroscience*, *27*(23), 6197–6206. https://doi.org/10.1523/JNEUROSCI.1833-07.2007

Fan, J., Flombaum, J. I., McCandliss, B. D., Thomas, K. M., & Posner, M. I. (2003). Cognitive and Brain Consequences of Conflict. *NeuroImage*, *18*(1), 42–57. https://doi.org/10.1006/nimg.2002.1319

Fan, J., McCandliss, B. D., Sommer, T., Raz, A., & Posner, M. I. (2002). Testing the Efficiency and Independence of Attentional Networks. *Journal of Cognitive Neuroscience*, *14*(3), 340–347. https://doi.org/10.1162/089892902317361886

Fan, J., Mccandliss, B., Fossella, J., Flombaum, J., & Posner, M. (2005). The activation of attentional networks. *NeuroImage*, *26*(2), 471–479. https://doi.org/10.1016/j.neuroimage.2005.02.004

Franzkowiak, S., Pollok, B., Biermann-Ruben, K., Südmeyer, M., Paszek, J., Thomalla, G., Jonas, M., Orth, M., Münchau, A., & Schnitzler, A. (2012). Motor-Cortical Interaction in Gilles de la Tourette Syndrome. *PLOS ONE*, *7*(1), e27850. https://doi.org/10.1371/journal.pone.0027850

Freed, R. D., Coffey, B. J., Mao, X., Weiduschat, N., Kang, G., Shungu, D. C., & Gabbay, V. (2016). Decreased Anterior Cingulate Cortex γ-Aminobutyric Acid in Youth With Tourette's Disorder. *Pediatric Neurology*, *65*, 64–70. https://doi.org/10.1016/j.pediatrneurol.2016.08.017

Ganos, C., Bongert, J., Asmuss, L., Martino, D., Haggard, P., & Münchau, A. (2015). The somatotopy of tic inhibition: Where and how much? *Movement Disorders*, *30*(9), 1184–1189. https://doi.org/10.1002/mds.26188

Ganos, C., Kahl, U., Brandt, V., Schunke, O., Bäumer, T., Thomalla, G., Roessner, V., Haggard, P., Münchau, A., & Kühn, S. (2014). The neural correlates of tic inhibition in Gilles de la Tourette syndrome. *Neuropsychologia*, *65*, 297–301. https://doi.org/10.1016/j.neuropsychologia.2014.08.007

Ganos, C., Kühn, S., Kahl, U., Schunke, O., Feldheim, J., Gerloff, C., Roessner, V., Bäumer, T., Thomalla, G., Haggard, P., & Münchau, A. (2014). Action inhibition in Tourette syndrome. *Movement Disorders*, *29*(12), 1532–1538. https://doi.org/10.1002/mds.25944

Ganos, C., Roessner, V., & Münchau, A. (2013). The functional anatomy of Gilles de la Tourette syndrome. *Neuroscience & Biobehavioral Reviews*, *37*(6), 1050–1062. https://doi.org/10.1016/j.neubiorev.2012.11.004

Ganos, C., Rothwell, J., & Haggard, P. (2018). Voluntary inhibitory motor control over involuntary tic movements. *Movement Disorders*, *33*(6), 937–946. https://doi.org/10.1002/mds.27346

Grados, M., Huselid, R., & Duque-Serrano, L. (2018). Transcranial Magnetic Stimulation in Tourette Syndrome: A Historical Perspective, Its Current Use and the Influence of Comorbidities in Treatment Response. *Brain Sciences*, *8*(7). https://doi.org/10.3390/brainsci8070129

Grandchamp, R., Braboszcz, C., Makeig, S., & Delorme, A. (2012). Stability of ICA decomposition across within-subject EEG datasets. *2012 Annual International Conference of the IEEE Engineering in Medicine and Biology Society*, 6735–6739. https://doi.org/10.1109/EMBC.2012.6347540

Greene, D. J., Williams Iii, A. C., Koller, J. M., Schlaggar, B. L., & Black, K. J. (2017). Brain structure in pediatric Tourette syndrome. *Molecular Psychiatry*, *22*(7), 972–980. https://doi.org/10.1038/mp.2016.194

Groppe, D. M., Urbach, T. P., & Kutas, M. (2011). Mass univariate analysis of event-related brain potentials/fields I: A critical tutorial review. *Psychophysiology*, *48*(12), 1711–1725. https://doi.org/10.1111/j.1469-8986.2011.01273.x

Hämäläinen, M. S., & Ilmoniemi, R. J. (1994). Interpreting magnetic fields of the brain: Minimum norm estimates. *Medical & Biological Engineering & Computing*, *32*(1), 35–42. https://doi.org/10.1007/BF02512476

Hampson, M., Tokoglu, F., King, R. A., Constable, R. T., & Leckman, J. F. (2009). Brain Areas Coactivating with Motor Cortex During Chronic Motor Tics and Intentional Movements. *Biological Psychiatry*, *65*(7), 594–599. https://doi.org/10.1016/j.biopsych.2008.11.012

Hashemiyoon, R., Kuhn, J., & Visser-Vandewalle, V. (2017). Putting the Pieces Together in Gilles de la Tourette Syndrome: Exploring the Link Between Clinical Observations and the Biological Basis of Dysfunction. *Brain Topography*, *30*(1), 3–29. https://doi.org/10.1007/s10548-016-0525-z

Herrmann, K., Sprenger, A., Baumung, L., Alvarez-Fischer, D., Münchau, A., & Brandt, V. (2019). Help or hurt? How attention modulates tics under different conditions. *Cortex*, *120*, 471–482. https://doi.org/10.1016/j.cortex.2019.06.016

Himle, M. B., & Woods, D. W. (2005). An experimental evaluation of tic suppression and the tic rebound effect. *Behaviour Research and Therapy*, *43*(11), 1443–1451. https://doi.org/10.1016/j.brat.2004.11.002

Hirschtritt, M. E., Lee, P. C., Pauls, D. L., Dion, Y., Grados, M. A., Illmann, C., King, R. A., Sandor, P., McMahon, W. M., Lyon, G. J., Cath, D. C., Kurlan, R., Robertson, M. M., Osiecki, L., Scharf, J. M., Mathews, C. A., & for the Tourette Syndrome Association International Consortium for Genetics. (2015). Lifetime Prevalence, Age of Risk, and Genetic Relationships of Comorbid Psychiatric Disorders in Tourette Syndrome. *JAMA Psychiatry*, *72*(4), 325–333. https://doi.org/10.1001/jamapsychiatry.2014.2650

Hong, H. J., Sohn, H., Cha, M., Kim, S., Oh, J., Chu, M. K., Namkoong, K., & Jeong, J. (2013). Increased Frontomotor Oscillations During Tic Suppression in Children With Tourette Syndrome. *Journal of Child Neurology*, *28*(5), 615–624. https://doi.org/10.1177/0883073812450317

Hsu, S.-H., Pion-Tonachini, L., Palmer, J., Miyakoshi, M., Makeig, S., & Jung, T.-P. (2018). Modeling brain dynamic state changes with adaptive mixture independent component analysis. *NeuroImage*, *183*, 47–61. https://doi.org/10.1016/j.neuroimage.2018.08.001

Hu, S., Ide, J. S., Zhang, S., & Li, C. R. (2016). The Right Superior Frontal Gyrus and Individual Variation in Proactive Control of Impulsive Response. *Journal of Neuroscience*, *36*(50), 12688–12696. https://doi.org/10.1523/JNEUROSCI.1175-16.2016

Jackson, S. R., Loayza, J., Crighton, M., Sigurdsson, H. P., Dyke, K., & Jackson, G. M. (2020). The role of the insula in the generation of motor tics and the experience of the premonitory urge-to-tic in Tourette syndrome. *Cortex*, *126*, 119–133. https://doi.org/10.1016/j.cortex.2019.12.021

Jackson, S. R., Parkinson, A., Jung, J., Ryan, S. E., Morgan, P. S., Hollis, C., & Jackson, G. M. (2011). Compensatory Neural Reorganization in Tourette Syndrome. *Current Biology*, *21*(7), 580–585. https://doi.org/10.1016/j.cub.2011.02.047

Jackson, S. R., Parkinson, A., Kim, S. Y., Schüermann, M., & Eickhoff, S. B. (2011). On the functional anatomy of the urge-for-action. *Cognitive Neuroscience*, *2*(3–4), 227–243. https://doi.org/10.1080/17588928.2011.604717

Jung, J., Jackson, S. R., Parkinson, A., & Jackson, G. M. (2013). Cognitive control over motor output in Tourette syndrome. *Neuroscience & Biobehavioral Reviews*, *37*(6), 1016–1025. https://doi.org/10.1016/j.neubiorev.2012.08.009

Jurgiel, J., Miyakoshi, M., Dillon, A., Piacentini, J., Makeig, S., & Loo, S. K. (2021). Inhibitory control in children with tic disorder: Aberrant fronto-parietal network activity and connectivity. *Brain Communications*, *3*(2), fcab067. https://doi.org/10.1093/braincomms/fcab067

Karp, B. I., Porter, S., Toro, C., & Hallett, M. (1996). Simple motor tics may be preceded by a premotor potential. *Journal of Neurology, Neurosurgery & Psychiatry*, *61*(1), 103–106. https://doi.org/10.1136/jnnp.61.1.103

Korn, E. L., Troendle, J. F., McShane, L. M., & Simon, R. (2004a). Controlling the number of false discoveries: Application to high-dimensional genomic data. *Journal of Statistical Planning and Inference*, *124*(2), 379–398. https://doi.org/10.1016/S0378-3758(03)00211-8

Korn, E. L., Troendle, J. F., McShane, L. M., & Simon, R. (2004b). Controlling the number of false discoveries: Application to high-dimensional genomic data. *Journal of Statistical Planning and Inference*, *124*(2), 379–398. https://doi.org/10.1016/S0378-3758(03)00211-8

Korzeniewska, A., Crainiceanu, C. M., Kuś, R., Franaszczuk, P. J., & Crone, N. E. (2008). Dynamics of event-related causality in brain electrical activity. *Human Brain Mapping*, *29*(10), 1170–1192. https://doi.org/10.1002/hbm.20458

Koshiyama, D., Miyakoshi, M., Joshi, Y. B., Molina, J. L., Tanaka-Koshiyama, K., Sprock, J., Braff, D. L., Swerdlow, N. R., & Light, G. A. (2020). Abnormal Effective Connectivity Underlying Auditory Mismatch Negativity Impairments in Schizophrenia. *Biological Psychiatry: Cognitive Neuroscience and Neuroimaging*, *5*(11), 1028–1039. https://doi.org/10.1016/j.bpsc.2020.05.011

Kothe, C. A., & Makeig, S. (2013). BCILAB: A platform for brain–computer interface development. *Journal of Neural Engineering*, *10*(5), 056014. https://doi.org/10.1088/1741-2560/10/5/056014

Kriegeskorte, N., Simmons, W. K., Bellgowan, P. S., & Baker, C. I. (2009). Circular analysis in systems neuroscience – the dangers of double dipping. *Nature Neuroscience*, *12*(5), 535–540. https://doi.org/10.1038/nn.2303

Kumar, A., Trescher, W., & Byler, D. (2016). Tourette Syndrome and Comorbid Neuropsychiatric Conditions. *Current Developmental Disorders Reports*, *3*(4), 217–221. https://doi.org/10.1007/s40474-016-0099-1

Kwon, H. J., Lim, W. S., Lim, M. H., Lee, S. J., Hyun, J. K., Chae, J.-H., & Paik, K. C. (2011). 1-Hz low frequency repetitive transcranial magnetic stimulation in children with Tourette's syndrome. *Neuroscience Letters*, *492*(1), 1–4. https://doi.org/10.1016/j.neulet.2011.01.007

Lacadie, C. M., Fulbright, R. K., Constable, R. T., & Papademetris, X. (2008). More Accurate Talairach Coordinates for NeuroImaging using Nonlinear Registration. *NeuroImage*, *42*(2), 717–725. https://doi.org/10.1016/j.neuroimage.2008.04.240

Le, K., Liu, L., Sun, M., Hu, L., & Xiao, N. (2013). Transcranial magnetic stimulation at 1Hertz improves clinical symptoms in children with Tourette syndrome for at least 6 months. *Journal of Clinical Neuroscience*, *20*(2), 257–262. https://doi.org/10.1016/j.jocn.2012.01.049

Leckman, J. F., Bloch, M. H., Scahill, L., & King, R. A. (2006). Tourette Syndrome: The Self Under Siege. *Journal of Child Neurology*, *21*(8), 642–649. https://doi.org/10.1177/08830738060210081001

Leckman, J. F., Riddle, M. A., Hardin, M. T., Ort, S. I., Swartz, K. L., Stevenson, J., & Cohen, D. J. (1989). The Yale Global Tic Severity Scale: Initial Testing of a Clinician-Rated Scale of Tic Severity. *Journal of the American Academy of Child & Adolescent Psychiatry*, *28*(4), 566–573. https://doi.org/10.1097/00004583-198907000-00015

Lerner, A., Bagic, A., Boudreau, E. A., Hanakawa, T., Pagan, F., Mari, Z., Bara-Jimenez, W., Aksu, M., Garraux, G., Simmons, J. M., Sato, S., Murphy, D. L., & Hallett, M. (2007). Neuroimaging of neuronal circuits involved in tic generation in patients with Tourette syndrome. *Neurology*, *68*(23), 1979–1987. https://doi.org/10.1212/01.wnl.0000264417.18604.12

Lerner, A., Bagic, A., Hanakawa, T., Boudreau, E. A., Pagan, F., Mari, Z., Bara-Jimenez, W., Aksu, M., Sato, S., Murphy, D. L., & Hallett, M. (2009). Involvement of Insula and Cingulate Cortices in Control and Suppression of Natural Urges. *Cerebral Cortex*, *19*(1), 218–223. https://doi.org/10.1093/cercor/bhn074

Little, S., Beudel, M., Zrinzo, L., Foltynie, T., Limousin, P., Hariz, M., Neal, S., Cheeran, B., Cagnan, H., Gratwicke, J., Aziz, T. Z., Pogosyan, A., & Brown, P. (2016). Bilateral adaptive deep brain stimulation is effective in Parkinson's disease. *Journal of Neurology, Neurosurgery & Psychiatry*, *87*(7), 717–721. https://doi.org/10.1136/jnnp-2015-310972

Little, S., Pogosyan, A., Neal, S., Zavala, B., Zrinzo, L., Hariz, M., Foltynie, T., Limousin, P., Ashkan, K., FitzGerald, J., Green, A. L., Aziz, T. Z., & Brown, P. (2013). Adaptive deep brain stimulation in advanced Parkinson disease. *Annals of Neurology*, *74*(3), 449–457. https://doi.org/10.1002/ana.23951

Loo, S. K., Miyakoshi, M., Tung, K., Lloyd, E., Salgari, G., Dillon, A., Chang, S., Piacentini, J., & Makeig, S. (2019). Neural activation and connectivity during cued eye blinks in Chronic Tic Disorders. *NeuroImage: Clinical*, *24*, 101956. https://doi.org/10.1016/j.nicl.2019.101956

Maiquez, B. M., Jackson, G. M., & Jackson, S. R. (2020). *Examining the neural antecedents of tics in Tourette syndrome using electroencephalography* [Preprint]. Neuroscience. https://doi.org/10.1101/2020.05.01.071837

Margulies, D. S., Vincent, J. L., Kelly, C., Lohmann, G., Uddin, L. Q., Biswal, B. B., Villringer, A., Castellanos, F. X., Milham, M. P., & Petrides, M. (2009). Precuneus shares intrinsic functional architecture in humans and monkeys. *Proceedings of the National Academy of Sciences of the United States of America*, *106*(47), 20069–20074. https://doi.org/10.1073/pnas.0905314106

Marsh, R., Zhu, H., Wang, Z., Skudlarski, P., & Peterson, B. S. (2007). A Developmental fMRI Study of Self-Regulatory Control in Tourette's Syndrome. *American Journal of Psychiatry*, *164*(6), 955–966. https://doi.org/10.1176/ajp.2007.164.6.955

McDermott, T. J., Wiesman, A. I., Proskovec, A. L., Heinrichs-Graham, E., & Wilson, T. W. (2017). Spatiotemporal oscillatory dynamics of visual selective attention during a flanker task. *NeuroImage*, *156*, 277–285. https://doi.org/10.1016/j.neuroimage.2017.05.014

McGuire, J. F., Sturm, A., Ricketts, E. J., Montalbano, G. E., Chang, S., Loo, S. K., Woods, D. W., McCracken, J., & Piacentini, J. (2022). Cognitive control processes in behavior therapy for youth with Tourette's disorder. *Journal of Child Psychology and Psychiatry*, *63*(3), 296–304. https://doi.org/10.1111/jcpp.13470

Misirlisoy, E., Brandt, V., Ganos, C., Tübing, J., Münchau, A., & Haggard, P. (2015). The Relation Between Attention and Tic Generation in Tourette Syndrome. *Neuropsychology*, *29*(4), 658–665. https://doi.org/10.1037/neu0000161

Morand-Beaulieu, S., Grot, S., Lavoie, J., Leclerc, J. B., Luck, D., & Lavoie, M. E. (2017). The puzzling question of inhibitory control in Tourette syndrome: A meta-analysis. *Neuroscience & Biobehavioral Reviews*, *80*, 240–262. https://doi.org/10.1016/j.neubiorev.2017.05.006

Mueller, S. C., Jackson, G. M., Dhalla, R., Datsopoulos, S., & Hollis, C. P. (2006). Enhanced Cognitive Control in Young People with Tourette's Syndrome. *Current Biology*, *16*(6), 570–573. https://doi.org/10.1016/j.cub.2006.01.064

Mullen, T. R., Kothe, C. A. E., Chi, Y. M., Ojeda, A., Kerth, T., Makeig, S., Jung, T.-P., & Cauwenberghs, G. (2015). Real-time neuroimaging and cognitive monitoring using wearable dry EEG. *IEEE Transactions on Biomedical Engineering*, *62*(11), 2553–2567. https://doi.org/10.1109/TBME.2015.2481482

Müller-Vahl, K. R., Kaufmann, J., Grosskreutz, J., Dengler, R., Emrich, H. M., & Peschel, T. (2009). Prefrontal and anterior cingulate cortex abnormalities in Tourette Syndrome: Evidence from voxel-based morphometry and magnetization transfer imaging. *BMC Neuroscience*, *10*(1), 47. https://doi.org/10.1186/1471-2202-10-47

Nachev, P., Kennard, C., & Husain, M. (2008). Functional role of the supplementary and pre-supplementary motor areas. *Nature Reviews Neuroscience*, *9*(11), 856–869. https://doi.org/10.1038/nrn2478

Nagahama, Y., Okada, T., Katsumi, Y., Hayashi, T., Yamauchi, H., Sawamoto, N., Toma, K., Nakamura, K., Hanakawa, T., Konishi, J., Fukuyama, H., & Shibasaki, H. (1999). Transient Neural Activity in the Medial Superior Frontal Gyrus and Precuneus Time Locked with Attention Shift between Object Features. *NeuroImage*, *10*(2), 193–199. https://doi.org/10.1006/nimg.1999.0451

Neuner, I., Werner, C. J., Arrubla, J., Stöcker, T., Ehlen, C., Wegener, H. P., Schneider, F., & Shah, N. J. (2014). Imaging the where and when of tic generation and resting state networks in adult Tourette patients. *Frontiers in Human Neuroscience*, *8*. https://doi.org/10.3389/fnhum.2014.00362

Nielsen, A. N., Gratton, C., Church, J. A., Dosenbach, N. U. F., Black, K. J., Petersen, S. E., Schlaggar, B. L., & Greene, D. J. (2020). Atypical Functional Connectivity in Tourette Syndrome Differs Between Children and Adults. *Biological Psychiatry*, *87*(2), 164–173. https://doi.org/10.1016/j.biopsych.2019.06.021

Nunez, P. L., Srinivasan, R., Westdorp, A. F., Wijesinghe, R. S., Tucker, D. M., Silberstein, R. B., & Cadusch, P. J. (1997). EEG coherency: I: statistics, reference electrode, volume conduction, Laplacians, cortical imaging, and interpretation at multiple scales. *Electroencephalography and Clinical Neurophysiology*, *103*(5), 499–515. https://doi.org/10.1016/S0013-4694(97)00066-7

Obeso, J. A., Rothwell, J. C., & Marsden, C. D. (1981). Simple tics in Gilles de la Tourette's syndrome are not prefaced by a normal premovement EEG potential. *Journal of Neurology, Neurosurgery & Psychiatry*, *44*(8), 735–738. https://doi.org/10.1136/jnnp.44.8.735

O'Neill, J., Piacentini, J. C., & Peterson, B. S. (2019). Cingulate role in Tourette syndrome. In *Handbook of Clinical Neurology* (Vol. 166, pp. 165–221). Elsevier. https://doi.org/10.1016/B978-0-444-64196-0.00011-X

Oostenveld, R., Fries, P., Maris, E., & Schoffelen, J.-M. (2010a). FieldTrip: Open Source Software for Advanced Analysis of MEG, EEG, and Invasive Electrophysiological Data. *Computational Intelligence and Neuroscience*, *2011*, e156869. https://doi.org/10.1155/2011/156869

Oostenveld, R., Fries, P., Maris, E., & Schoffelen, J.-M. (2010b, December 23). *FieldTrip: Open Source Software for Advanced Analysis of MEG, EEG, and Invasive Electrophysiological Data* [Research Article]. Computational Intelligence and Neuroscience; Hindawi. https://doi.org/10.1155/2011/156869

Openneer, T. J. C., Marsman, J.-B. C., van der Meer, D., Forde, N. J., Akkermans, S. E. A., Naaijen, J., Buitelaar, J. K., Dietrich, A., & Hoekstra, P. J. (2020). A graph theory study of resting-state functional connectivity in children with Tourette syndrome. *Cortex*, *126*, 63–72. https://doi.org/10.1016/j.cortex.2020.01.006

Ozonoff, S., Strayer, D. L., McMahon, W. M., & Filloux, F. (1998). Inhibitory Deficits in Tourette Syndrome: A Function of Comorbidity and Symptom Severity. *Journal of Child Psychology and Psychiatry*, *39*(8), 1109–1118. https://doi.org/10.1111/1469-7610.00415

Palmer, J. A., Kreutz-Delgado, K., & Makeig, S. (2011). *AMICA: An Adaptive Mixture of Independent Component Analyzers with Shared Components*. 15.

Paus, T. (2001). Primate anterior cingulate cortex: Where motor control, drive and cognition interface. *Nature Reviews Neuroscience*, *2*(6), 417–424. https://doi.org/10.1038/35077500

Pedroarena-Leal, N., & Ruge, D. (2017). Toward a Symptom-Guided Neurostimulation for Gilles de la Tourette Syndrome. *Frontiers in Psychiatry*, *8*. https://doi.org/10.3389/fpsyt.2017.00029

Pernet, C. R., Latinus, M., Nichols, T. E., & Rousselet, G. A. (2015). Cluster-based computational methods for mass univariate analyses of event-related brain potentials/fields: A simulation study. *Journal of Neuroscience Methods*, *250*, 85–93. https://doi.org/10.1016/j.jneumeth.2014.08.003

Peterson, B., Skudlarski, P., Anderson, A., Zhang, H., Gatenby, C., Lacadie, C., Leckman, J., & Gore, J. (1998). A Functional Magnetic Resonance Imaging Study of Tic Suppression in Tourette Syndrome. *Archives of General Psychiatry*, *55*, 326–333. https://doi.org/10.1001/archpsyc.55.4.326

Peterson, B., Thomas, P., Kane, M. J., Scahill, L., Zhang, H., Bronen, R., King, R. A., Leckman, J. F., & Staib, L. (2003). Basal Ganglia Volumes in Patients With Gilles de la Tourette Syndrome. *Archives of General Psychiatry*, *60*(4), 415–424. https://doi.org/10.1001/archpsyc.60.4.415

Pion-Tonachini, L., Makeig, S., & Kreutz-Delgado, K. (2017). Crowd labeling latent Dirichlet allocation. *Knowledge and Information Systems*, *53*(3), 749–765. https://doi.org/10.1007/s10115-017-1053-1

Polyanska, L., Critchley, H. D., & Rae, C. L. (2017). Centrality of prefrontal and motor preparation cortices to Tourette Syndrome revealed by meta-analysis of task-based neuroimaging studies. *NeuroImage: Clinical*, *16*, 257–267. https://doi.org/10.1016/j.nicl.2017.08.004

R Core Team. (2020). *R: A Language and Environment for Statistical Computing*. R Foundation for Statistical Computing, Vienna, Austria. http://www.R-project.org

Rae, C. L., Polyanska, L., Gould van Praag, C. D., Parkinson, J., Bouyagoub, S., Nagai, Y., Seth, A. K., Harrison, N. A., Garfinkel, S. N., & Critchley, H. D. (2018). Face perception enhances insula and motor network reactivity in Tourette syndrome. *Brain*, *141*(11), 3249–3261. https://doi.org/10.1093/brain/awy254

Ramkiran, S., Heidemeyer, L., Gaebler, A., Shah, N. J., & Neuner, I. (2019). Alterations in basal ganglia-cerebello-thalamo-cortical connectivity and whole brain functional network topology in Tourette's syndrome. *NeuroImage. Clinical*, *24*, 101998. https://doi.org/10.1016/j.nicl.2019.101998

Robertson, M. M. (2008). The prevalence and epidemiology of Gilles de la Tourette syndrome: Part 1: The epidemiological and prevalence studies. *Journal of Psychosomatic Research*, *65*(5), 461–472. https://doi.org/10.1016/j.jpsychores.2008.03.006

Roessner, V., Albrecht, B., Dechent, P., Baudewig, J., & Rothenberger, A. (2008). Normal response inhibition in boys with Tourette syndrome. *Behavioral and Brain Functions*, *4*(1), 29. https://doi.org/10.1186/1744-9081-4-29

Roessner, V., Overlack, S., Schmidt-Samoa, C., Baudewig, J., Dechent, P., Rothenberger, A., & Helms, G. (2011). Increased putamen and callosal motor subregion in treatment-naïve boys with Tourette syndrome indicates changes in the bihemispheric motor network. *Journal of Child Psychology and Psychiatry*, *52*(3), 306–314. https://doi.org/10.1111/j.1469-7610.2010.02324.x

Ruhrman, D., Mikulincer, M., Apter, A., Benaroya-Milshtein, N., & Steinberg, T. (2021). Emotion regulation and tic disorders in children. *European Child & Adolescent Psychiatry*. https://doi.org/10.1007/s00787-021-01912-5

Santhana Gopalan, P. R., Loberg, O., Hämäläinen, J. A., & Leppänen, P. H. T. (2019). Attentional processes in typically developing children as revealed using brain event-related potentials and their source localization in Attention Network Test. *Scientific Reports*, *9*(1), 2940. https://doi.org/10.1038/s41598-018-36947-3

Scahill, L., Riddle, M. A., McSwiggin-Hardin, M., Ort, S. I., King, R. A., Goodman, W. K., Cicchetti, D., & Leckman, J. F. (1997). Children's Yale-Brown Obsessive Compulsive Scale: Reliability and Validity. *Journal of the American Academy of Child & Adolescent Psychiatry*, *36*(6), 844–852. https://doi.org/10.1097/00004583-199706000-00023

Schelter, B., Timmer, J., & Eichler, M. (2009). Assessing the strength of directed influences among neural signals using renormalized partial directed coherence. *Journal of Neuroscience Methods*, *179*(1), 121–130. https://doi.org/10.1016/j.jneumeth.2009.01.006

Schilling, C., Kühn, S., Romanowski, A., Schubert, F., Kathmann, N., & Gallinat, J. (2012). Cortical thickness correlates with impulsiveness in healthy adults. *NeuroImage*, *59*(1), 824–830. https://doi.org/10.1016/j.neuroimage.2011.07.058

Seghier, M. L. (2013). The Angular Gyrus: Multiple Functions and Multiple Subdivisions. *The Neuroscientist*, *19*(1), 43–61. https://doi.org/10.1177/1073858412440596

Serrien, D. J., Orth, M., Evans, A. H., Lees, A. J., & Brown, P. (2005). Motor inhibition in patients with Gilles de la Tourette syndrome: Functional activation patterns as revealed by EEG coherence. *Brain*, *128*(1), 116–125. https://doi.org/10.1093/brain/awh318

Shackman, A. J., Salomons, T. V., Slagter, H. A., Fox, A. S., Winter, J. J., & Davidson, R. J. (2011). The integration of negative affect, pain and cognitive control in the cingulate cortex. *Nature Reviews Neuroscience*, *12*(3), 154–167. https://doi.org/10.1038/nrn2994

Silverman, W. K. (1996). *Anxiety Disorders Interview Schedule for DSM-IV.: Parent interview schedule*. Oxford University Press.

Sowell, E. R., Kan, E., Yoshii, J., Thompson, P. M., Bansal, R., Xu, D., Toga, A. W., & Peterson, B. S. (2008). Thinning of sensorimotor cortices in children with Tourette syndrome. *Nature Neuroscience*, *11*(6), 637–639. https://doi.org/10.1038/nn.2121

Stern, E., Silbersweig, D. A., Chee, K.-Y., Holmes, A., Robertson, M. M., Trimble, M., Frith, C. D., Frackowiak, R. S. J., & Dolan, R. J. (2000). A Functional Neuroanatomy of Tics in Tourette Syndrome. *Archives of General Psychiatry*, *57*(8), 741–748. https://doi.org/10.1001/archpsyc.57.8.741

Stevens, F. L., Hurley, R. A., Taber, K. H., Hurley, R. A., Hayman, L. A., & Taber, K. H. (2011). Anterior Cingulate Cortex: Unique Role in Cognition and Emotion. *The Journal of Neuropsychiatry and Clinical Neurosciences*, *23*(2), 121–125. https://doi.org/10.1176/jnp.23.2.jnp121

Swanson, J. M., Schuck, S., Porter, M. M., Carlson, C., Hartman, C. A., Sergeant, J. A., Clevenger, W., Wasdell, M., McCleary, R., Lakes, K., & Wigal, T. (2012). Categorical and Dimensional Definitions and Evaluations of Symptoms of ADHD: History of the SNAP and the SWAN Rating Scales. *The International Journal of Educational and Psychological Assessment*, *10*(1), 51–70.

Tinaz, S., Belluscio, B. A., Malone, P., Veen, J. W. van der, Hallett, M., & Horovitz, S. G. (2014). Role of the sensorimotor cortex in tourette syndrome using multimodal imaging. *Human Brain Mapping*, *35*(12), 5834–5846. https://doi.org/10.1002/hbm.22588

Tinaz, S., Malone, P., Hallett, M., & Horovitz, S. G. (2015). Role of the right dorsal anterior insula in the urge to tic in tourette syndrome. *Movement Disorders*, *30*(9), 1190–1197. https://doi.org/10.1002/mds.26230

Tzourio-Mazoyer, N., Landeau, B., Papathanassiou, D., Crivello, F., Etard, O., Delcroix, N., Mazoyer, B., & Joliot, M. (2002). Automated Anatomical Labeling of Activations in SPM Using a Macroscopic Anatomical Parcellation of the MNI MRI Single-Subject Brain. *NeuroImage*, *15*(1), 273–289. https://doi.org/10.1006/nimg.2001.0978

Van Veen, V., & Carter, C. (2002). The anterior cingulate as a conflict monitor: FMRI and ERP studies. *Physiology & Behavior*, *77*(4–5), 477–482. https://doi.org/10.1016/S0031-9384(02)00930-7

Wang, Z., Maia, T. V., Marsh, R., Colibazzi, T., Gerber, A., & Peterson, B. S. (2011). The Neural Circuits That Generate Tics in Tourette's Syndrome. *American Journal of Psychiatry*, *168*(12), 1326–1337. https://doi.org/10.1176/appi.ajp.2011.09111692

Wechsler, D. (1999). *Wechsler Abbreviated Scale of Intelligence WASI: Manual*. Pearson/PsychCorpl.

Wen, H., Liu, Y., Rekik, I., Wang, S., Zhang, J., Zhang, Y., Peng, Y., & He, H. (2017). Disrupted topological organization of structural networks revealed by probabilistic diffusion tractography in Tourette syndrome children. *Human Brain Mapping*, *38*(8), 3988–4008. https://doi.org/10.1002/hbm.23643

Wen, H., Liu, Y., Wang, J., Rekik, I., Zhang, J., Zhang, Y., Tian, H., Peng, Y., & He, H. (2016). Combining tract- and atlas-based analysis reveals microstructural abnormalities in early Tourette syndrome children. *Human Brain Mapping*, *37*(5), 1903–1919. https://doi.org/10.1002/hbm.23146

Woods, D. W., Piacentini, J., Himle, M. B., & Chang, S. (2005). Premonitory Urge for Tics Scale (PUTS): Initial Psychometric Results and Examination of the Premonitory Urge Phenomenon in Youths with Tic Disorders. *Journal of Developmental & Behavioral Pediatrics*, *26*(6), 397–403.

Worbe, Y., Malherbe, C., Hartmann, A., Pélégrini-Issac, M., Messé, A., Vidailhet, M., Lehéricy, S., & Benali, H. (2012). Functional immaturity of cortico-basal ganglia networks in Gilles de la Tourette syndrome. *Brain*, *135*(6), 1937–1946. https://doi.org/10.1093/brain/aws056

Worbe, Y., Marrakchi-Kacem, L., Lecomte, S., Valabregue, R., Poupon, F., Guevara, P., Tucholka, A., Mangin, J.-F., Vidailhet, M., Lehericy, S., Hartmann, A., & Poupon, C. (2015). Altered structural connectivity of cortico-striato-pallido-thalamic networks in Gilles de la Tourette syndrome. *Brain*, *138*(2), 472–482. https://doi.org/10.1093/brain/awu311

Wylie, S. A., Claassen, D. O., Kanoff, K. E., Ridderinkhof, K. R., & van den Wildenberg, W. P. M. (2013). Impaired inhibition of prepotent motor actions in patients with Tourette syndrome. *Journal of Psychiatry & Neuroscience : JPN*, *38*(5), 349–356. https://doi.org/10.1503/jpn.120138

Xia, M., Wang, J., & He, Y. (2013). BrainNet Viewer: A Network Visualization Tool for Human Brain Connectomics. *PLoS ONE*, *8*(7), e68910. https://doi.org/10.1371/journal.pone.0068910

Xuan, B., Mackie, M.-A., Spagna, A., Wu, T., Tian, Y., Hof, P. R., & Fan, J. (2016). The activation of interactive attentional networks. *NeuroImage*, *129*, 308–319. https://doi.org/10.1016/j.neuroimage.2016.01.017

Zapparoli, L., Macerollo, A., Joyce, E. M., Martino, D., & Kilner, J. M. (2019). Voluntary tic suppression and the normalization of motor cortical beta power in Gilles de la Tourette syndrome: An EEG study. *European Journal of Neuroscience*, *50*(12), 3944–3957. https://doi.org/10.1111/ejn.14548

Zapparoli, L., Porta, M., & Paulesu, E. (2015). The anarchic brain in action: The contribution of task-based fMRI studies to the understanding of Gilles de la Tourette syndrome. *Current Opinion in Neurology*, *28*(6), 604–611. https://doi.org/10.1097/WCO.0000000000000261

Zapparoli, L., Tettamanti, M., Porta, M., Zerbi, A., Servello, D., Banfi, G., & Paulesu, E. (2017). A tug of war: Antagonistic effective connectivity patterns over the motor cortex and the severity of motor symptoms in Gilles de la Tourette syndrome. *European Journal of Neuroscience*, *46*(6), 2203–2213. https://doi.org/10.1111/ejn.13658